THE DEVELOPMENT AND EVALUATION OF A Nd:YAG LASER INCORPORATING AN UNSTABLE RESONATOR

by

Trevor Neil de Kock

A thesis submitted in fulfilment of the requirements for the degree of Master of Science of Rhodes University.

Pretoria
December 1985

ACKNOWLEDGEMENTS

I wish to express my thanks to my supervisors, Drs D J Brink and L M G Poole for the help and useful guidance which has been given me during the project.

The other members of the Laser Section of the National Physical Research Laboratory (NPRL) are thanked for the assistance and useful discussions on various aspects of the project. Messrs. J A Strauss and E J de Kock are thanked for the proofreading of the manuscript.

Finally, I must thank Mrs J Turnbull who did the drawings and Mrs L King and I Uytenbogaardt for the many hours of typing which were spent on the manuscript.

CONTENTS

CHAPTER 1

INTRODUCTION

For approximately the last eight years the Laser Section of the National Physical Research Laboratory (NPRL) has been interested in inter alia, pulsed solid-state lasers and in particular, Nd:YAG. Investigations of various resonator types were undertaken with a view to the improvement of the laser parameters such as output energy, pulse width, beam quality and sensitivity to mirror misalignment.

In 1980 a Nd:YAG laser employing a rotating prism Q-switch was constructed (Preussler (1980)). It involves rotating one of the two cavity reflectors so that they are parallel for only a brief instant in time. Typically the prism must rotate at a speed of 20 000 r.p.m. to ensure a single pulse output. Such lasers suffer from the tendency to emit multiple pulses, they are very noisy and they require frequent maintenance because of the short lifetime of the bearings.

A resonator employing conventional curved mirrors and an electro-optical Q-switch was constructed in 1980 (Robertson & Preussler (1982)). In 1981 an electro-optically Q-switched laser making use of a crossed Porro-prism resonator was investigated due to its relative insensitivity to misalignment of the reflectors compared with the conventional mirror resonator (Nortier (1981)).

Improvements in terms of output power, beam divergence and beam quality can be achieved by making use of a so-called unstable resonator. Such a laser has been investigated and is reported on in this study. Chapter 2 provides some background into laser theory and operation while chapter 3 deals with the theory of the unstable resonator. Chapter 4 provides details of the experimental equipment and techniques used in the work and chapter 5 discusses the evaluation of the project and results obtained.

CHAPTER 2

BASIC LASER THEORY

2.1 INTRODUCTION

The first demonstration of laser action, or the "optical maser" as it was then known, was achieved by Maiman (1960) using ruby as the active medium. The neodymium ion (Nd^{3+}) was recognized as having ideal characteristics for laser action but the host materials available at the time showed some shortcomings either because of their intrinsic physical properties or because of the way in which they interacted with the Nd^{3+} ions. These were overcome by Geusic et al. (1964) with the use of yttrium aluminium garnet (YAG) as host. Nd:YAG lasers displayed the lowest thresholds for CW operation at room temperature of any known host-dopant combination. Today, Nd:YAG is one of the most commonly used solid-state laser materials.

The underlying principles upon which all lasers operate are essentially the same except, for example, in the excitation mechanisms. In this chapter these principles are described in a classical rather than a quantum mechanical way, since the classical way is sufficient to outline the concepts involved.

2.2 REQUIREMENTS FOR LASER ACTION

For successful operation, lasers require an active medium in which a population inversion is created, and an optical resonator. The active medium may be in a solid, liquid or gaseous form. The condition of a population inversion is highly abnormal in nature and is created in a laser by a process known as pumping. Finally, some form of optical feedback is necessary to ensure laser oscillation and this is achieved with the optical resonator. These concepts are dealt with in greater detail in the following subsections.

2.2.1 ACTIVE MEDIUM: EMISSION AND ABSORPTION OF RADIATION

The active medium is a collection of atoms, molecules or ions that amplify radiation in the optical part of the electromagnetic spectrum. Such an atomic system is characterized by discrete energy states and, for simplicity, we assume that there are only two energy states. These states are described by energies E_0, for the lower level and E_1 for the single excited state ($E_1 > E_0$). When an electromagnetic field is incident on the system, radiation is either absorbed or emitted by the atoms at a defined frequency ν_{10} which is given by the Bohr relation

$$\nu_{10} = \frac{E_1 - E_0}{h} \tag{2.1}$$

where h is Planck's constant = $6{,}6 \times 10^{-34}$ J.s

The absorption and emission of radiation in an atomic system can take place by essentially three processes illustrated in Fig. 2.1. Atoms can be stimulated by the incident radiation at frequency ν_{10} to undergo transitions from the ground state to the excited state. Since incident radiation is needed for this absorption process to occur it is referred to as stimulated absorption (Fig. 2.1(a)).

Soon after being excited to the higher energy state, an atom emits a quantum of energy at frequency ν_{10} and so returns to the ground state. This emission process can take place in two forms. In contrast to the absorption transition, the emission of radiation by an excited atom can occur spontaneously (spontaneous emission), or it can be stimulated to occur by the presence of radiation at the transition frequency (stimulated emission). These two processes are illustrated in Fig. 2.1(b) and (c). The stimulated emission process is an essential part of the operation of a laser.

Atoms emitting radiation by the spontaneous emission process do so randomly in space and time. Atoms undergoing stimulated emission radiate

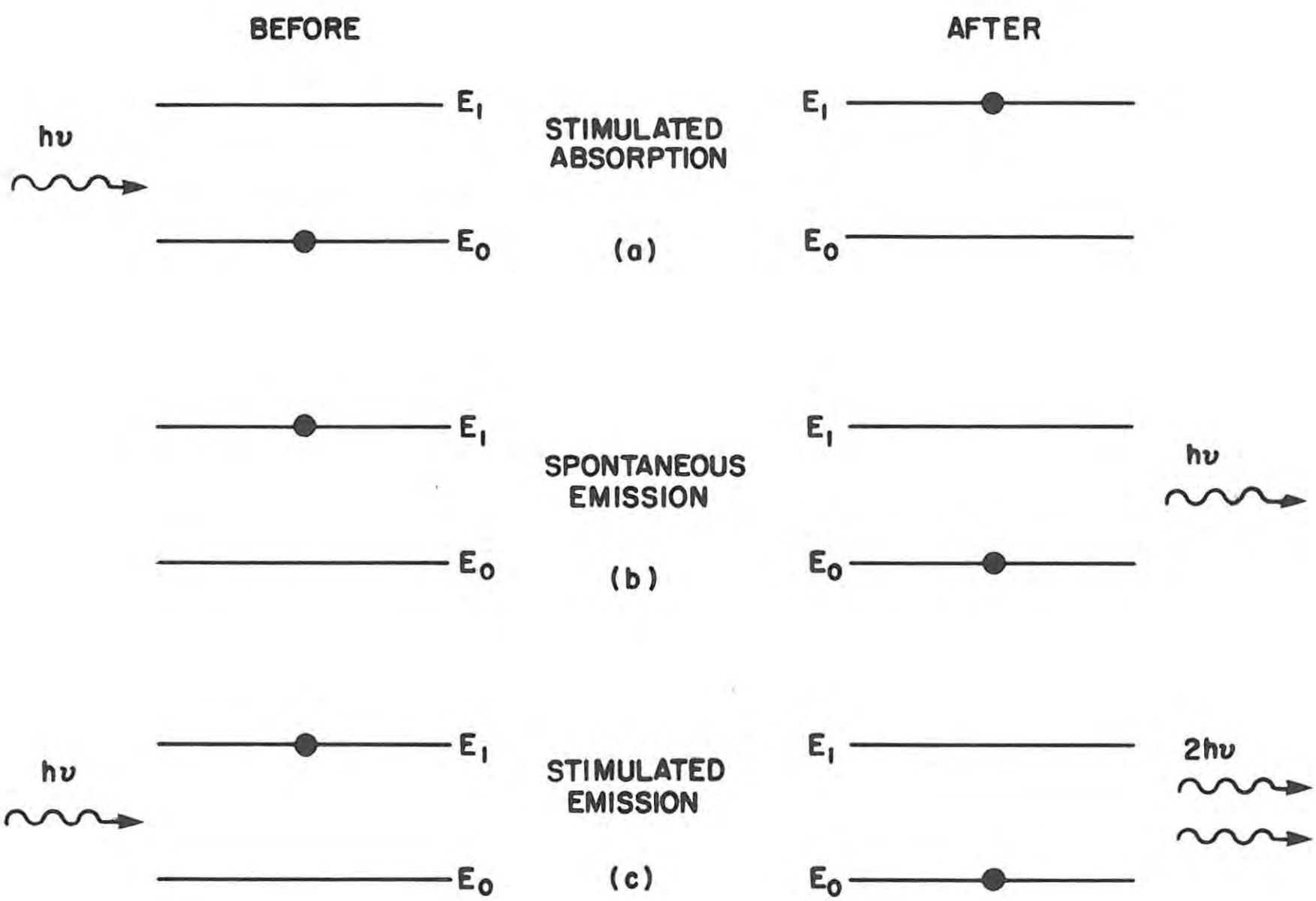

FIG. 2.1 INITIAL AND FINAL STATES OF ABSORPTION AND EMISSION PROCESSES

photons in phase and at the same frequency as the stimulating radiation. This means that the additional photon liberated in the process adds to the radiation on a constructive basis, thereby increasing its amplitude.

The average fractional rate at which atoms in energy state E_1 spontaneously drop to the lower state E_0 is designated by a constant, the Einstein coefficient of spontaneous emission, A_{10}. The time for the transition to occur is the transition lifetime of the state, τ_{10}, and is equal to the reciprocal of A_{10} for a two-level system. If there are N_1 atoms with energy E_1, the number of atoms per second which undergo spontaneous emission to the lower state is given by

spontaneous emission transition rate = $N_1 A_{10}$

$$\left(\frac{\partial N_1}{\partial t}\right)_{spont} = -N_1 A_{10} \tag{2.2}$$

Incident radiation energy must be present for the stimulated processes to occur. The number of atoms undergoing absorption transitions per second is proportional to the number of atoms in the lower state, N_0, and to the spectral energy density of the radiation, ρ_ν, at the transition frequency, ν_{10}.

stimulated absorption transition rate = $N_0 \rho_\nu B_{01}$

$$\left(\frac{\partial N_0}{\partial t}\right)_{stim} = -N_0 \rho_\nu B_{01} \tag{2.3}$$

where B_{01} is a proportionality constant, the Einstein coefficient of stimulated absorption.

Similarly, the stimulated emission rate is given by the number of atoms in the excited state times the spectral energy density times the proportionality constant, B_{10}, the Einstein coefficient of stimulated emission,

stimulated emission transition rate = $N_1 \rho_\nu B_{10}$

$$\left(\frac{\partial N_1}{\partial t}\right)_{stim} = -N_1 \rho_\nu B_{10} \tag{2.4}$$

If thermal equilibrium conditions are assumed, it can be shown that the coefficients of stimulated absorption and stimulated emission are related by

$$g_0 B_{01} = g_1 B_{10} \tag{2.5}$$

where g_i is the statistical weight of level i.
The coefficient of spontaneous emission can be shown to be related to the coefficient of stimulated emission by the equation

$$A_{10} = \frac{8\pi h \nu_{10}^3}{c^3} B_{10} \tag{2.6}$$

where $c = c_o/n$ c_o, speed of light in vacuum
n, index of refraction

Equations (2.5) and (2.6) are known as the Einstein relations and were derived by him in 1917 (Einstein (1917)).

Although the discussion above has been in terms of transitions between the ground state and a single excited state, in real systems characterized by a number of different energy states, absorption and emission transitions are, in principle, possible between any of the states. For such real systems the Einstein relations can be extended for an arbitrary pair of atomic energy states, E_i and E_j $(E_j > E_i)$ simply by substituting E_j for E_1 and E_i for E_0.

2.2.2 CREATION OF A POPULATION INVERSION AND PUMPING

If we consider a collection of atoms in a medium in thermal equilibrium at room temperature then the population in the ground electronic state is normally much larger than that of a higher electronic state. At higher temperatures the fraction of atoms in excited states is larger. The population densities of any two levels i and j $(E_j > E_i)$ can be determined by the Boltzmann distribution to be

$$\frac{N_j}{N_i} = \frac{g_j}{g_i} \exp\left(\frac{-(E_j - E_i)}{kT}\right) \qquad (2.7)$$

where k = Boltzmann's constant = $1{,}38 \times 10^{-23}$ J/K

T = absolute temperature in Kelvin

As T is increased (for $g_j \approx g_i$) in equation (2.7) N_j approaches N_i but it cannot exceed it. The essential condition, however, for amplification and hence lasing is that we must have, at a given instant, more atoms in an upper energy level than in a lower level i.e.

$$N_j > N_i \quad \text{if} \quad (E_j > E_i)$$

This is an abnormal situation which is never observed at thermal equilibrium and is called a population inversion. Such a population inversion can only be achieved by some external energy source, the pump source. Once a population inversion is achieved, amplification can take place by stimulated emission. Typical pump sources include flashlamps and electric discharges.

Optical pumping schemes require processes more complicated than the pumping of atoms from the ground state directly to the upper laser level of a laser transition. Two-, three- and four-level schemes are common pumping schemes. Here we will only consider the four-level pumping scheme which is characteristic of the rare earth ions in host materials such as YAG.

The population of energy levels in a four-level system is shown in Fig. 2.2. It can be seen that the pump excitation lifts atoms from the ground state to the highest of the four "levels" E_3, the so-called pump band which is a wide absorption band. From this band the atoms proceed rapidly to the sharply defined level E_2. The laser transition now occurs with the atoms proceeding to a terminal level, E_1, which is situated above the ground state. From this level the atom undergoes a rapid non-radiative transition to the ground level. If the lifetimes of the $(3 \rightarrow 2)$ and $(1 \rightarrow 0)$ transition are short compared with the spontaneous emission lifetime of the laser transition $(2 \rightarrow 1)$, a population inversion on the $(2 \rightarrow 1)$ transition can be achieved.

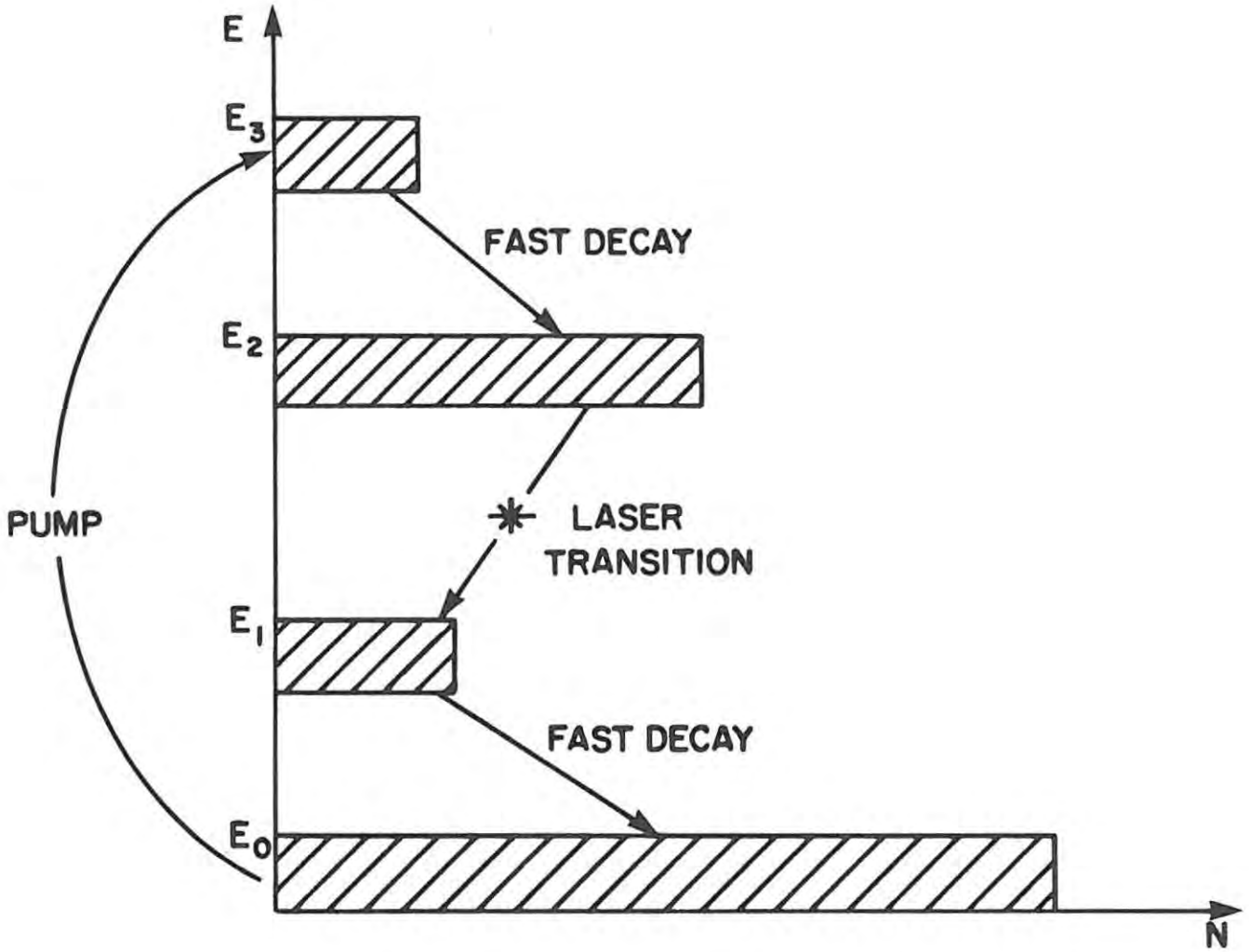

FIG. 2.2 POPULATION OF ENERGY LEVELS IN A FOUR-LEVEL SYSTEM

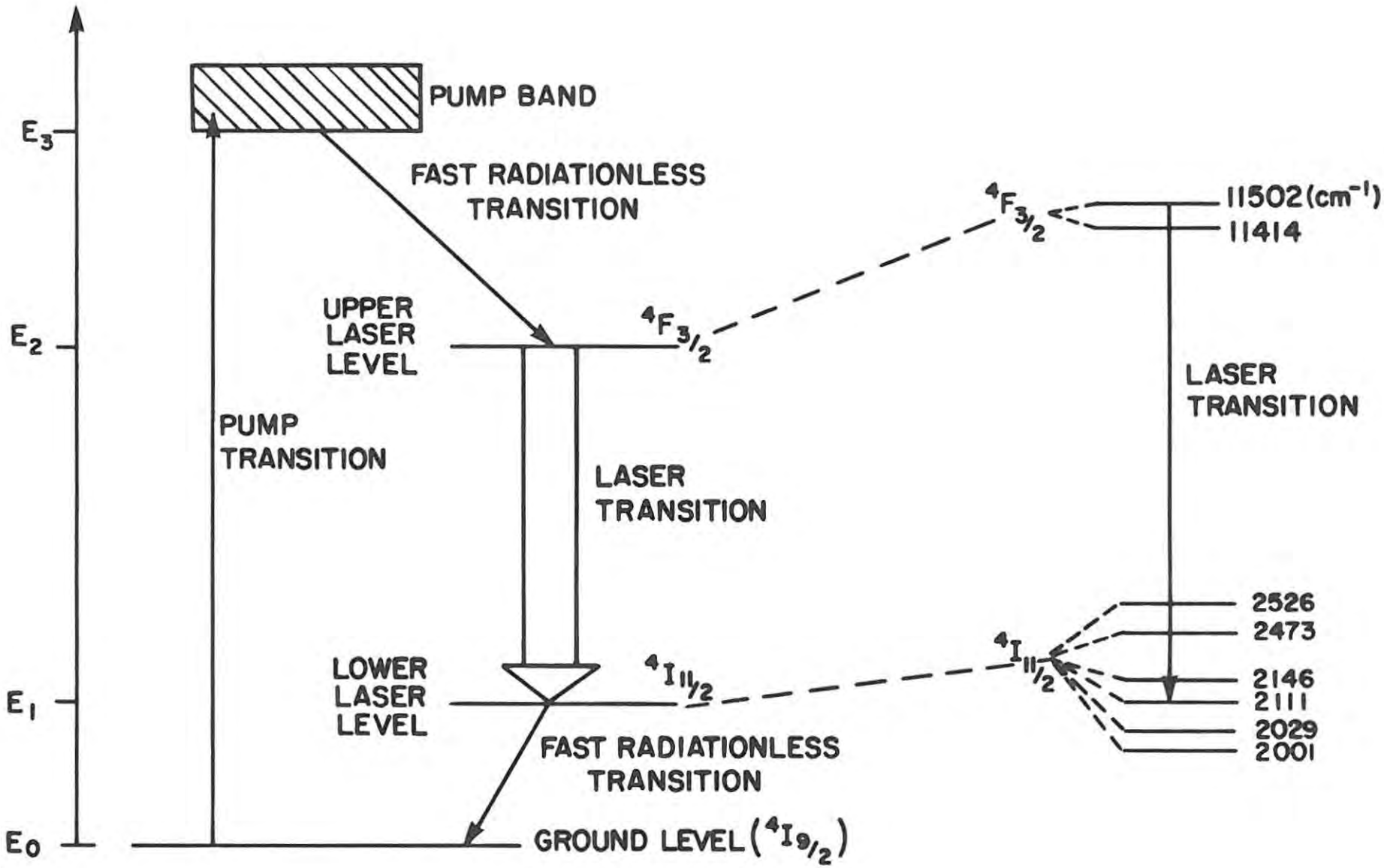

FIG. 2.3 ENERGY LEVEL DIAGRAM OF Nd:YAG

Fig. 2.3 shows the energy level diagram of Nd:YAG. The laser transition at a wavelength of 1,064 μm, originates from the 11502 cm^{-1} component of the $^4F_{3/2}$ level and terminates at the 2111 cm^{-1} component of the $^4I_{11/2}$ level. The ground level is the $^4I_{9/2}$ level. A number of relatively broad, closely spaced, energy levels comprise the pump level 3. The lifetimes of the (3 → 2) and (1 → 0) transitions are approximately 0,1 ns and 30 ns respectively compared to the spontaneous fluorescence lifetime of 230 μs. The terminology used here is standard to the spectroscopy of rare earth ions in crystals and can be found in, for example, Lengyel (1971). The terminology is essentially the same as for atomic spectroscopy with the level being designated

$$2S + 1\,L_J$$

where the resultant orbital quantum numbers L = 0,1,2,3 .... are expressed by the capital letters S,P,D,F,G, ...

$2S + 1$ represents the multiplicity of the state due to the resultant spin S.

J is the resultant combination of L and S.

When an ion is located in a crystal lattice, the electric and magnetic fields prevailing at the position of the ion may exert a considerable influence on the energy level structure of the ion. The subject of crystal field theory, also called Ligand field theory, is used to describe the splitting of energy levels of ions in a crystal field (Ballhausen (1962)). Koningstein and Geusic (1964) have studied the energy levels and crystal fields in Nd:YAG.

The dynamic behaviour of the laser can be described reasonably accurately by a set of coupled rate equations. A pair of simultaneous differential equations describes the population inversion and the radiation density within a spatially uniform laser medium. Such a set of rate equations is useful in predicting some features of laser outputs such as average and peak powers, Q-switched pulse-envelope shape and threshold conditions. Many details are inaccessible from the rate equations such as spectral, temporal and spatial distributions of the laser emission. Such details can fortunately be accounted for by other means.

Assuming that the transition from the pump band to the upper laser level occurs very rapidly we can neglect the population of the pump band (i.e. $N_3 \approx 0$) and find the rate of change of the population of the two laser levels to be (Koechner (1976)):

$$\frac{dN_2}{dt} = W_p N_o - (N_2 - \frac{g_2}{g_1} N_1)\sigma\phi c - N_2(\frac{1}{\tau_{21}} + \frac{1}{\tau_{20}}) \tag{2.8}$$

$$\frac{dN_1}{dt} = (N_2 - \frac{g_2}{g_1} N_1)\sigma\phi c + \frac{N_2}{\tau_{21}} - \frac{N_1}{\tau_{10}} \tag{2.9}$$

and

$$N_{TOT} = N_0 + N_1 + N_2 \tag{2.10}$$

where W_p is the pumping rate (s^{-1})

σ is the stimulated emission cross section

ϕ is the photon density

$c = \frac{c_0}{n}$ is the speed of light in the material

$g_{1,2}$ are the level degeneracies

$\tau_{i,j}$ is the lifetime of the transition ($i \rightarrow j$).

By defining the inversion population density by

$$N = N_2 - \frac{g_2}{g_1} N_1$$

and by making the assumption that $\tau_{10} = 0$, implying that $N_1 = 0$, the equations can be combined to give (Koechner (1976))

$$\frac{\partial N}{\partial t} = -N\,\sigma\phi c - \frac{N}{\tau_f} + W_p(N_{TOT} - N) \tag{2.11}$$

where τ_f is the fluorescence decay time of the upper laser level given by

$$\frac{1}{\tau_f} = \frac{1}{\tau_{21}} + \frac{1}{\tau_{20}}$$

Another equation describes the rate of change of photon density in the resonator (Koechner (1976)):

$$\frac{\partial \phi}{\partial t} = c\phi\sigma N - \frac{\phi}{\tau_c} + S \qquad (2.12)$$

where τ_c is the decay time for photons in the resonator and
S is the rate at which spontaneous emission is added to the laser emission.

Computer solutions of the laser rate equations predict a train of regular and damped spikes at the output of the laser (Röss (1969), Steele (1968) and Robertson & Preussler (1982)). However, most lasers show irregular undamped spikes caused by mechanical and thermal shocks and disturbances present in many real lasers act to continually reexcite the spiking behaviour and keep it from damping out (see Section 5.2).

2.2.3 OPTICAL FEEDBACK - THE LASER RESONATOR

The final basic requirement for laser action to take place is that there should be some form of optical feedback in the laser system. This is achieved by the optical resonator which comprises two mirrors which are perpendicular to the optical axis of the active medium. The optical resonator together with the active medium and the pump source form the laser oscillator.

The pump source, in our case a flashlamp, inverts the population in the laser material, leading to energy storage in the upper laser level. Photons spontaneously emitted along the optical axis of the laser are reflected by the resonator mirrors and cause the stimulated emission of further photons. If the feedback is sufficiently large to compensate for the losses of the system, the system will oscillate. The reflectivity of the mirrors determines the amount of feedback.

It is possible to calculate the threshold condition for laser oscillation by means of a simple laser oscillator model. We assume a gain per

unit length of g, an active medium of length ℓ and mirrors of reflectivity $R_1 \approx 1$ and $0 < R_2 < 1$. For convenience, all nonoutput losses are represented by a single parameter α, the absorption coefficient per unit length. A gain which is exponential with length can be shown to be a realistic choice (Steele (1968)). If we assume a photon density of ϕ photons/cm^3, the threshold condition requires that after one round trip in the resonator the final photon density should be equal to the initial photon density. Note that one round trip entails two traversals of the active medium and one reflection by each mirror.

The threshold condition then requires that

$$\phi \exp[+2(g-\alpha)\ell] R_1 R_2 = \phi$$

or

$$\exp[-2(g-\alpha)\ell] = R_1 R_2 \tag{2.13}$$

Taking the logarithm of both sides we can obtain an expression for g,

$$g = \alpha + \frac{1}{2\ell} \ln \frac{1}{R_1 R_2} = \alpha + \alpha_0 \tag{2.14}$$

The form of (2.14) emphasizes the similar nature of the two terms as losses: α represents losses of cavity radiation resulting from absorption and scattering in the medium, α_0 represents the radiation lost in the form of useful output. When the useful output is regarded as a loss, the condition for steady-state laser oscillation may be stated as: the gain is equal to the sum of the losses in the laser.

It should be noted that for laser emission to occur the rate of change of photon density must be equal to or greater than zero. So at laser threshold to maintain oscillation we need the condition

$$\frac{\partial \phi}{\partial t} \geq 0 \tag{2.15}$$

From (2.12) ignoring the contribution from spontaneous emission processes (i.e. S = 0) we can get the inversion density at threshold,

$$N > \frac{1}{c\sigma\tau_c} \tag{2.16}$$

2.3 THE LASER OUTPUT

2.3.1 RELAXATION OSCILLATIONS - SPIKING

The most notable transient effect in solid-state lasers is the phenomenon of relaxation oscillations resulting in the spiking behaviour as mentioned in Section 2.2.2. The phenomenon of spike formation can be explained with the aid of Fig. 2.4.

At the onset of pumping there are a negligible number of photons in the cavity at the appropriate frequency. The pump radiation causes the population to become inverted. Under steady-state oscillation conditions N_2 can never exceed N_t, the threshold inversion. However, under transient conditions N_2 goes above N_t, because no laser oscillation has has been built up and no radiation exists to reduce N_2 by means of stimulated emission. Laser oscillation only begins to build up after N_2 exceeds N_t so that the net round-trip gain exceeds unity. Then because N_2 is considerably larger than N_t, the oscillation level builds up rapidly to a value of a photon flux which is considerably larger than the steady-state value for the particular pumping level.

With a high photon flux, the upper level rate of depletion by stimulated emission becomes large, even larger than the pumping rate. Consequently, the upper population level passes through a maximum value and then decreases rapidly due to the large photon flux level. The population of the upper level goes below the threshold level N_t and the net gain in the cavity becomes less than unity. The existing oscillation in the cavity thus begins to die out and once the radiation level has decreased below the steady-state level, the stimulated emission rate again becomes small. After this point has been reached the pumping process builds the population level N_2 back up toward and

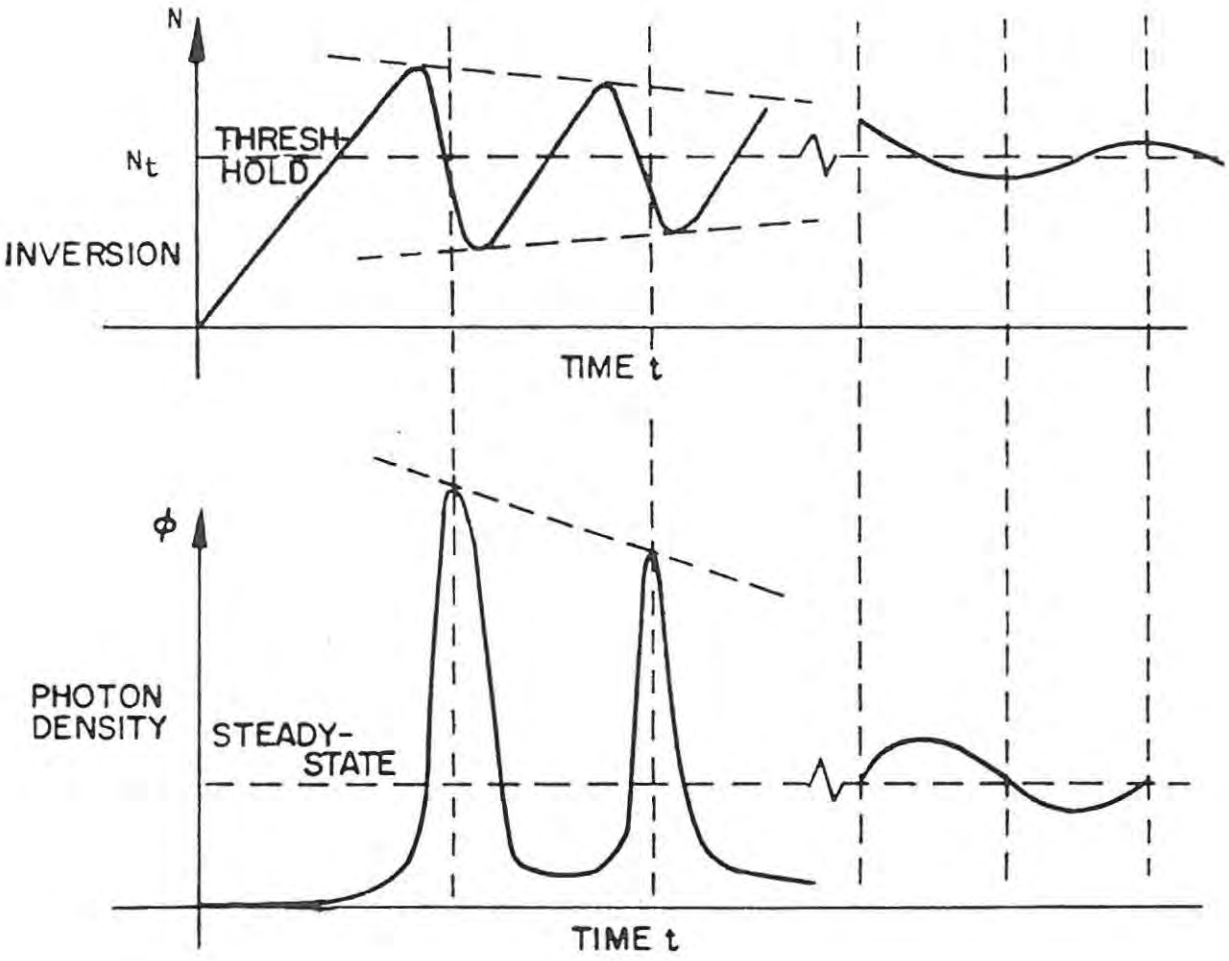

FIG. 2.4 SPIKING BEHAVIOUR IN A SOLID-STATE LASER OSCILLATOR

through the threshold value again. This causes another burst of laser action and the system can repeat in the same or a similar cycle. The time scale over which the spiking occurs is typically the duration of the pump cycle ≈100 μs while individual spikes are typically 0,1 to 1 μs in duration.

For some laser applications, e.g. materials processing, the laser can be operated as described above, the so-called long-pulse mode operation. The energy contained in the train of pulses is spread out over such a long time that powers are low with lasers using this mode of operation. For other laser applications, however, for example, non-linear optics and ranging, it is desirable to have a high peak power and a smooth, single output pulse. This may be achieved by a technique known as Q-switching.

2.3.2 Q-SWITCHING

The name of this technique is derived from the fact that it is based on the alteration of the optical Q of the laser cavity. The quality factor, Q, is defined as the ratio of the energy stored in the cavity to the energy loss per cycle, hence, the higher the quality factor the lower are the losses. The generation of a Q-switched laser pulse can be explained with reference to Fig. 2.5.

By lowering the Q of the cavity, lasing can be prevented even during the pumping process. Energy stored in the laser rod cannot be emitted and the population inversion reaches a level much higher than the threshold for normal lasing action. The lifetime of the upper laser level determines the maximum time for which energy may be stored. The population inversion reaches a maximum value towards the end of the flashlamp pulse as shown in Fig. 2.5(a) and (c). At this point a high Q is quickly restored, i.e. losses are reduced, and the photon flux builds up due to the gain created by the stored energy. The upper level population is depleted very rapidly and a single extremely short pulse of light is emitted, a Q-switched pulse, sometimes also called a giant pulse. The peak power of this pulse is larger than that obtainable from an ordinary long pulse by orders of magnitude.

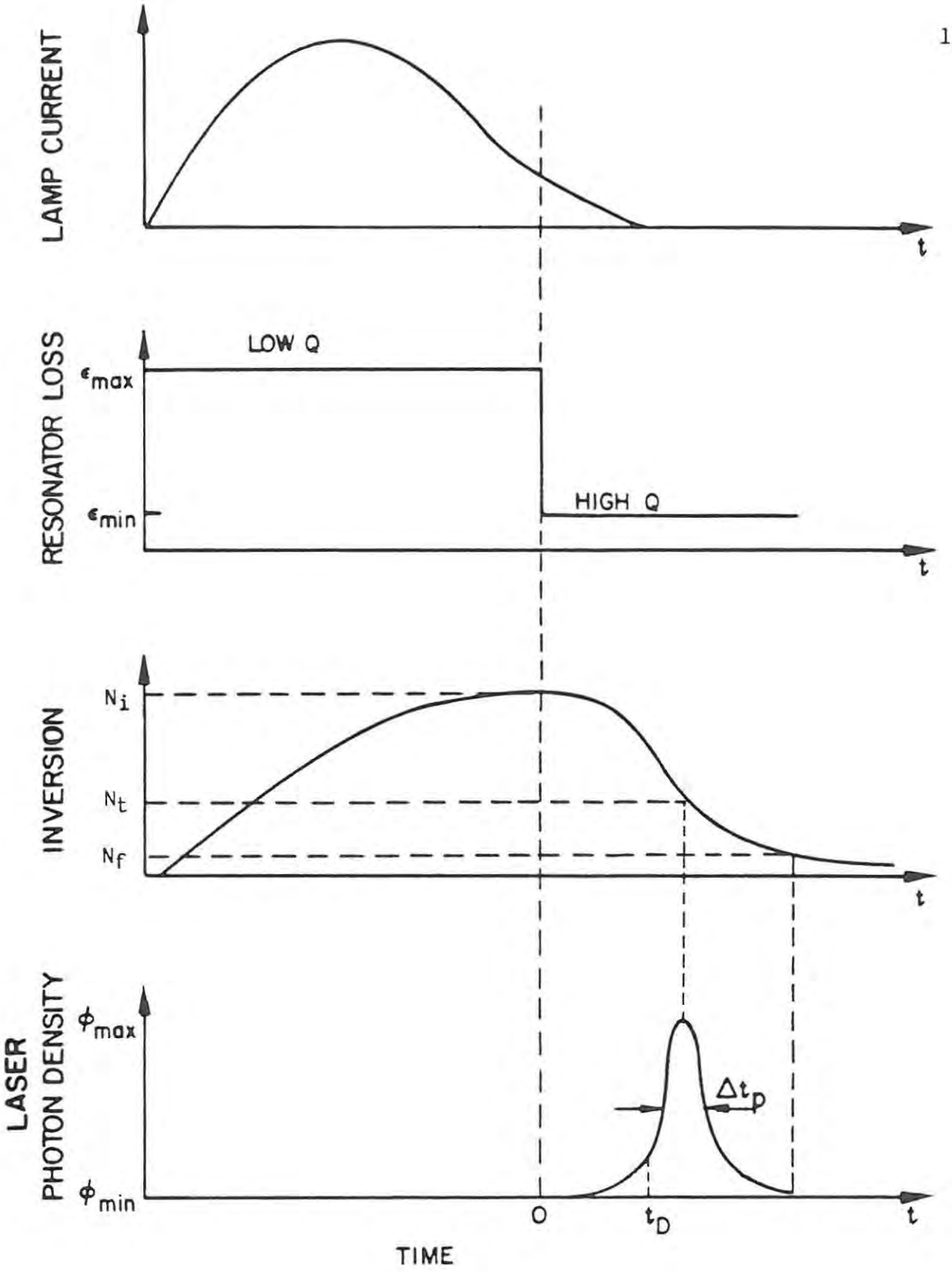

FIG. 2.5. DEVELOPMENT OF A Q-SWITCHED LASER PULSE. SHOWN ARE THE FLASHLAMP CURRENT, RESONATOR LOSS, POPULATION INVERSION AND LASER PHOTON DENSITY AS A FUNCTION OF TIME.

The Q-switched pulse duration is very short and one can neglect the optical pumping and spontaneous emission when writing the rate equations. From (2.11) and (2.12) we then have

$$\frac{\partial \phi}{\partial t} = c\phi\sigma N \frac{\ell}{\ell'} - \frac{\phi}{\tau_c}$$

$$= c\phi\sigma N \frac{\ell}{\ell'} - \frac{\phi\varepsilon}{t_R} \qquad (2.17)$$

and

$$\frac{\partial N}{\partial t} = -N\sigma\phi c \qquad (2.18)$$

The factor $\frac{\ell}{\ell'}$ in (2.17) arises if we distinguish between the length of the active medium ℓ and the length of the resonator ℓ'. τ_c, the decay time constant of the radiation, can also be defined as the average lifetime of photons in the resonator. A photon will have some average lifetime in the cavity before being scattered, emitted or lost in other ways. Relating τ_c to the fractional power loss ε per round trip we get (Koechner (1976))

$$\varepsilon = \frac{t_R}{\tau_c} \qquad (2.19)$$

where $t_R = \frac{2\ell'}{c}$ is the round-trip time of a photon in a resonator of optical length ℓ'. The relation (2.19) was used to express τ_c as a function of ε and t_R in (2.17). Q-switching is accomplished by making ε a function of time (e.g. Pockels cell Q-switches) or a function of photon density (e.g. saturable absorber Q-switching).

Dividing (2.17) by (2.18) to eliminate time as a parameter we get

$$\frac{d\phi}{dN} = -\frac{\ell}{\ell'}\left(1 - \frac{\varepsilon}{2\ell N\sigma}\right)$$

$$= -\frac{\ell}{\ell'}\left(1 - \frac{N_t}{N}\right) \qquad (2.20)$$

where $N_t = \frac{\varepsilon}{2\sigma\ell}$, is the population inversion at threshold obtained from (2.16) (which has been modified to take into account the distinction between active medium length, ℓ, and resonator length ℓ') and (2.19).

It is important to note that (2.16) was obtained from (2.12) which made no distinction between the two lengths. Taking these lengths into account, it can be shown from (2.17) that (2.16) would then become

$$N > \frac{\ell'}{\ell c \sigma \tau_c}$$

From this and (2.19) it can be seen that $N_t = \frac{\varepsilon}{2\sigma\ell}$.

According to (2.17), peak output occurs when $\frac{d\phi}{dt} = 0$ or when $N = \frac{\varepsilon}{2\sigma\ell}$. This is exactly the threshold inversion and so peak power occurs when the inversion has fallen to the threshold value N_t as shown in Fig. 2.5. Equation (2.20) can be integrated to give

$$\phi(t) = \frac{\ell}{\ell'} \{N_t \ln \frac{N(t)}{N_i} + N_i - N(t)\} \qquad (2.21)$$

and with $N(t) = N_t$ we get $\phi(t) = \phi_{max}$.

The inversion remaining in the active material after the Q-switched pulse has been emitted can be found by setting $\phi(t) = 0$ in (2.21) which gives

$$N_f - N_i = N_t \ln \frac{N_f}{N_i} \qquad (2.22)$$

2.3.2.1 ELECTRO-OPTICAL (E-O) Q-SWITCHING

The key element in this form of Q-switching is a very fast electronically controlled element which becomes birefringent under the influence of an external electric field. Such an element is said to exhibit an electro-optic effect. In our case this element is a Pockels cell which consists of a crystal of potassium dideuterium phosphate (KD*P). The Pockels effect is a linear electro-optical effect and was studied extensively by the German physicist Friederich Pockels in 1893.

Birefringence is characterized in a medium by two orthogonal directions, the fast and slow axes, which have differing indices of refraction. A beam polarized linearly at 45 ° to these axes and propagating perpendicular to their plane, splits into two orthogonal components

which travel along the same path but at different velocities. This results in a phase difference between the two components and the resulting combination is either an elliptically, circularly or linearly polarized beam depending on the applied voltage (Born & Wolf (1980)). In our case only one voltage is of interest, the quarter-wave voltage in which linearly polarized light is circularly polarized after passing through the cell, i.e. quarter-wave retardation has taken place.

Before describing the theory of operation in more detail the basic principle of E-O Q-switching can be explained with the aid of Fig. 2.6. The quarter-wave voltage, $V_{1/4}$, is applied to the cell while the flashlamp is pulsed. At this voltage the polarizing effect of the Pockels cell reduces the cavity Q. As the laser begins to emit spontaneously, the linearly polarized radiation passing through the cell becomes circularly polarized. After reflection from mirror M1, the radiation again passes through the cell and undergoes another $\lambda/4$ retardation and becomes linearly polarized at 90 ^{o} to the original linear polarization. The radiation is deflected out of the cavity by the polarizer and so prevents feedback. Near the end of the flashlamp pulse when the stored energy in the laser rod is a maximum, the voltage is switched to zero resulting in no retardation and allowing lasing to take place which results in the emission of a high power, Q-switched laser pulse.

Pockels cell Q-switches may have the electric field applied either parallel or perpendicular to the direction of the optical beam. In the former type, longitudinal field Q-switches, the crystals are uniaxial in the absence of an electric field. The dependence of refractive index on the electric field can be described by the change in orientation and dimensions of the index ellipsoid (Koechner (1976), Wahlstrom (1960)). Figure 2.7(a) shows a block of suitable uniaxial material and the orientation of the index ellipsoid relative to the crystallographic axes. The index ellipsoid is an ellipse of revolution about the optic axis (Z). Figure 2.7(b) shows that the index ellipsoid projects as a circle on a plane perpendicular to the optic axis indicating no birefringence in the optical axis direction. Application of an electric field parallel to the optical axis results in a change in shape but not

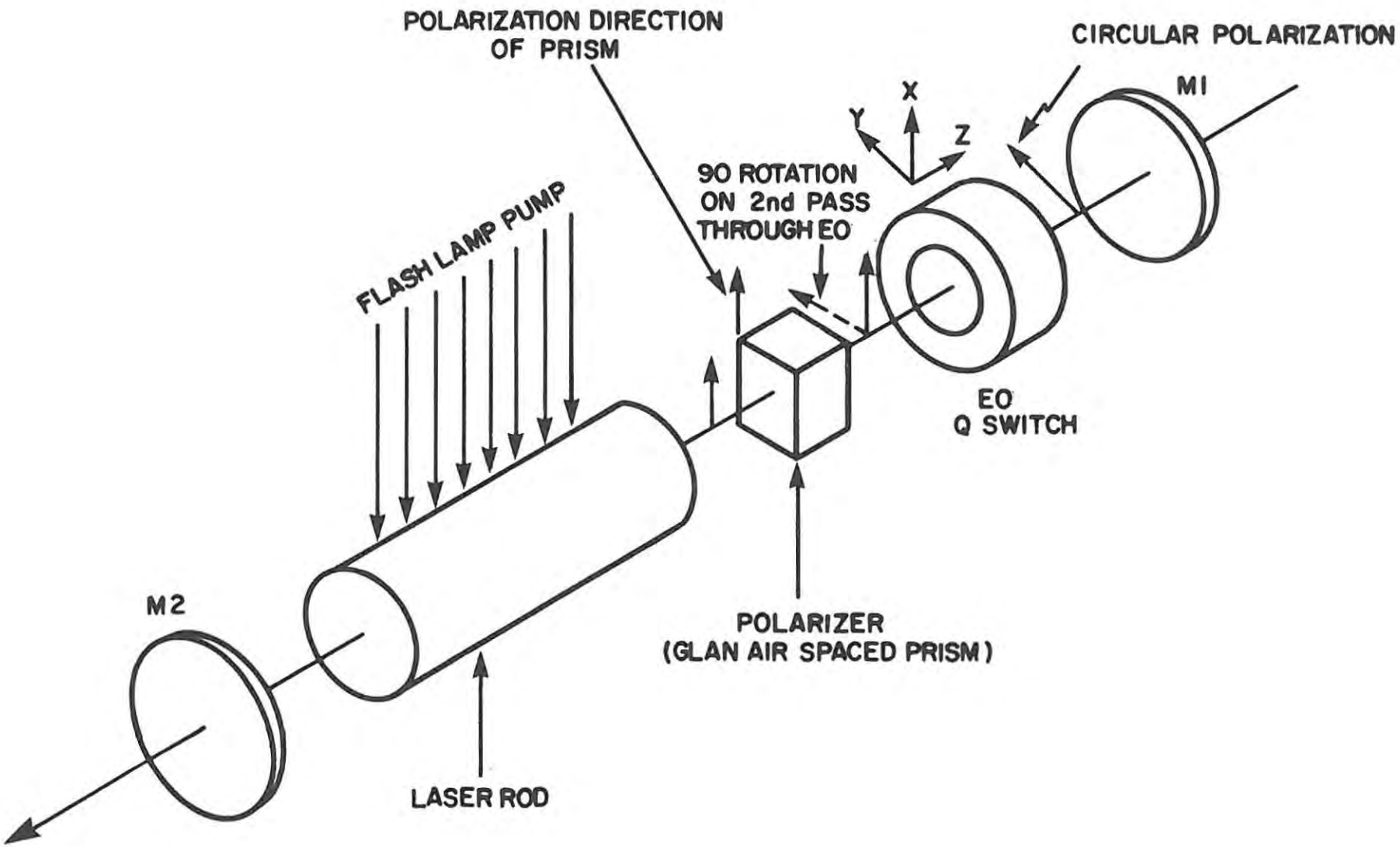

FIG. 2.6 ELEMENT ORIENTATION FOR E-O Q-SWITCHING.

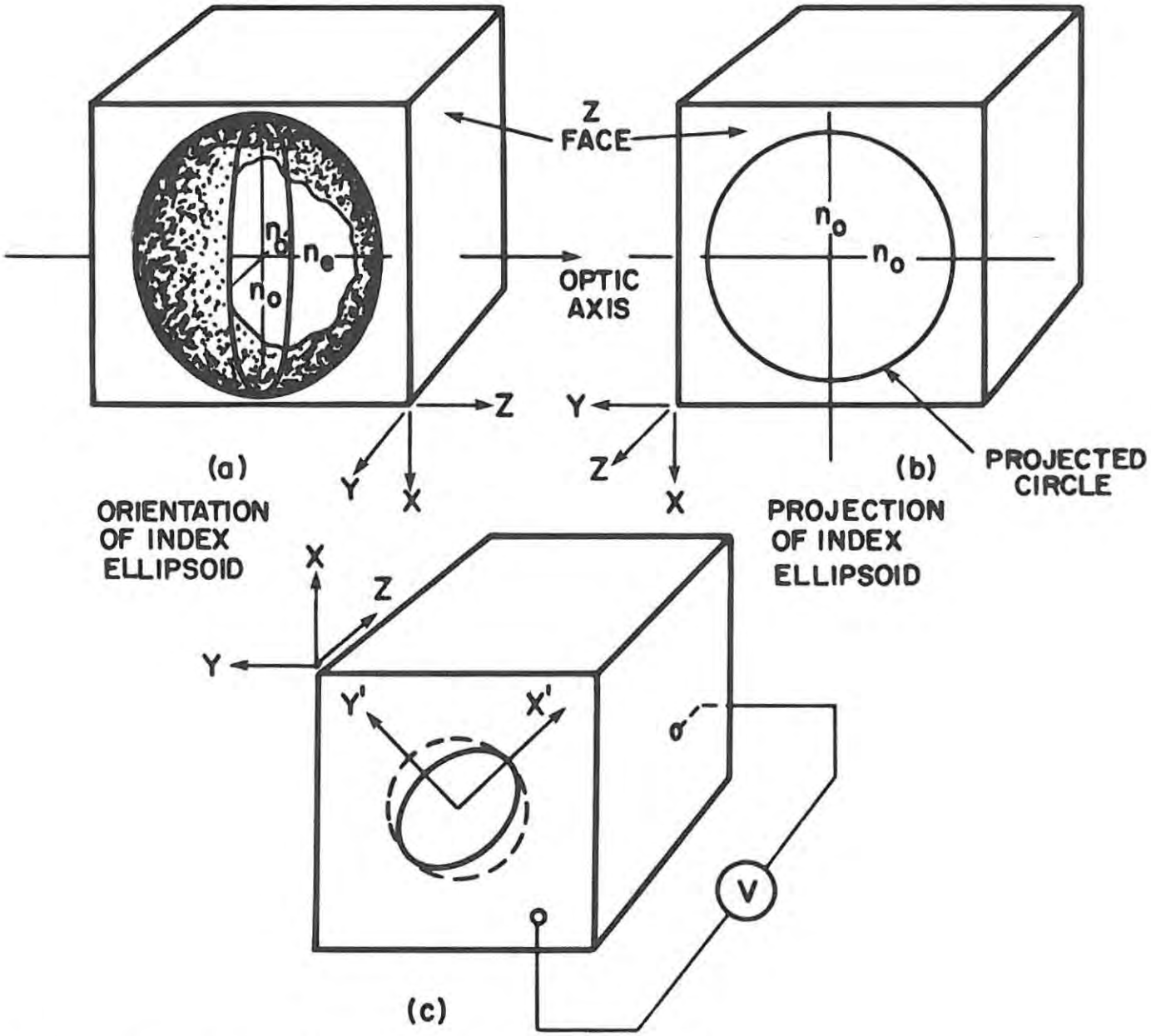

FIG. 2.7 THE INDEX ELLIPSOID IN A Q-SWITCHING CRYSTAL

orientation of the index ellipsoid as shown in Fig. 2.7(c). This results in a change in the projection of the ellipsoid from a circle at no voltage, to an ellipse with axes (X',Y') at 45 ° to the crystallographic axes (X,Y). The length of the ellipse axes are proportional to the reciprocals of the indices of refraction in the axes directions. The crystal is now linearly birefringent for light propagating in the direction of the optical axis.

If a voltage V_z is applied across a crystal of length ℓ, then $V_z = E_z\ell$ where E_z is the applied electric field, and the phase difference between the ordinary and extraordinary rays is given by

$$\delta = \frac{2\pi}{\lambda} n_o^3 r_{63} V_z \qquad (2.23)$$

where n_o is the refractive index for the ordinary ray

r_{63} is the relevant electro-optic coefficient for light propagating in the z direction and

λ is the wavelength.

For KD*P, $n_o \approx 1{,}52$; $r_{63} \approx 26{,}4 \times 10^{-12}$ m/V and $V_{1/4} \approx 3$ kV for $\lambda = 1{,}06$ μm. It can be seen that for a given wavelength of light, the retardation is independent of the crystal dimensions and is directly proportional to the applied voltage.

If linearly polarized light is propagated through the crystal with polarization parallel to the X or Y axis as shown in Fig. 2.7(c), the components of this vector parallel to the induced axes X' and Y' undergo a relative phase shift δ given by eqn. (2.23). In general, the phase shift produces elliptically polarized light. If the light then passes through a polarizer, the resulting intensity will be a function of the ellipticity and therefore of the applied voltage. Born & Wolf (1980) show that with the analyser at right angles to the input polarization, the voltage and transmitted light intensity are related by

$$I = I_o \sin^2 \frac{\delta}{2} \qquad (2.24)$$

where I_o is the input light intensity.

We are specifically interested in the $\lambda/4$ voltage ($V_{1/4}$) which produces a phase shift of $\pi/2$. From (2.23) we find

$$V_{1/4} = \frac{\lambda}{4n_o^3 r_{63}} \tag{2.25}$$

So using (2.23), (2.24) and (2.25), the Pockels cell transmission will change with voltage according to:

$$T = \frac{I}{I_o} = \sin^2 \left(\frac{\pi}{4} \frac{V}{V_{1/4}}\right) \tag{2.26}$$

Further details of the Pockels cell used are given in Section 4.2.4.

2.3.2.2 SATURABLE ABSORBER Q-SWITCHING

The saturable absorber or dye Q-switch is a very simple device. It consists of a thin absorption cell, filled with appropriate dye, placed in the laser cavity usually between the rod and the rear mirror as shown in Fig. 2.8. In the liquid dye the absorption coefficient decreases with increasing light intensity. Initially the dye absorbs the emission from the rod so that the rear mirror is optically isolated from the rest of the cavity. As the light becomes more intense the transparency increases and the dye "bleaches" resulting in the laser radiation reaching the rear mirror enabling lasing to occur. The decrease of the absorption coefficient for a saturable absorber is related to the incident light intensity, I, by (Koechner (1976))

$$\gamma = \frac{\gamma_o}{1 + I/I_s} \tag{2.27}$$

where γ_o is the absorption coefficient at zero intensity

I_s is the saturation intensity, at which γ decreases by a half.

A number of disadvantages are associated with dye Q-switches. There is a large jitter between the flashlamp triggering and the emission of the laser pulse typically of the order of 10 to 100 μs. The dye degrades quickly due to the UV emitted by the flashlamp. Absorption in the cell

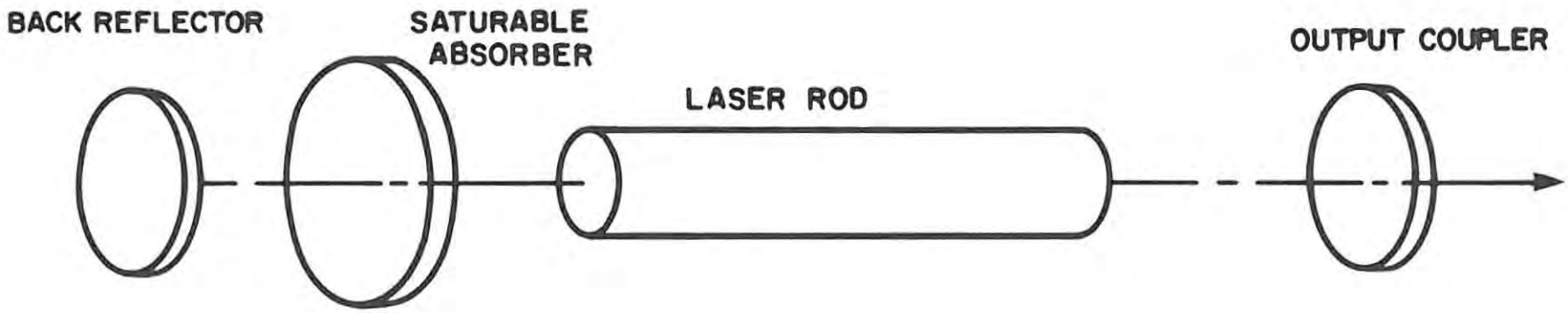

FIG. 2.8 LASER WITH SATURABLE ABSORBER Q-SWITCH.

due to incomplete bleaching results in lowered energy output.

Advantages of dye Q-switches include economy and simplicity of operation. A variation of the dye Q-switch is one which is made from transparent plastic impregnated with dye solution.

2.4 THERMAL LENSING IN THE LASER ROD

Thermal effects in laser rods arise due to a combination of heat generated because of absorption of pump radiation and the cooling processes on the surface of the rod. This results in a radial thermal gradient in the rod, which leads to a distortion of the laser beam due to induced temperature and stress-dependent variation of the refractive index. The distortions which occur in the rod due to the nonuniform temperature distribution are thermal lensing and thermally induced birefringence because of the photoelastic effect of thermal strains. Foster & Osterink (1970) have developed a theoretical model for the thermal effects in a continuously pumped Nd:YAG rod. In our case we are mainly concerned with the thermal lensing effect of the laser rod (it acts as a thick positive lens) and the resulting effect on the laser resonator (see Section 3.4.2).

The refractive index variation in the laser rod due to the above effects varies quadratically with radius (Koechner (1976)) and so results in an equivalent spherical lens effect. Koechner (1970) has shown that the focal length of the laser rod due to thermal effects is given by the relation

$$f = \frac{2K\pi r_o^2}{P_{in}\eta} \left[\frac{\partial n}{\partial T} - \frac{n_o^3 \alpha C_x'}{48(1-\nu)} + \frac{2(n_o-1)\alpha \ell_o}{L} \right]^{-1} \qquad (2.28)$$

where $\frac{\partial n}{\partial T} = 7{,}3 \times 10^{-6} K^{-1}$ is the refractive index change with temperature

K is the thermal conductivity of YAG at 300 K (= 0,11 W/cmK)

T is the temperature in Kelvin

r_o is the rod radius = 3,175 mm

P_{in} is the electrical input power

η is the fraction of heat dissipated by the crystal to electri-

cal input power, i.e. $\eta = P_a/P_{in} = 0{,}05$ (P_a is the heat dissipated by the crystal)

n, n_o = 1,818 is the refractive index of Nd:YAG at 1,06 μm, 300 K

α = $7{,}9 \times 10^{-6} K^{-1}$ is the thermal expansion of Nd:YAG at 300 K

C_x' = -1,311 is a parameter related to the thermally induced, radial photoelastic effects

ν = 0,3 is the Poisson ratio

$\ell_o \approx r$, is the length of the end section of the rod over which thermal expansion occurs

L = 80 mm is the rod length.

The first term in the bracket of (2.28) represents the change of the refractive index with temperature. The second term represents the stress dependent change of refractive index. The last term gives the distortion caused by the end face curvature of the rod. Substitution of the known constants into (2.28) shows that the temperature dependent change of the refractive index represents approximately 75 % of the total contribution to thermal lensing.

In fact, (2.28) actually predicts to two focal lengths (Koechner (1970)) since the parameter C_x' can be replaced by C_y' which is related to the tangential photoelastic effects. This essentially means that the second term in (2.28) takes on two different values, one for the radial and one for the tangential component of the polarized light. Here, the radial component is along a radius of the laser rod with the tangential component being perpendicular to it. Under thermal stress the indicatrix, which specifies the refractive index of the crystal, changes its shape, size and orientation (Born & Wolf (1980)). From a sphere under no stress in YAG it becomes an ellipsoid with the radial and tangential components forming the two axes (Koechner (1970)). This unequal change of the refractive index for light polarized in the two directions results in two focal lengths being obtained. A difference in focal length between different polarizations means that a resonator designed to compensate for laser rod lensing for light of radial polarization will not compensate for the lensing of tangentially polarized light. With the above values and with C_y' = 0,1682 (Koechner (1970)), Robertson & Preussler (1982) of this laboratory have found

$$f_{radial} = \frac{1,73}{P_{in}} \tag{2.29}$$

and $$f_{tan} = \frac{2,18}{P_{in}} \tag{2.30}$$

where f is in metres and P_{in} is in kilowatts.

These two equations imply quite a bad astigmatism for light polarized in the radial and tangential directions. However, for the input powers which we were concerned with, approximately 300 W, the focal lengths given by the equations are relatively long, 5,8 and 7,3 metres respectively. The change in length of the resonator to compensate for the two focal lengths is only approximately 5 mm (see Fig. 5.22) which according to Table 5-2 does not significantly affect the far-field beam divergence. For this reason, and due to the experimental difficulty in measuring the two focal lengths accurately, only one focal length was measured.

Robertson & Preussler (1982) have experimentally measured the focal length of the laser rod used in our setup and found it to be given by

$$f = \left(\frac{2,1}{P_{in}} + 0,5 \right) \text{ m} \tag{2.31}$$

The measured focal lengths show good agreement with Herbst et al (1977) but are longer than those reported by Hotz (1973) and Andreou (1978), for the same input powers. Herbst et al (1977) and Andreou (1978) also only measure one rod focal length for their unstable resonator laser rods and make no comment regarding astigmatism.

In stable laser resonators the thermal lensing effect of the rod is not particularly important. However, in unstable resonators the effects of thermal lensing are most marked and should therefore be compensated for. The spherical lens effect can be compensated for by grinding concave spherical surfaces on the ends of the laser rod, introducing a negative lens into the resonator or by suitably designing the resonator. The latter approach was the one used in this study and is discussed in more detail in the next chapter.

CHAPTER 3

UNSTABLE RESONATOR THEORY

3.1 INTRODUCTION

The initial paper on unstable resonators was published by Siegman (1965). There it was stated that "there are ... good reasons for believing that ... unstable resonators will be of practical utility in laser applications." In a later paper Siegman & Arrathoon (1967) stated three reasons why unstable resonators were attractive for laser applications:

(1) they can have large mode volumes even in very short resonators
(2) the unstable configuration is readily adapted to adjustable diffraction output coupling
(3) they should have very substantial discrimination against higher order transverse modes.

The publications and review articles of Siegman (1965, 1971, 1974) and Siegman & Arrathoon (1967) form the cornerstone of this area of laser theory. Unstable resonators have been used in many high energy lasers and are especially suited for lasers with high gain media. This is because a high gain requires only a few passes thus limiting "walk-off" problems. In the past this has restricted the use of unstable resonators to gas lasers like CO_2, HF, KrF, etc.

To be effective as an unstable resonator the laser medium must be of high optical quality. This requirement has also limited applications of unstable resonators to gaseous media because the time-and power-dependent thermal distortions occurring in solid state lasers make this type of resonator unattractive (Koechner (1976)). However, contrary to this statement, Byer & Herbst (1978) state that a properly designed Nd:YAG unstable resonator could provide marked improvements in performance, reliability and cost over conventional stable resonators.

A few Nd:YAG unstable resonator lasers have been described in the literature and will be referred to in due course. In fact, Nd:YAG laser systems incorporating unstable resonator configurations are now also available commercially.

The remainder of this chapter will deal with a discussion of unstable resonator properties, the design of the laser used in this study and some results of the optimization of the design.

3.2 THE STABILITY OF LASER RESONATORS

Laser resonators are classified as being either stable or unstable according to the stability condition defined in (3.1)

$$0 < g_1 g_2 < 1 \qquad (3.1)$$

or $$0 < (1 - \frac{L}{R_1})(1 - \frac{L}{R_2}) < 1$$

where $g_i = 1 - \frac{L}{R_i}$ are the so-called g-parameters of the empty resonator

L is the separation of the mirrors

R_i is the radius of curvature of the mirror i and is by convention positive if the mirror is concave inward toward the resonator, otherwise negative

As long as condition (3.1) is satisfied by the resonator it is termed a stable resonator. If, on the other hand

$$g_1 g_2 < 0 \quad \text{or} \quad g_1 g_2 > 1$$

the resonator is classified as unstable. In cases where the $g_1 g_2$ product equals zero or one, the laser is on the boundary between stability and instability and is termed marginally stable. The stability condition (3.1) can be represented graphically by the stability diagram shown in Fig. 3.1. Any optical resonator can then be represented by a point on the diagram and only resonators whose point falls within the shaded region of the diagram are stable.

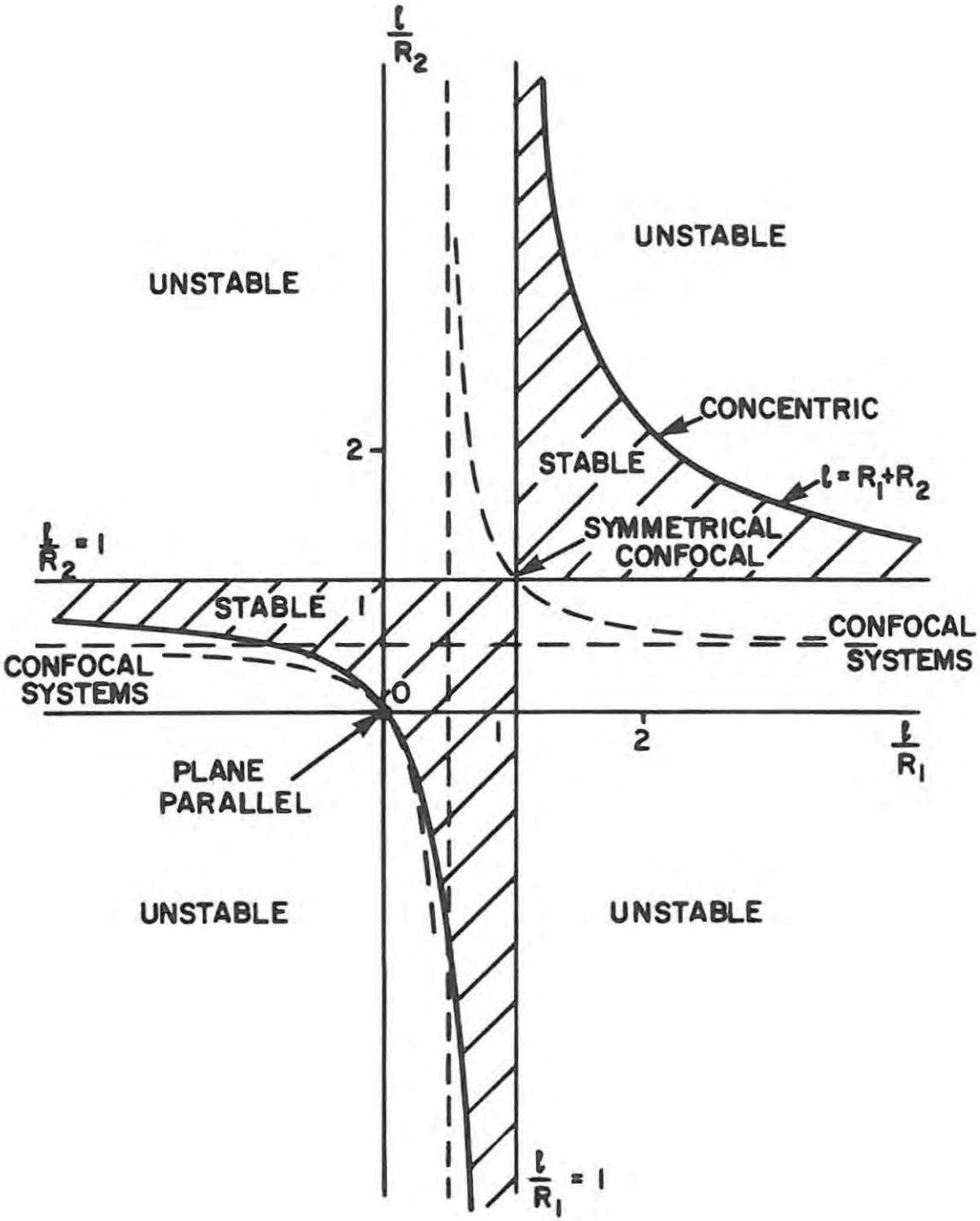

FIG. 3.1 RESONATOR STABILITY DIAGRAM

In a stable resonator, if a narrow ray of light is injected into the resonator at a small angle and initial displacement relative to the resonator axis, it will oscillate between the mirrors but will always stay trapped within a finite distance about the axis. Stable resonators thus correspond to stable periodic focussing systems and are low-loss devices. In contrast, a bouncing ray of light in an unstable resonator expands on repeated bounces to fill the entire cross section of at least one of the laser mirrors however large it may be. The laser output is taken as a diffraction coupled beam passing around rather than through (stable case) the output mirror. Unstable resonators thus correspond to divergent periodic focussing systems and are consequently high-loss devices. The above concepts are shown graphically in Fig. 3.2.

The most useful form of unstable resonator is the confocal unstable resonator introduced by Ananév et al (1970) and by Krupke & Sooy (1969). Its advantage is that it automatically produces a collimated output beam. Confocal configurations can be divided into positive and negative branches as shown in Fig. 3.3. In practice the positive branch is usually employed because of possible optical breakdown at the internal focal point in the negative branch case.

3.3 DISCUSSION OF THE TRANSVERSE MODES IN LASER RESONATORS

A comprehensive review of the theory of modes in stable optical resonators is given by Kogelnik & Li (1966) but here only the main points will be given.

When two curved mirrors of appropriate curvature and spacing are set up facing each other, the lowest order resonant mode of the resonator is a Gaussian light beam of appropriate curvature and spot size trapped between the mirrors. This can be demonstrated by approaching the problem from the other direction, by starting with a Gaussian light beam and fitting resonator mirrors to it (Siegman (1971a)). This beam is called the fundamental or TEM_{00} mode and it obeys certain propagation laws which can be found in, for example, Kogelnik & Li (1966).

STABLE

UNSTABLE

FIG. 3.2 STABLE AND UNSTABLE RESONATOR CONFIGURATIONS

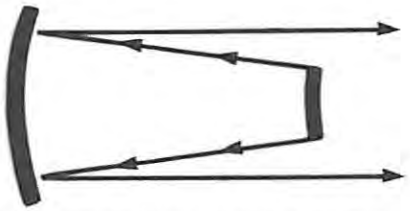

POSITIVE BRANCH

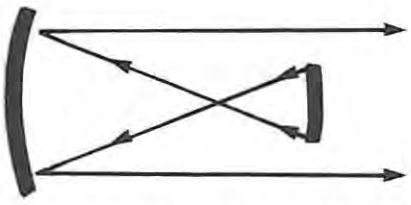

NEGATIVE BRANCH

FIG. 3.3 POSITIVE- AND NEGATIVE-BRANCH UNSTABLE RESONATORS

Gaussian stable resonator modes are generally slender and threadlike and are much smaller than the bore diameters of most high-power lasers. This is how the stable resonator was depicted in Fig. 3.2. A stable mode volume filling the gain medium would essentially require flat mirrors which introduce further problems with respect to the optical homogeneity of the medium. These limitations are avoided in unstable resonators.

There are other resonant modes which can also exist in the resonator. All the modes together form a complete and orthogonal set of functions known as the propagation modes. The higher-order modes are expressed in terms of Hermite or Laguerre polynomials depending on whether rectangular or cylindrical coordinates are being used. The exact form of these modes is beyond the scope of this work, but what is important is that the modes in stable resonators are well-known and the lowest-order mode is Gaussian in form.

In a stable resonator both the phase front radius of curvature and mode radius are repeated after one round trip, whereas in the unstable resonator only the phase front radius of curvature is repeated.

The spot size on the mirrors in a stable resonator is always finite. As the resonator parameters are moved to the unstable regions, the spot sizes begin to equal and eventually exceed the mirror sizes. Radiation then spills over the mirrors and the losses become very high. The Gaussian beam approach to optical resonators then ceases to be valid and more complex analyses must be used.

A useful but not entirely detailed picture of the mode properties of an unstable resonator can be obtained from a purely geometrical or spherical-wave approach (Siegman (1965), Kahn (1966)). The discussion refers to Fig. 3.4. We assume a spherical wave of uniform intensity is travelling to the right, say, inside the resonator. This wave originates from a point (virtual centre) P_1 behind mirror M_1, which is not, in general, the centre of curvature of M_1. The wave then reflects from M_2 and creates a spherical wave as if it came from a point P_2 behind M_2. For self-consistency this new wave must then reflect from M_1 again

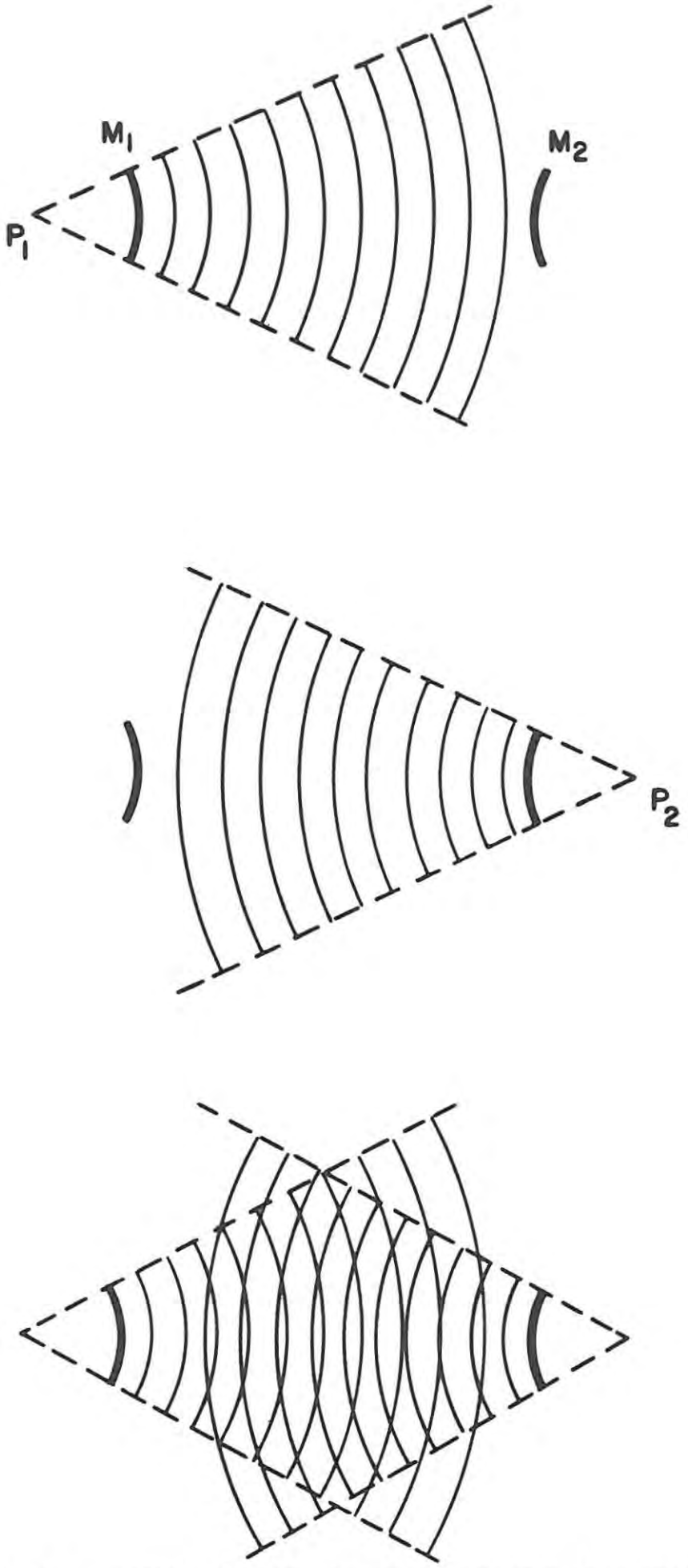

FIG. 3.4 SPHERICAL-WAVE PICTURE OF THE MODE IN AN UNSTABLE RESONATOR

in such a way as to create the initial spherical wave. If one applies the lens formulas connecting virtual centres and focal properties of mirrors, one finds that only one unique pair of points P_1 and P_2 exists which makes the spherical waves self-consistent (Siegman (1965). These two self-consistent uniform, spherical waves form the geometrical picture of the lowest order mode in an unstable resonator. It is possible that the virtual centres described above may become a real centre or focal points inside the resonator.

Directly from this geometrical picture arises an important resonator parameter, the round-trip magnification M as illustrated in Fig. 3.5. The loss in an unstable resonator arises from the fact that the magnified wave couples past one of the resonator mirrors. The geometrical coupling ratio is independent of the mirror sizes and depends only on the linear magnification M. It can be seen from this simple analysis that the two oppositely travelling waves in an unstable resonator have different transverse sizes and different phase front radii of curvature at any point in the resonator. This is in contrast to the stable modes where the two waves, (coming from opposite mirrors), are identical at every point in the cavity.

The simple geometrical description of unstable resonator modes described above gives a useful though limited zeroth-order approximation to the modes. The uniform intensity distribution given above clearly does not account for diffraction effects in the waves; a more accurate description of the modes requires analysis that includes the effects of diffraction.

The modes of the empty unstable resonator with diffraction included are found by solving an integral equation derived from Kirchoff's equation of the form (Siegman (1974))

$$\gamma_n U_n(x,y) = \iint K(x,y;\, x',y')\, U_n(x',y')\, dx'dy' \qquad (3.2)$$

where the Huygen's kernel $K(x,y;x',y')$ accounts for the wave propagation through one round trip in the resonator and γ_n is the complex eigenvalue corresponding to the eigenfunction $U_n(x,y)$.

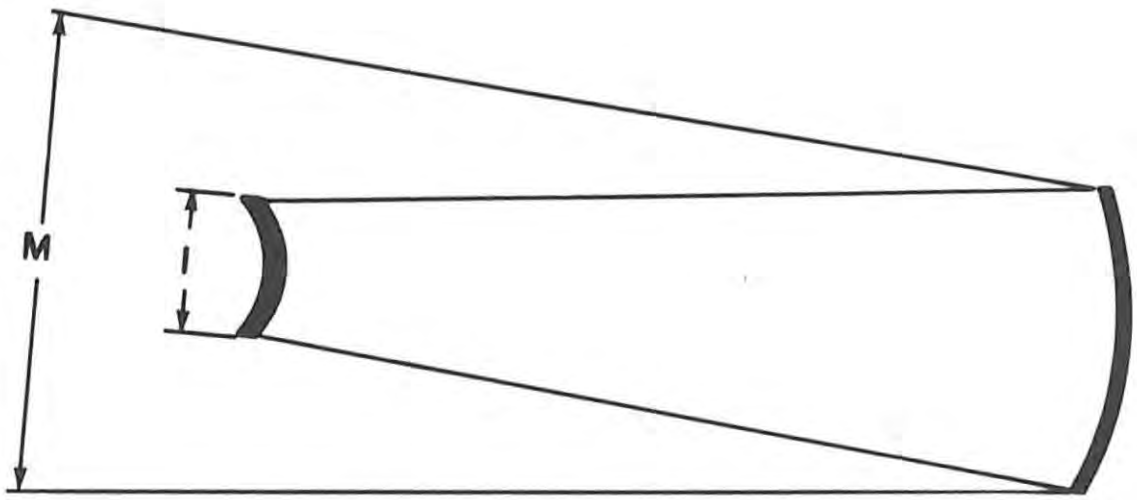

$$\frac{\text{LOSS}}{\text{BOUNCE}} = 1 - \left(\frac{1}{M}\right)^2$$

FIG. 3.5 THE MAGNIFICATION, M, WHICH CHARACTERIZES THE GEOMETRICAL PROPERTIES OF AN UNSTABLE RESONATOR

Analytical solutions to this equation are not known and extensive computer calculations are needed using the techniques developed by Fox & Li (1961). Their technique essentially involves arbitrarily choosing an initial amplitude function $U_0(x,y)$ and applying the integral transformation (3.2) to compute the new amplitude $U_1(x,y)$ after one bounce. This new function $U_1(x,y)$ is then used as input to (3.2) to compute another function $U_2(x,y)$, and so on. Repeated iterations of the process continues until the amplitude converges to a function $U_n(x,y)$ which remains constant in shape on further transformations, i.e.

$$U_{n+1}(x,y) = \iint K(x,y;x',y')\, U_n(x',y')\, dx'dy' = \gamma_n U_n(x,y) \qquad (3.2a)$$

This function $U_n(x,y)$ must then be one of the normal modes of the resonator. The method will always converge to the lowest-loss mode of the system which, in most cases, is the mode of most interest for lasers. Three hundred bounces are typically required to obtain steady-state results.

Other computational techniques have been used to solve the problem of modes in unstable resonators (Chen & Felson (1973), Rensch & Chester (1973), Horwitz (1976)). Siegman & Miller (1970) used the Prony technique which gives the losses and mode patterns for higher-order unstable resonator modes as well.

In general, the above analyses show that the lowest order mode patterns have considerable amplitude ripple superimposed on the uniform geometrical solution, and a phase front which closely follows the geometrical solution. Some typical results are shown in Fig. 3.6 and 3.7 (Rensch & Chester (1973)). The upper two parts of the figures show the near-field intensity and phase at the output mirror, the vertical lines marking the edges of the output mirror. The third part shows the far-field intensity as a function of far-field angle.

A very important parameter in the study of the modes in unstable resonators is the equivalent Fresnel number, N_{eq}, which is proportional to the square of the resonator's output coupler diameter (see Section 3.4.1). A remarkable feature of the mode behaviour is that at

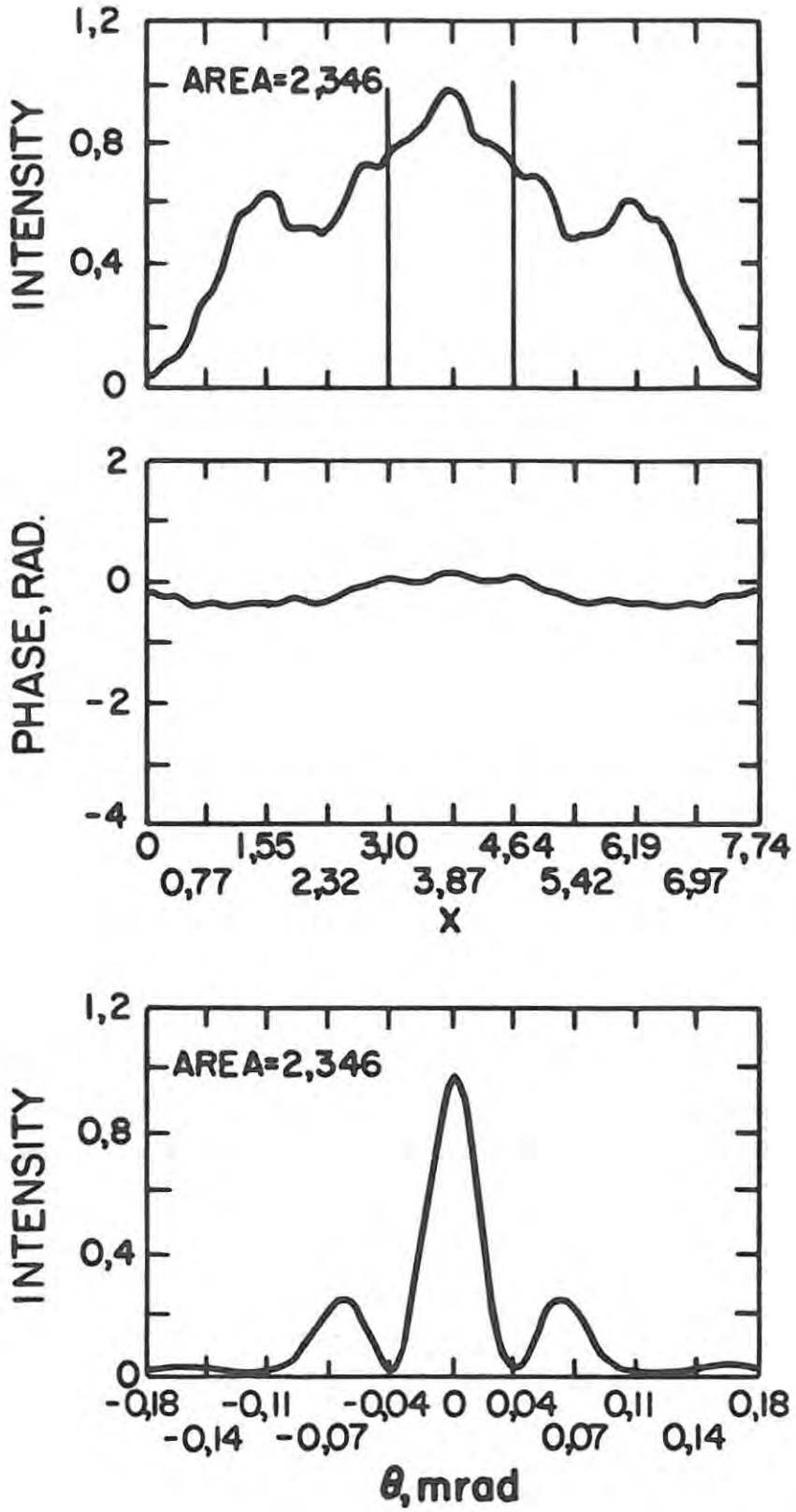

FIG. 3.6 NORMALIZED NEAR- AND FAR-FIELD INTENSITY DISTRIBUTIONS FOR N_{eq} = 0,4 AND M = 5 (RENSCH & CHESTER (1973)). SEE TEXT FOR AXES DESCRIPTIONS.

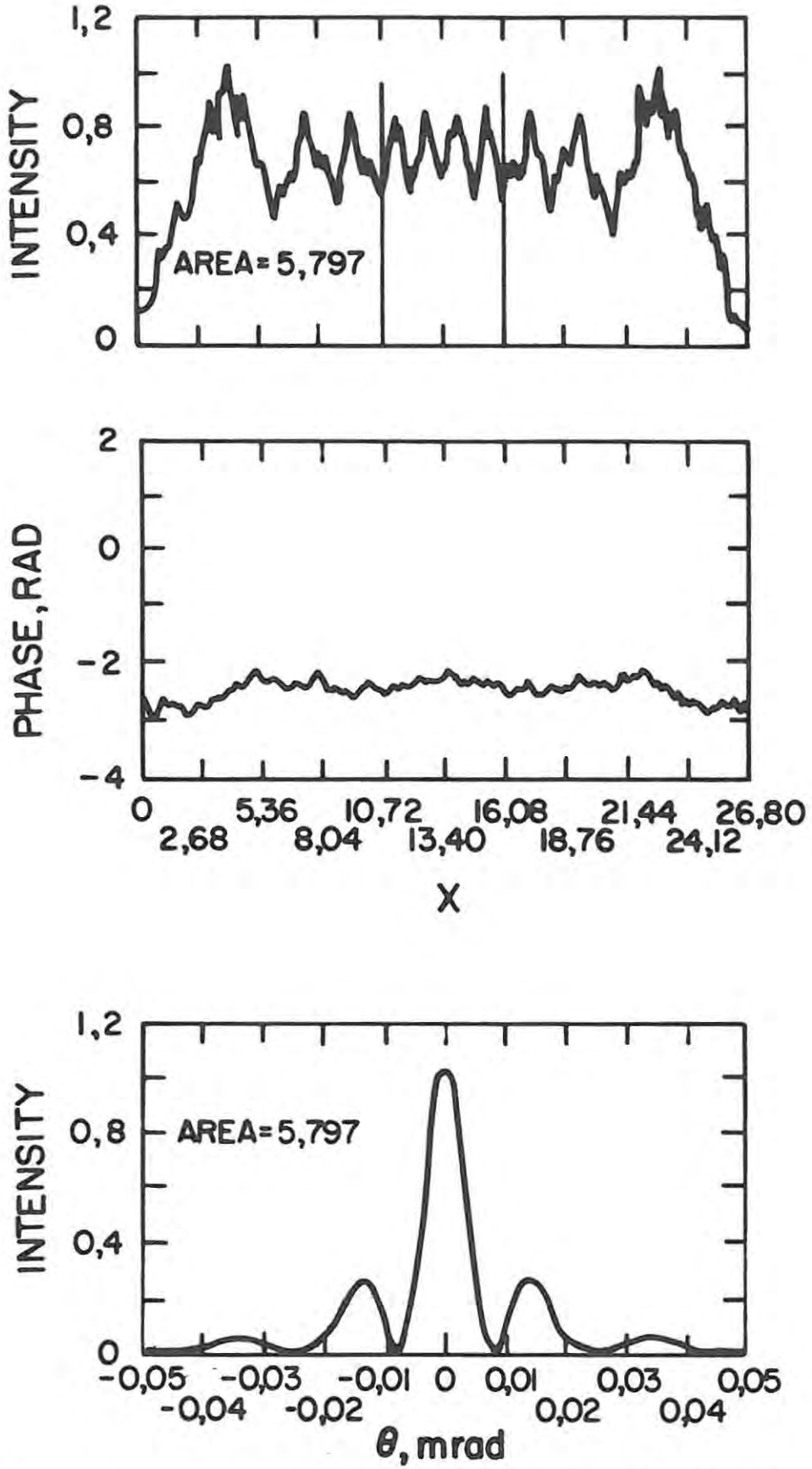

FIG. 3.7 NORMALIZED NEAR- AND FAR-FIELD INTENSITY DISTRIBUTIONS FOR $N_{eq} = 4,8$; M = 5 (RENSCH & CHESTER (1973)). SEE TEXT FOR AXES DESCRIPTIONS.

each half-integer value $N_{eq} = \frac{m}{2}$ (m = 1,3,5,...) a different, distinct mode, i.e. one with a different spatial pattern, becomes the lowest-order resonator mode (Siegman & Miller (1970)). What this means is that good transverse mode discrimination will be obtained in an unstable resonator which is designed to operate at one of the dominant mode peaks which occur at every half-integer value of N_{eq}. This is indicated in Fig. 3.8 where the numbers (1), (2) refer to the axially symmetric modes of the resonator. Excellent transverse mode discrimination will be obtained in particular if one operates with $N_{eq} = 0,5$.

The Soviet workers, Ananév & Sherstobitov (1971), have given a basic physical interpretation of the equivalent Fresnel number. Figure 3.9 illustrates this for a symmetric unstable resonator. The distance between the outer edge of the output coupler and the nearest point on the outgoing geometrical wave when that wave just touches the centre of the mirror is just equal to N_{eq} half wavelengths. The outer edge of the output coupler may be regarded as a discrete scattering point. Light rays incident on this edge will be scattered in all directions. Only the ray directed back into the resonator exactly along the ray direction of the outgoing spherical wave should be important in determining the mode properties since it is trapped along the resonator axis whereas other rays are deflected out of the cavity after a few reflections. In Fig. 3.9 the solid lines represent the geometrical rays of the mode incident on the mirror edge, and the dashed lines represent rays of the resulting edge wave. The edge wave can, therefore, be considered the feedback mechanism for the unstable resonator.

3.4 DESIGN PHILOSOPHY OF THE UNSTABLE RESONATOR

The design of an unstable resonator cavity is a more complicated procedure than for a stable resonator because of the interdependence of cavity length, output coupling and mirror radii of curvature. The desire to have a collimated output beam, and to avoid problems with breakdown at an internal focal point resulted in the choice of a confocal positive branch unstable resonator. The fact that we had to stick to standard available mirror radii of curvature further complicated the design.

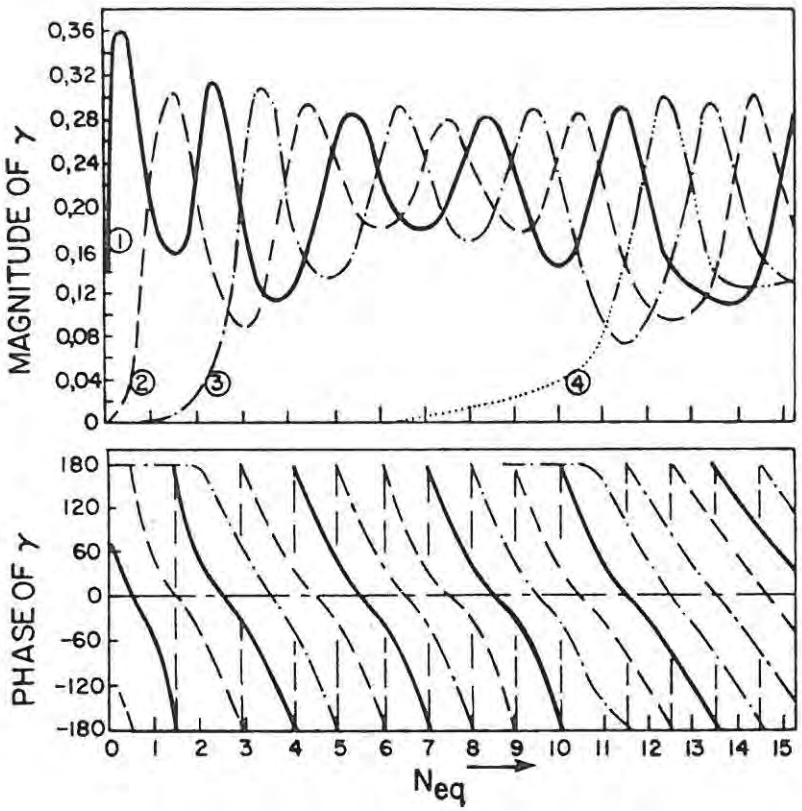

FIG. 3.8 MAGNITUDE & PHASE OF EIGENVALUES OF THE AXIALLY SYMMETRIC MODES OF A CIRCULAR MIRROR SYMMETRIC UNSTABLE RESONATOR WITH M = 5 AS A FUNCTION OF N_{eq} (FROM SIEGMAN & MILLER (1970)).

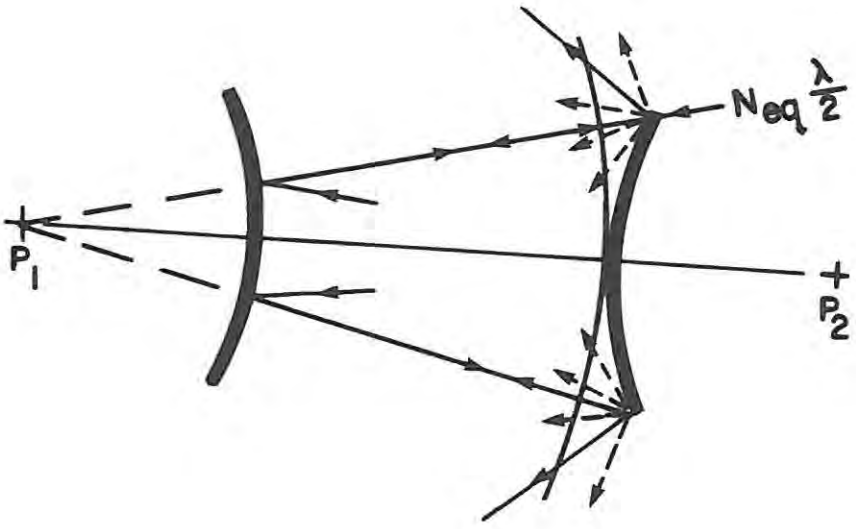

FIG. 3.9 SYMMETRIC UNSTABLE RESONATOR SHOWING THE EDGE-DIFFRACTED WAVES (DASHED LINES) AND THE PHYSICAL SIGNIFICANCE OF N_{eq}. (FROM STEIER (1979)).

The basic design philosophy was as follows. The resonator was designed according to the equations given in Section 3.4.1. These equations essentially describe a design for a resonator which is empty, as they take no account of refractive index variations. Having designed the empty resonator according to these equations and the available radii of curvature, the thermal lensing of the laser rod and the refractive indices of the laser rod and Pockels cell were introduced and the component separations optimized by means of computer calculations to obtain the confocal condition. The design procedure and component optimization are given in the next section.

3.4.1 BASIC DESIGN PROCEDURE AND EQUATIONS

The basic equations for a confocal, positive branch unstable resonator are given here and can be found in numerous publications (Siegman (1971), Andreou (1978), Herbst et al (1977)).

The resonator magnification, M, is the ratio of the output beam diameter, D, to the output coupler diameter, d, i.e.

$$M = \frac{D}{d} \tag{3.3}$$

The output beam diameter is, in turn, fixed by the diameter of the laser rod which in our case was 6,35 mm (1/4 inch). The geometrical output coupling is related to the magnification, M, by

$$\delta_g = 1 - \frac{1}{M^2} \tag{3.4}$$

The equivalent Fresnel number, N_{eq}, discussed in Section 3.3 is given by the relation

$$N_{eq} = \left(\frac{M-1}{2M^2}\right) \frac{D^2}{4\lambda L} \tag{3.5}$$

where L is the cavity length

λ is the laser wavelength

As mentioned in Section 3.3 N_{eq} takes the values 0,5; 1,5; 2,5; ...

For a confocal resonator the mirror radii of curvature are given by

$$R_1 = \frac{-2L}{M-1} \quad \text{(output coupler)} \tag{3.6}$$

$$R_2 = \frac{2ML}{M-1} \quad \text{(back reflector)} \tag{3.7}$$

It should be noted that the output coupler has a negative curvature and is thus convex (see convention with eqn. (3.1)) while the back reflector is concave.

By using M from equation (3.6) in equation (3.5) the length of the resonator can be found to be

$$L = -\frac{1}{2}|R_1| + \frac{D}{4}\left(\frac{|R_1|}{\lambda N_{eq}}\right)^{1/2} \tag{3.8}$$

The design procedure was then to choose a standard radius of curvature for R_1 of 30 cm.

i.e. $R_1 = -30$ cm (convex)

With D = 6,35 mm and λ = 1,064 μm equation (3.8) can be used to calculate the resonator length if N_{eq} is known. It can be shown that resonator lengths of 104 cm, 54 cm and 38,4 cm are obtained for N_{eq} = 0,5; 1,5 and 2,5 respectively. We chose to use a resonator of length 38 cm due to its convenient size for possible further portability. Using this value in equation (3.6) we get that

$$M = 3,56$$

and from equation (3.7) we then get

$$R_2 = 106,8 \text{ cm (concave)}$$

This being a non-standard curvature forces us to choose a curvature for R_2 of 1 m. This obviously affects the confocal condition and to obtain collimated output we have to change the mirror separation which in turn affects the equivalent Fresnel number. These unfortunately

are restrictions which are imposed and which we cannot control more rigidly. From equation (3.3) we can calculate that the output coupler mirror is 1,8 mm in diameter and the geometrical output coupling for the resonator is 92 %.

The unstable resonator resulting from this design is shown in Fig. 3.10. More details of the individual components and specifications are given in Chapter 4.

3.4.2 RAY MATRIX APPROACH FOR THE INCLUSION OF THERMAL LENSING

Nd:YAG lasers using unstable resonators which have been designed to compensate for the thermal lensing effects of the laser rod, appear to have been designed to operate at only one repetition rate, i.e. only one focal length of the laser rod is important. (Herbst et al (1977), Andreou (1978)). In these cases the procedure has been the following: given the back mirror curvature R_2' and calculating the laser rod focal length, f, required to achieve an effective mirror curvature equal to R_2, the following expression is employed:

$$\frac{1}{f} = \frac{1}{R_2} - \frac{1}{R_2'} \qquad (3.9)$$

The available back mirror curvature R_2' is chosen such that the rod focal length corresponds to the desired average lamp input power.

It was desirable to use the present system at variable repetition rates (10; 5; 2,5 and 1,25 Hz) so the rod compensation had to be variable too. In order to be able to do this it was decided to put the back reflector on a translation stage and to vary its position from the laser rod as is described in greater detail in Section 3.4.2.2.

3.4.2.1 THEORY OF RAY TRANSFER MATRICES

The technique of ray transfer matrices is well known in the optics field and has been applied to laser resonators (Yariv (1975), Siegman (1971a) and Kogelnik & Li (1966)).

The ray transfer matrix, or ABCD matrix, describes the propagation of paraxial rays through an optical system. If r_i and α_i represent the

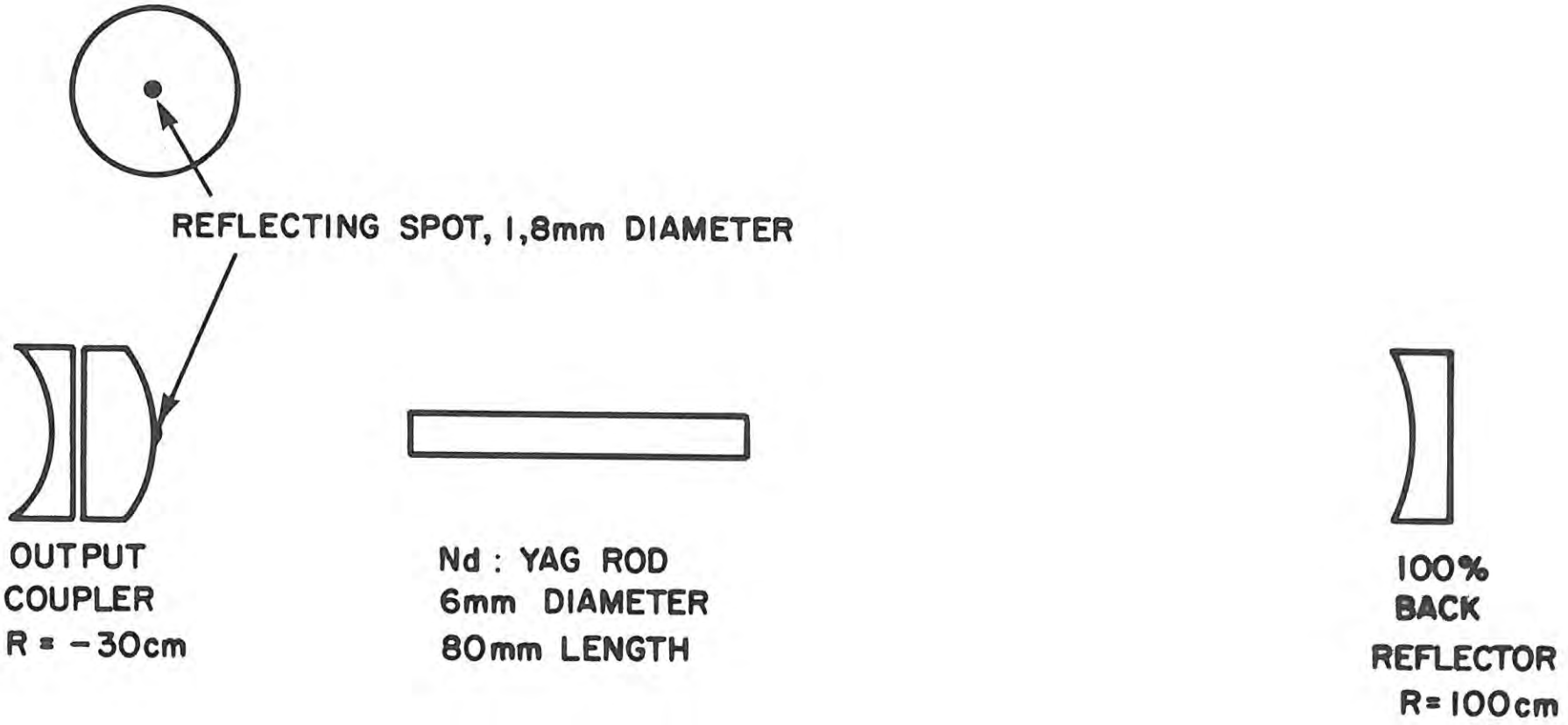

FIG. 3.10 THE BASIC COMPONENTS OF THE UNSTABLE RESONATOR

axial displacement and slope of a ray at plane i, which is perpendicular to the propagation axis, then r_i and α_i transform like a vector (r_i,α_i) on passing through any optical structure (including free space. The optical structure is characterized by an ABCD matrix and the axial displacement and slope of the ray at plane j, r_j and α_j, as shown in Fig. 3.11a is given by the so-called ABCD law,

$$\begin{bmatrix} r_j \\ \alpha_j \end{bmatrix} = \begin{bmatrix} A & B \\ C & D \end{bmatrix} \begin{bmatrix} r_i \\ \alpha_i \end{bmatrix} \tag{3.10}$$

The matrix ABCD represents everything lying between planes i and j. ABCD matrices for typical optical elements can be found in the cited references. This matrix usually has a unit determinant and for a system consisting of a number of optical elements, the matrix is obtained by multiplying the matrices for the individual sub-elements. Since matrices do not commute, the order of multiplying the sub-element matrices must be maintained. For ray propagation from left to right in Fig. 3.11b, the total ray transfer matrix M_t is given by

$$M_t = M_n M_{n-1} \cdots M_2 M_1 \tag{3.11}$$

where M_i = ABCD matrix of the ith element.
From equations (3.10) and (3.11) the transformed ray parameters would be

$$\begin{bmatrix} r_j \\ \alpha_j \end{bmatrix} = M_t \begin{bmatrix} r_i \\ \alpha_i \end{bmatrix} \tag{3.12}$$

3.4.2.2 OBTAINING THE CONFOCAL (COLLIMATION) CONDITION

The confocal condition can be obtained in two ways by making use of the ray transfer matrices. Both these methods require a defined reference plane in the resonator which for convenience is taken as the left surface of the laser rod as indicated in Fig. 3.12.

The first method then involves calculating the ABCD matrix for a ray moving to the right through the system from the reference plane. This

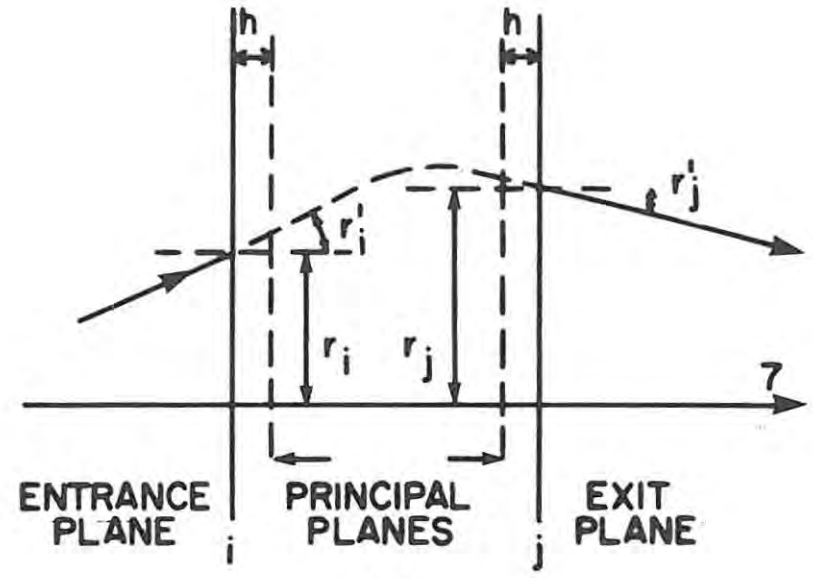

(a)

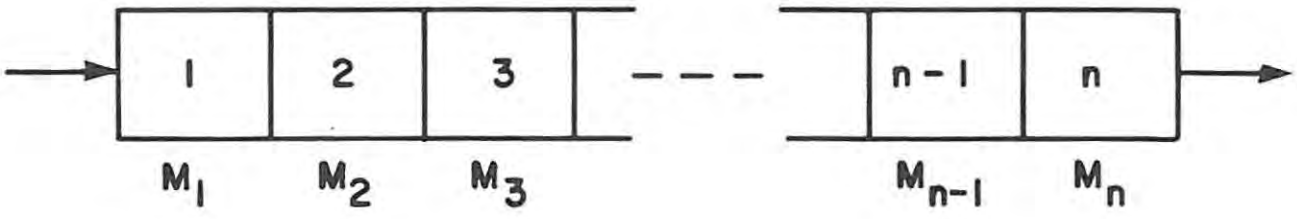

(b)

FIG. 3.11 ILLUSTRATIONS OF THE PRINCIPLES OF RAY TRANSFER MATRICES

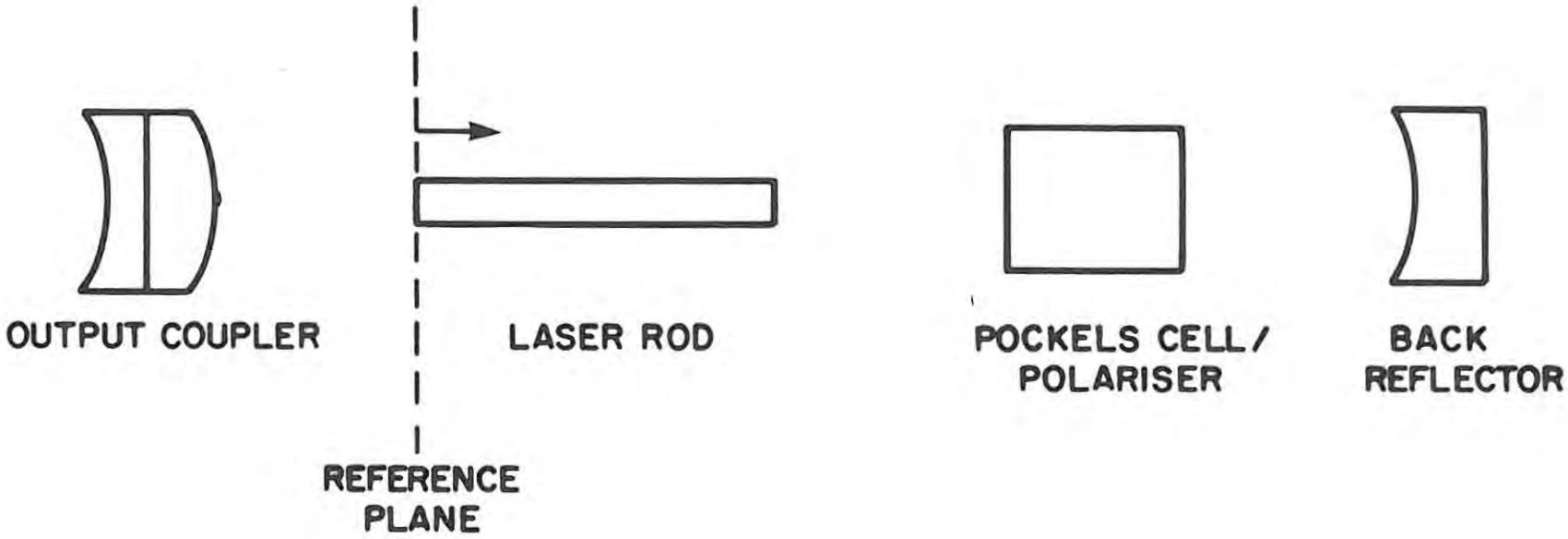

FIG. 3.12 DIAGRAM SHOWING THE REFERENCE PLANE USED IN THE RAY MATRIX ANALYSIS

means the ray passes through the laser rod, between the rod and Pockels cell (PC), between Pockels cell and back reflector, reflects off the back reflector and returns through the same sequence. The criterion for collimated output is then that the angle of the returning ray at the reference plane is close to zero.

The total ray transfer matrix of such a system would then be

$$M_T = M_{LR}\, M_D\, M_R\, M_D\, M_{LR} \qquad (3.13)$$

where M_{LR} = laser rod matrix

M_D = matrix of the combined system of: distance from rod to PC, PC thickness and distance from PC to back reflector

M_R = back reflector matrix.

Matrix M_R can be found in the cited references to be

$$M_R = \begin{bmatrix} 1 & 0 \\ \frac{-2}{R} & 1 \end{bmatrix}$$

with R = mirror radius of curvature.

M_D is a compound matrix consisting of the product of three matrices, say, M_1, M_{pc} and M_2

where M_1 = matrix of distance between rod and PC

$$= \begin{bmatrix} 1 & d_1 \\ 0 & 1 \end{bmatrix}, \quad d_1 = \text{distance between rod and PC}$$

M_2 = matrix of distance between PC and back reflector

$$= \begin{bmatrix} 1 & d_0 \\ 0 & 1 \end{bmatrix}, \quad d_0 = \text{distance between PC and back reflector}$$

$$M_{pc} = \begin{bmatrix} 1 & \frac{d_{pc}}{n} \\ 0 & 1 \end{bmatrix}$$

, d_{pc} = length of PC crystal = 40 mm

, n = PC refractive index = 1,48

From the discussion in the previous section

$$M_D = M_2\ M_{pc}\ M_1$$

$$= \begin{bmatrix} 1 & d_1 + d_0 + \frac{d_{pc}}{n} \\ 0 & 1 \end{bmatrix} \qquad (3.14)$$

The laser rod matrix, M_{LR}, can be found by assuming the rod to be a thick lens of homogeneous refractive index. The derivation of its matrix is given by Gleason (1971) and is

$$M_{LR} = \begin{bmatrix} 1 - \frac{\ell}{2n_o f} & \frac{\ell}{n_o} \\ -\frac{1}{f} & 1 - \frac{\ell}{2n_o f} \end{bmatrix}$$

where ℓ = rod length = 80 mm

n_o = rod refractive index = 1,818 for Nd:YAG

f = rod focal length

The focal lengths of the laser rod for various input energies and repetition rates have previously been measured by Robertson & Preussler (1982) and are given in Table 3.1.

An HP-86 computer programme to perform the M_T-computation from equation (3.13) and the above matrices, was written and is shown in Appendix I. Once M_T has been computed, say

$$M_T = \begin{bmatrix} A_T & B_T \\ C_T & D_T \end{bmatrix}$$

the outcoming ray height and angle is obtained by using equation (3.10) if the incoming ray height and angle are known, i.e.

$$\begin{bmatrix} r_{out} \\ \alpha_{out} \end{bmatrix} = \begin{bmatrix} A_T & B_T \\ C_T & D_T \end{bmatrix} \begin{bmatrix} r_{in} \\ \alpha_{in} \end{bmatrix}$$

TABLE 3.1

Measurements of the induced equilibrium focal lengths in the Nd:YAG laser rod

Rep. rate (Hz)	P_{in} (W)	$1/P_{in}$ (kW^{-1})	Average x (mm)	$f_{rod}^{632,8\ nm}$ (m)	$f_{rod}^{1064,1nm}$ (m)
5	50	20,0	95,177	42,8	44
5	60	16,7	95,132	35,9	37
5	75	13,3	95,034	26,8	28
10	100	10,0	94,917	20,8	21
10	120	8,33	94,792	16,9	17
10	150	6,67	94,708	15,1	16
20	200	5,00	94,405	11,1	11
20	240	4,17	94,089	8,91	9,2
20	300	3,33	93,955	8,27	8,5

If the output coupler is fixed at a known distance from the laser rod then the only variables are the rod to PC distance and the PC to back reflector distance. From the M_D matrix, equation (3.14), it can be seen that only the sum of these distances is important and not the relative magnitudes so that we can effectively group the distances into one and have a Pockels cell of known length and one space of known length.

The choice of incoming ray height and angle is governed only by the fact that the ray appears to originate from the known focal point of the output coupler. For convenience we chose the output coupler to laser rod length to be 80 mm which gives by simple trigonometry that, at the reference plane, r_{in} = 1,38 mm and α_{in} = 0,006 rads (α_{in} is the angle of a beam just grazing the output coupler from its known focal point).

The computer programme works briefly as follows:

It uses as inputs,

(1) the laser rod length and refractive index
(2) incoming ray height and angle, calculated above

(3) rod to PC distance
(4) laser rod focal length
(5) a "guess" of rod/back reflector length.

From these inputs the matrices are defined and M_T computed as well as the outcoming ray height and angle. The user then has the choice of another length if the outcoming angle is not close enough to zero in which case the calculations are repeated with the new length. If the user is satisfied with the α_{out}, he then has the choice of another laser rod focal length and repeating the process or of ending the programme. Figure 3.13 is a flowchart showing the processing of the programme.

The second method of calculating the confocal condition differs slightly from the first in that a few more calculations are performed. This method is based on the canonical formulation for analyzing unstable resonators as described by Siegman (1976). Using the techniques of ray transfer matrices one now calculates a round-trip matrix. From the reference plane of Fig. 3.12 one proceeds through the components as for the first method but instead of stopping after reaching the reference plane on the return trip, one continues to the output coupler and back to the reference plane in the same direction as one started. This requires the same procedures as before with the addition of the laser rod to output coupler distance matrix and the output coupler matrix which are defined as in the previous case. For collimation Siegman (1976) shows that with the total round-trip matrix, AD = 1.

A computer programme similar to that of the first method was written and is also shown in Appendix I. The programme runs in the same way except that one now decides on the closeness of the product AD to unity. Not surprisingly the programmes give identical results.

3.5 RESULTS

The results of the above confocal condition calculations are given in Fig. 3.14. For convenience, the parameters resulting in this curve are given here:

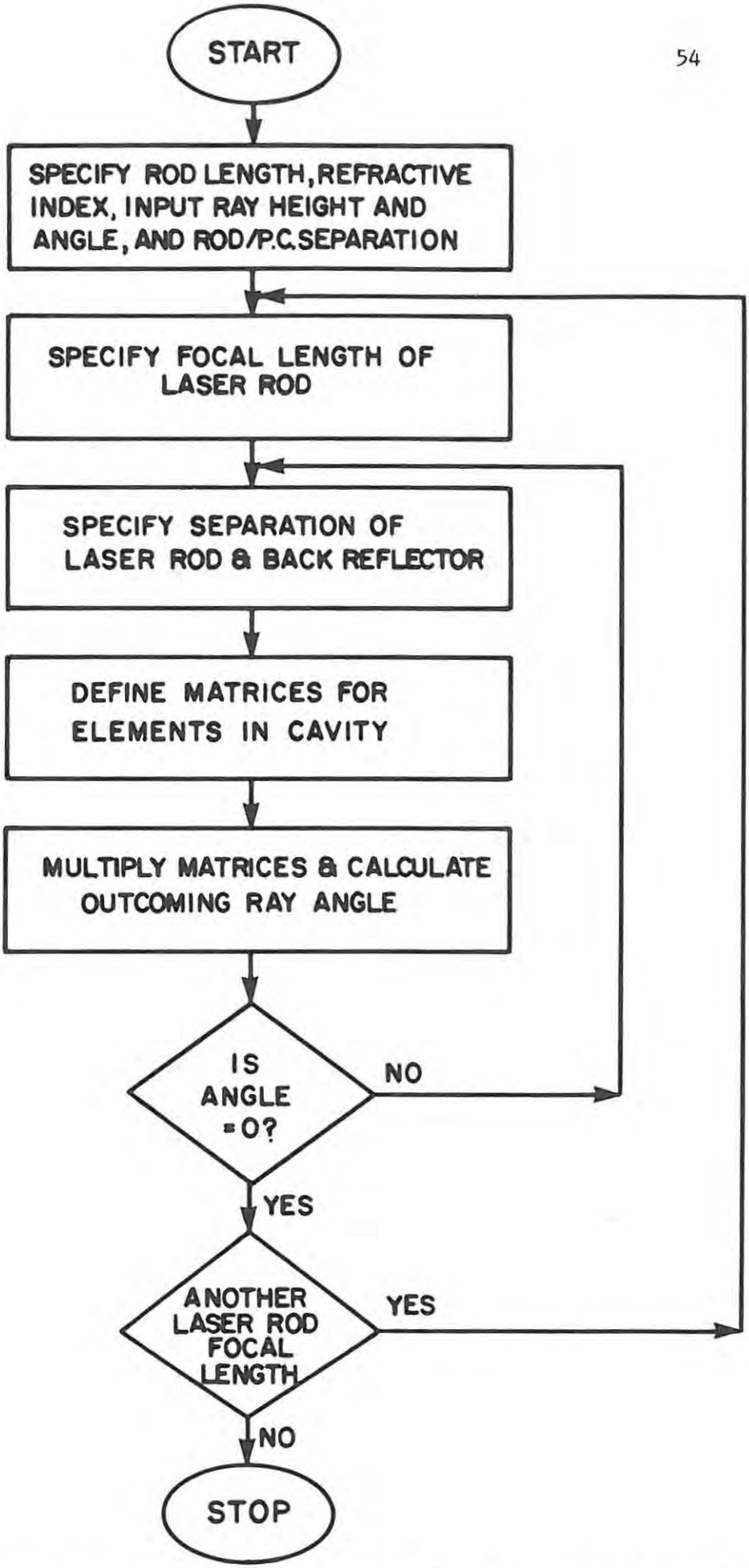

FIG. 3.13 FLOWCHART SHOWING THE METHOD OF CALCULATION OF THE CONFOCAL CONDITION

laser rod length:	80 mm
laser rod refractive index:	1,818
output coupler to laser rod distance:	80 mm
Laser rod/PC distance:	60 mm
Pockels cell length:	40 mm
Pockels cell refractive index:	1,48
laser rod focal length:	user defined
laser rod to back reflector distance:	user chosen and optimized.

Inspection of Fig. 3.14 and Table 3.1 shows that a considerable degree of adjustment is required if the repetition rate is changed from 1 to 20 Hz. For this reason many commercial lasers only operate at a pre-specified repetition rate.

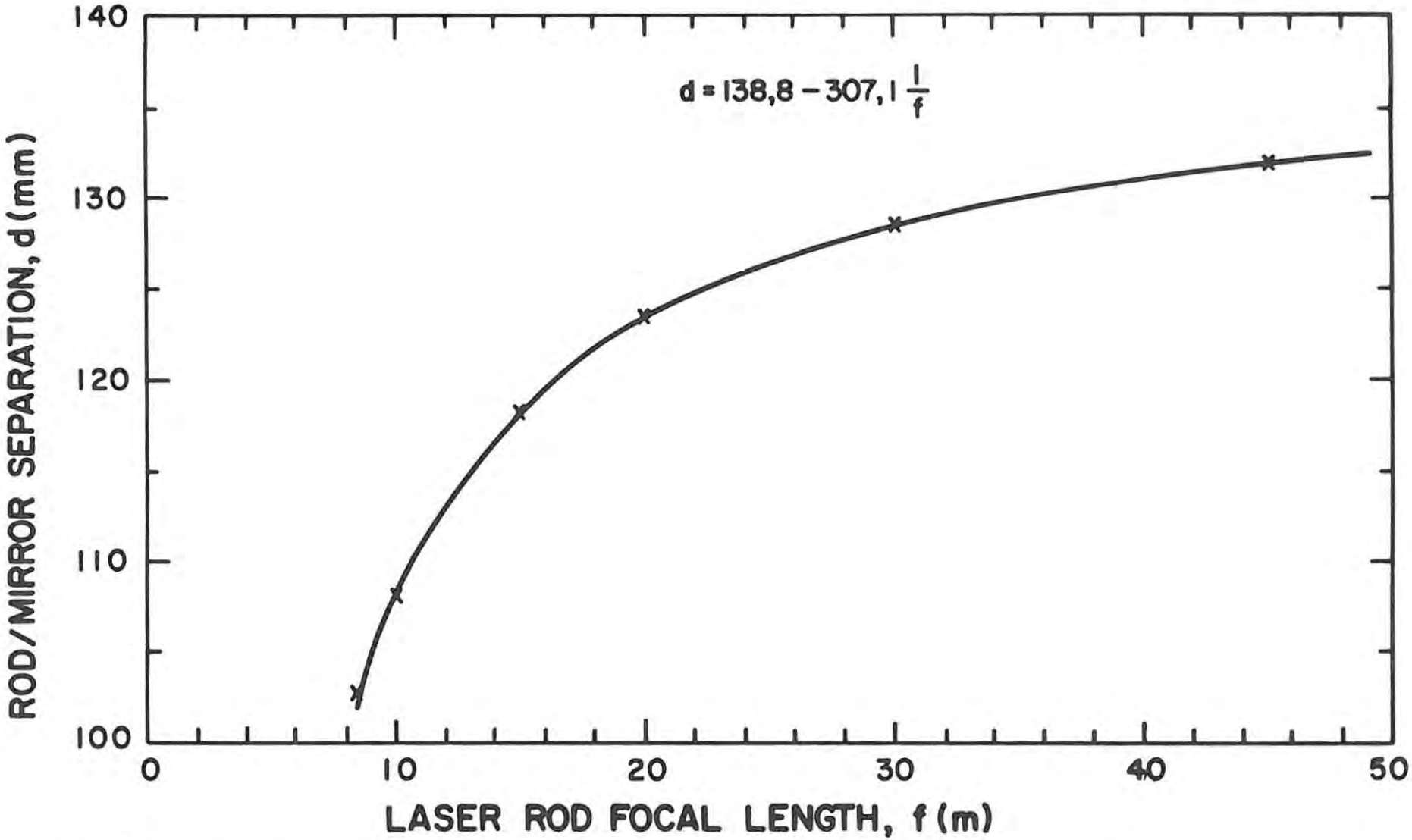

FIG. 3.14 SEPARATION OF THE LASER ROD AND BACK MIRROR FOR VARIOUS LASER ROD FOCAL LENGTHS

CHAPTER 4

EXPERIMENTAL APPARATUS, MEASURING EQUIPMENT AND OPTICAL ALIGNMENT METHODS

4.1 INTRODUCTION

In this chapter the experimental apparatus used in the construction and evaluation of the laser are discussed. This includes the components of the laser, control electronics, equipment used in the evaluation of the laser and the optical alignment of the laser.

4.2 THE LASER

The components of the unstable resonator laser are shown in Figs. 4.1 and 4.2. The components were screwed down on a steel U-channel.

4.2.1 THE LASER ROD

The Nd:YAG laser rod turns out to be a relatively expensive component due to a very slow growth rate (by the Czochralski method) of approximately 0,5 mm per hour. Boules are grown with the axis in the [111] direction and typical boules of 10 to 15 cm in length require a growth run of a number of weeks. In Nd:YAG a substitution of about 1 % of Y^{3+} by Nd^{3+} yields rods with good optical quality and lasing characteristics.

The laser rod used in this study was purchased from Union Carbide and was 80 mm long and 6,35 mm (1/4 inch) diameter. The ends were specified as being flat to $\frac{\lambda}{10}$ and parallel to less than 10 seconds of arc. The barrel of the rod was ground to a rough finish as it has been shown (Koechner (1976)) to give a more uniform pumplight distribution. The end faces of the rod were anti-reflection (AR) coated for 1,06 μm.

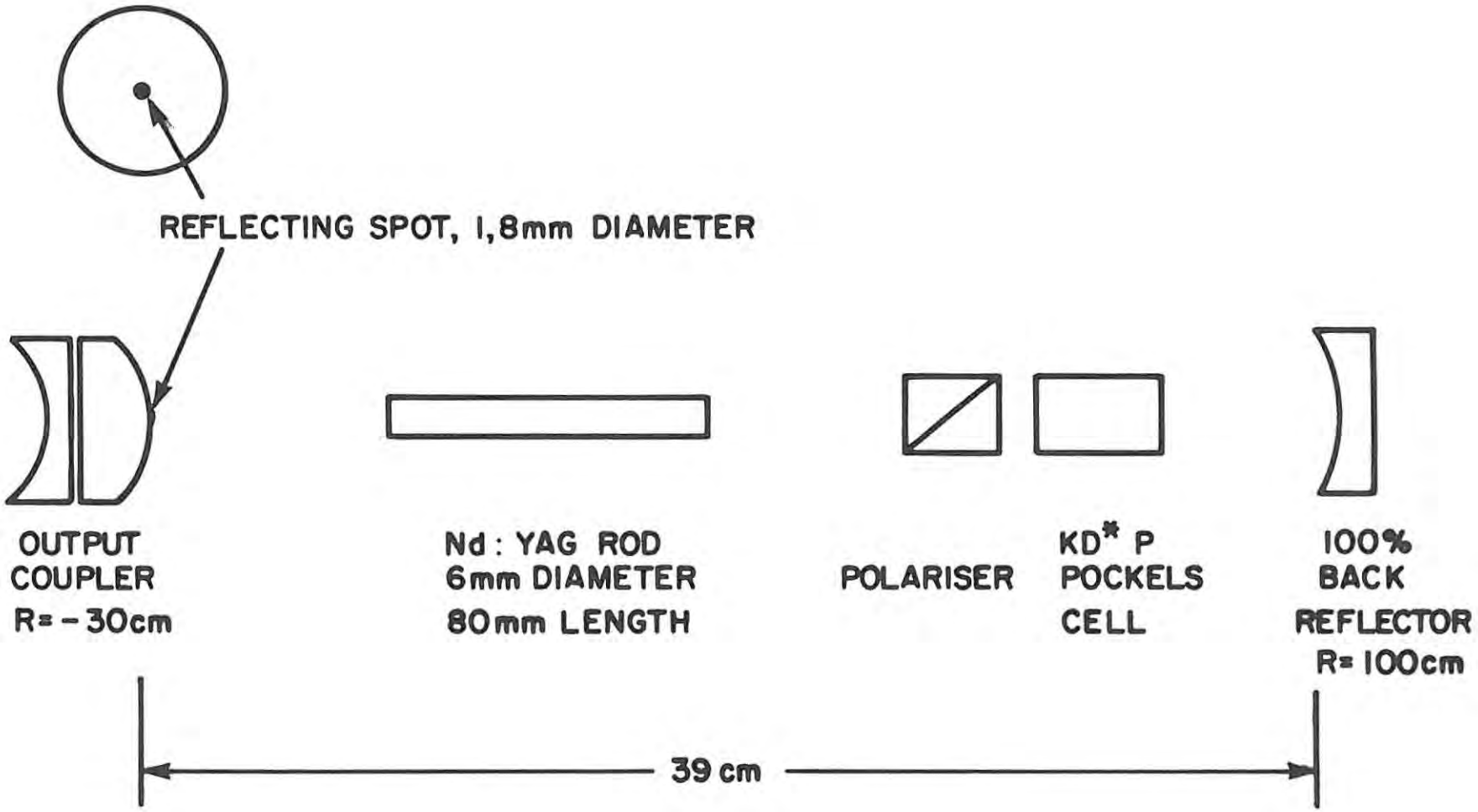

FIG. 4.1 THE COMPONENTS OF THE UNSTABLE RESONATOR LASER

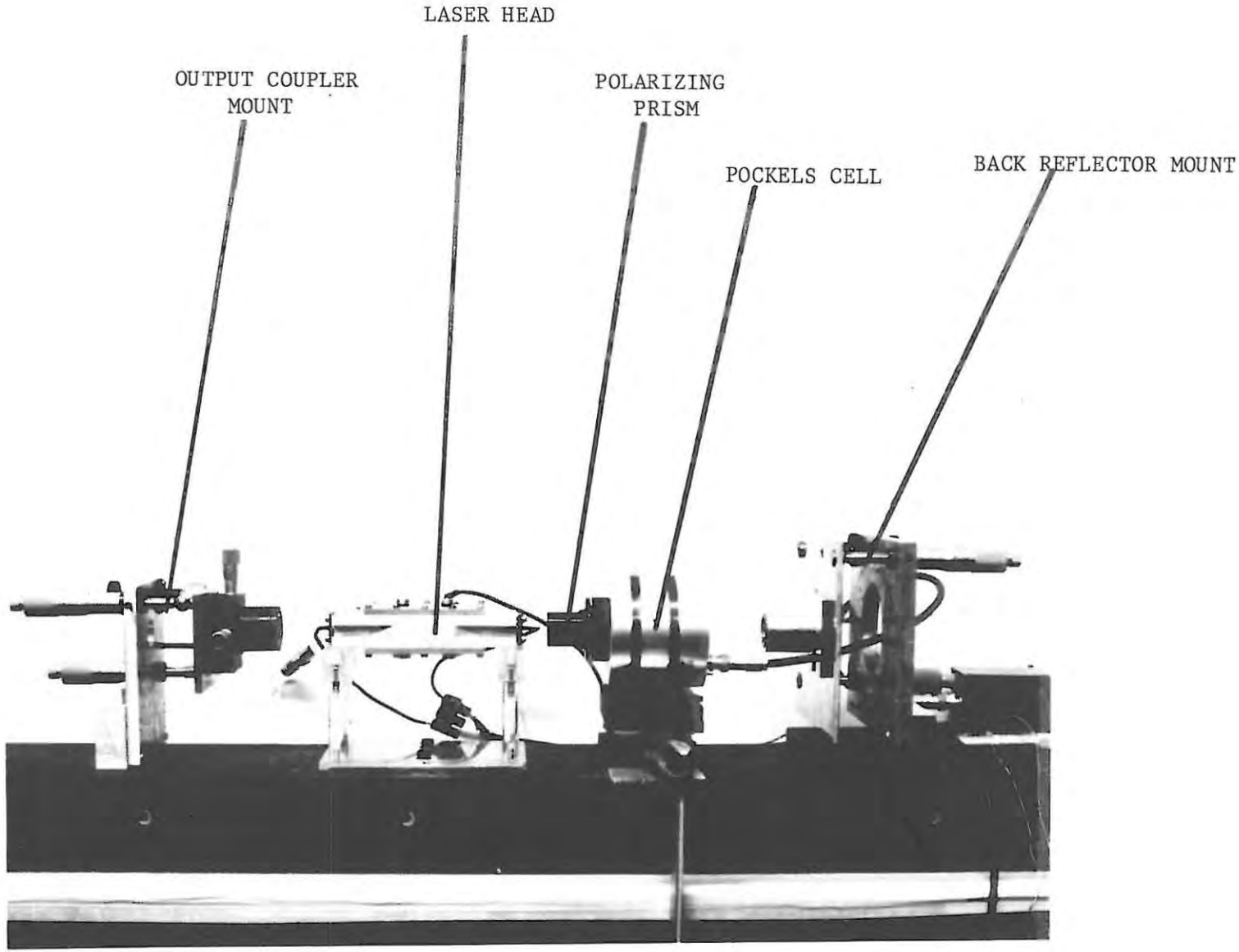

FIG. 4.2 PHOTOGRAPH SHOWING THE LASER MOUNTED ON A U-CHANNEL

4.2.2 THE FLASHLAMP

For pulsed laser operation noble gas flashlamps are most commonly used. These can be linear in form, as in the present case, or helical in which case the flashlamp is usually wrapped around the laser rod. Xenon is the gas which is usually used in pulsed flashlamp systems because it yields a higher radiation output for a given electrical input energy than other gases. Of the electrical input energy into the flashlamp, 40 to 50 % is converted to radiation in the 0,2 to 1 μm region which contains the pump bands of Nd:YAG (0,73 to 0,76 μm and 0,79 to 0,82 μm). A typical linear flashlamp is shown in Fig. 4.3.

A detailed discussion of the design considerations for the operation of these flashlamps is not applicable here since power supplies for previously investigated Nd:YAG laser systems in this laboratory are in existence and have already been documented (Nortier (1981), Robertson & Preussler (1982)). A few points are, however, mentioned in section 4.3. Triggering was achieved simply by applying a high voltage pulse (16 kV) to the aluminium laser rod and flashlamp housing (see Fig. 4.2). The electric field initiates a capacitive discharge between the electrodes which starts as a thin streamer and grows to fill the entire tube.

The flashlamp which was used in this study was a Xenon-filled linear flashlamp designated 4F3-G from ILC Technology. Inc. USA. This flashlamp had a bore diameter of 4 mm and a discharge length of 76 mm (3 inches) as shown in Fig. 4.3.

4.2.3 THE PUMP CAVITY AND COOLING SYSTEM

The efficient transfer of pump radiation from the flashlamp to the laser rod largely determines the overall efficiency of the laser system. This transfer of radiation is achieved by the pump cavity which also determines the pumplight distribution in the laser rod.

The most commonly used pump cavities in Nd:YAG lasers are a highly reflecting elliptical cylinder with the laser rod and flashlamp located at each focus (the close-coupled ellipse), and the diffuse cylinder.

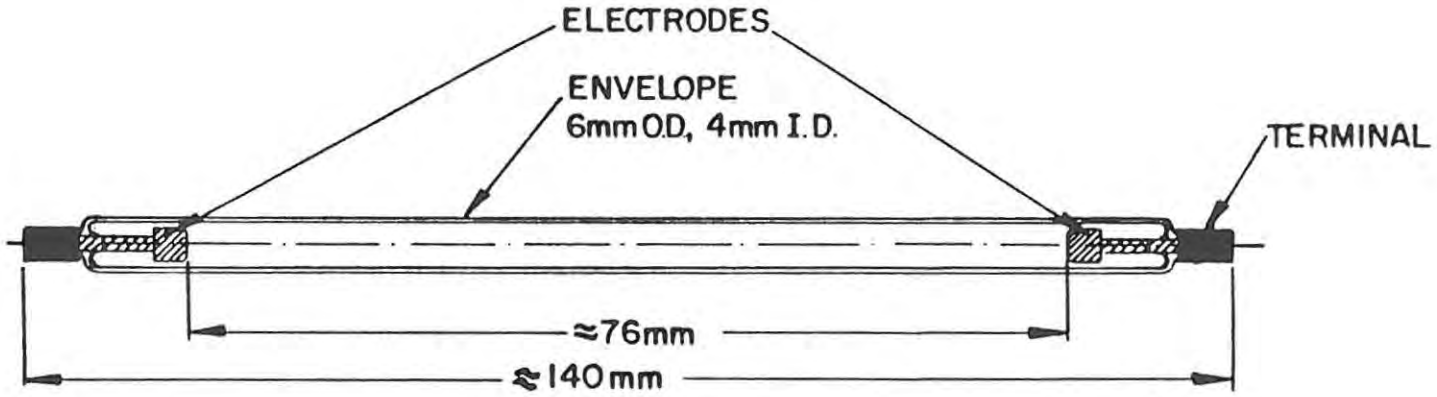

FIG. 4.3 FLASHLAMP DESIGN USED IN THIS WORK

These are shown in Fig. 4.4. The close-coupled ellipse is slightly more efficient than the diffuse cylinder. The latter consists of two concentric quartz tubes with MgO powder compressed in the space between them. The powder reflects between 90 and 98 % of the pumplight and results in a more uniform pumplight distribution in the laser rod. Since a diffuse reflector was available, the pump cavity used was of this type.

Due to the considerable amount of heat which is generated in a high repetition rate solid state laser, it is necessary that the flashlamp and laser rod are cooled. Liquid or air cooling can be used and in our case a water-ethylene glycol mixture was used. The closed-loop cooling system consisted of a reservoir, a pump, a deionizing chamber and a liquid-to-air heat exchanger. The laser head, which comprised an aluminium body, the pump cavity, laser rod and flashlamp, was designed in such a way that the cooling water floods the pump cavity and so surrounds the laser rod and flashlamp. The pump cavity consisted of two hemispherical sections which fit together into the laser head.

4.2.4 THE POCKELS CELL AND POLARIZING PRISM

As was stated in Section 2.3.2.1, the Pockels cell which was used in this study was a KD*P type (potassium dideuterium phosphate) cell with longitudinally applied electric field. A number of crystals are known to exhibit a linear electro-optic effect, amongst them are ammonium dihydrogen phosphate (ADP), potassium dihydrogen phosphate (KDP) and lithium niobate ($LiNbO_3$), the latter being of the transverse field type. All of these crystals have their own particular advantages and disadvantages. Lithium niobate is not suitable for high power density applications as its damage threshold is in the region of 10-50 MW/cm^2. Of the other crystals, KD*P has the lowest quarter-wave voltage (3,2 kV) by at least a factor of two. Typical damage thresholds of KD*P for 10 ns pulses are around 200 MW/cm^2. A disadvantage of KD*P, however, is its hygroscopic nature. This is circumvented by having the crystal immersed in a cell filled with index-matching fluid which makes it rather bulky. Since AR coatings cannot be applied to the crystal itself, the losses between the cell windows and the crystal faces are reduced by the index-matching fluid.

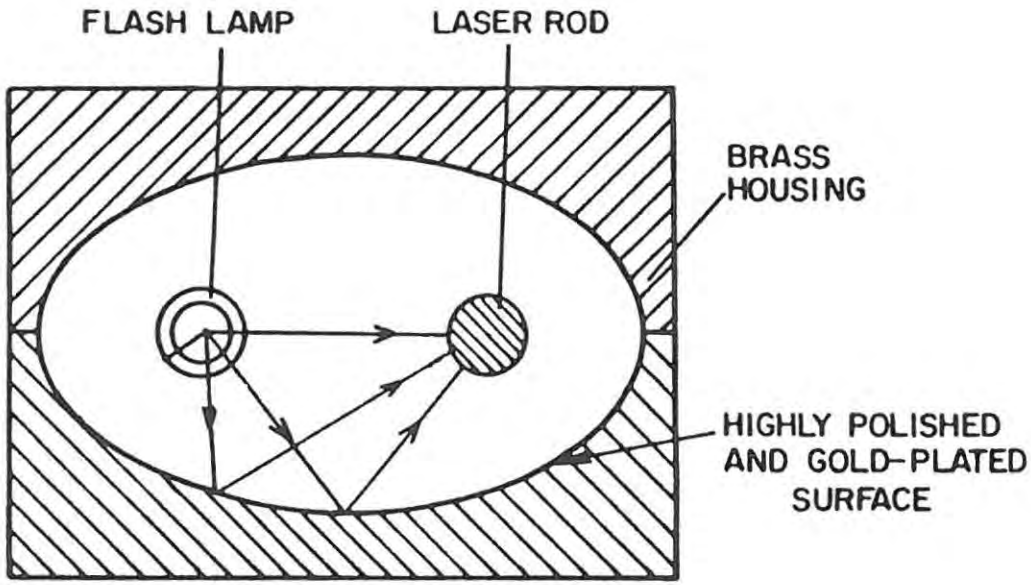

SINGLE ELLIPSE IMAGING REFLECTOR

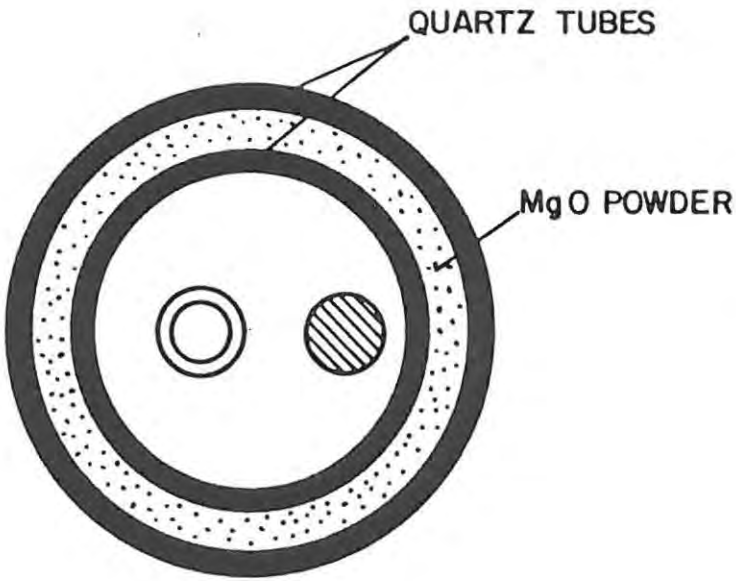

DIFFUSE REFLECTOR

FIG. 4.4 PUMP CAVITY CONFIGURATIONS USED FOR SOLID-STATE LASERS

The KD*P Pockels cell which was used in this study was a model 1056 from Lasermetrics Inc. USA. The stainless steel cell containing the crystal was fitted with AR coated windows for 1,06 μm. An extinction ratio of 800:1 was specified, quarter-wave voltage of 3,2 kV, risetime of less than 1 ns, capacitance of 10 pf and a damage threshold of 350 MW/cm^2.

The Pockels cell was supplied with a polarizer mounted with its plane of polarization at 45 ° to the fast axis of the cell. The polarizer was a calcite Glan-laser, air-spaced polarizing prism with double exit windows and AR coatings for 1,06 μm.

4.2.5 THE LASER MIRRORS

The mirrors used in the unstable resonator laser were purchased from CVI Laser Corp. USA. According to the design (see Section 3.4.1) the curvatures were

back reflector:	1 m concave
output coupler:	0,3 m convex with 1,8 mm reflecting spot as mirror.

Due to the availability of only plano-convex substrates, the resulting lens had to be compensated for by a plano-concave substrate. All surfaces were AR coated on both sides with the small mirror being coated in the centre of the convex side. This is how the output coupler has been shown in Fig. 4.1. All the mirrors and substrates were 25 mm (1 inch) in diameter and approximately 9 mm (3/8 inch) thick, and were made from Schlieren grade fused silica with appropriate high reflectivity coatings for 1,06 μm. The damage threshold for the 1,06 μm coating was specified as 5 GW/cm^2 for single pulses of 20 ns. The specifications by the manufacturer of the mirror were a surface figure of $\lambda/10$ at 632,8 nm and a surface quality of 10-5. For the latter, the first number gives the apparent width of a scratch (in μm) and the second number indicates the maximum bubble and dig diameter in 10 μm steps. Standard quality lenses have surfaces of 80-50. Laser mirrors require at least 15-5.

4.2.6 COMPONENT HARDWARE

4.2.6.1 MIRROR MOUNTS

The basic requirements for a good mirror mount are an independent, orthogonal and backlash-free tilt with sufficient resolution and good thermal and mechanical stability. We used a three-point suspension with torsion springs and 1 μm/div differential micrometers for the mirror mounts.

(i) Output coupler mount

The mount for the output coupler mirror is shown in the photograph in Fig. 4.5. The output coupler, being a small (1,8 mm diameter) spot, must be aligned vertically and horizontally on the optical axis as well as having the tilt facility for optimization. In order to achieve all these degrees of freedom, a commercial X-Y translation stage was mounted on to the tilt platform with the mirror holder mounted on the X-Y stage as shown in the photograph. The effect of this mount was to tilt the mirror about an axis which is relatively far behind the reflecting surface but it was felt that to tilt it about the plane of the mirror would require a rather elaborate mechanical design which was probably not worth the time spent. Fortunately the present design did not appear to have any drawbacks.

(ii) Back reflector mount

This mount is shown in Fig. 4.6. Due to the fact that the back reflector is theoretically more sensitive to misalignment than the output coupler (Section 5.3.4), it was mounted on a tilt platform with a longer leverage. This mount in turn was mounted on a 50 mm translation stage to be able to change the resonator length to compensate for the thermal lensing effect of the laser rod.

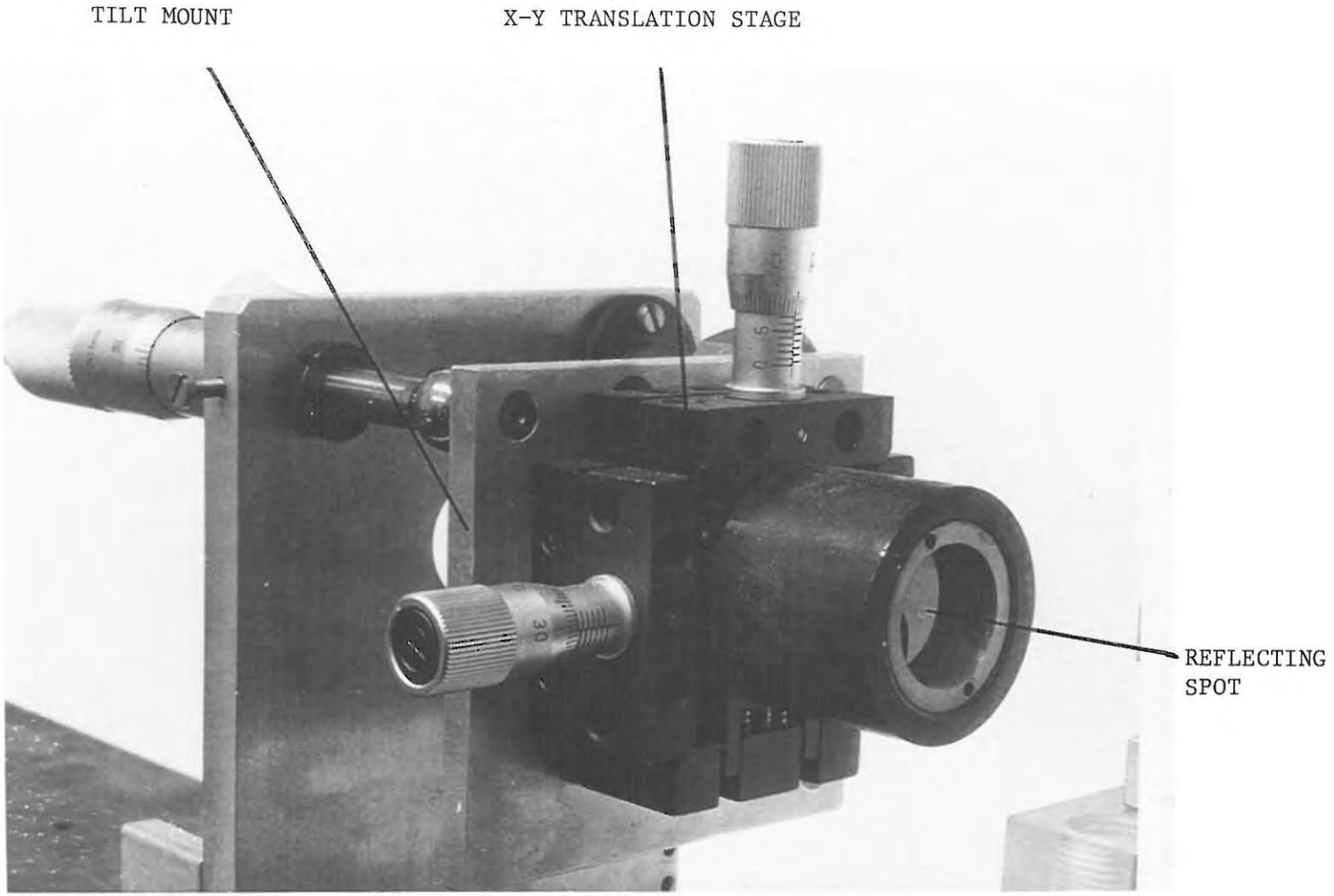

FIG. 4.5 PHOTOGRAPH SHOWING THE OUTPUT COUPLER MOUNT

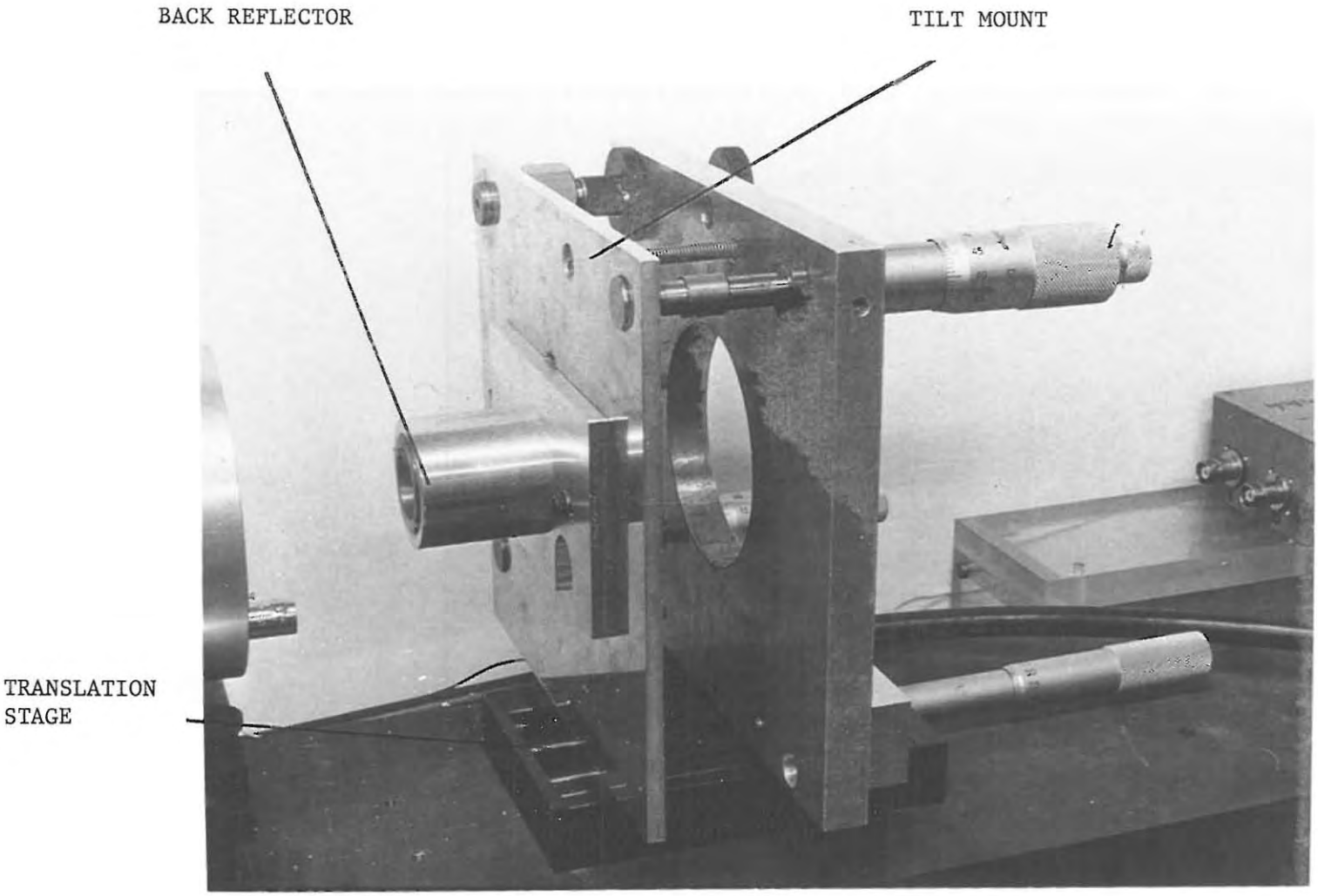

FIG. 4.6 PHOTOGRAPH SHOWING THE BACK REFLECTOR MOUNT

4.2.6.2 POCKELS CELL MOUNT

For accurate alignment of the Pockels cell one requires a number of different movements. These are X and Y translations to align the axis of the Pockels cell to that of the laser and then rotational movements about the 3 Cartesian axes. The mount which was used here was designed and used by Nortier (1981) and is shown in Fig. 4.7.

4.3 THE CONTROL ELECTRONICS

The laser power supply is a standard piece of equipment which has been used in the evaluation of a number of Nd:YAG lasers in this laboratory (Robertson & Preussler (1982), Preussler & De Kock (1983)). This control circuitry was designed and built in the Electronic Support Services Section of the Optics Division by W van den Berg. It is therefore only necessary to briefly outline its features and some important points. Figure 4.8 shows a block diagram of the high repetition rate electronic control circuit used in the experiments.

The pulse-forming network (PFN) in Fig. 4.8 is a single-mesh LC circuit which is designed to give a critically damped flashlamp pulse. The PFN integrates with what is known as the simmer-mode operation of the flashlamp. This technique, the circuitry of which is shown in Fig. 4.9, involves the maintenance of a low-current discharge between the main flashlamp pulses. After triggering of the flashlamp, a small current flows through the limiting resistor, which is in parallel with the pulse-forming inductor (L) and a thyristor. The main discharge is then initiated by triggering of the thyristor. The simmer-mode operation increases flashlamp life, reduces coolant degradation, reduces RF radiation and increases efficiency and pulse reproducibility.

The high voltage switch for switching the Pockels cell voltage consisted of a Krytron switch and is shown in Fig. 4.10. The output is initially at +HV and switches to 0V when triggered. This switching takes place on a time scale of ≈10 ns.

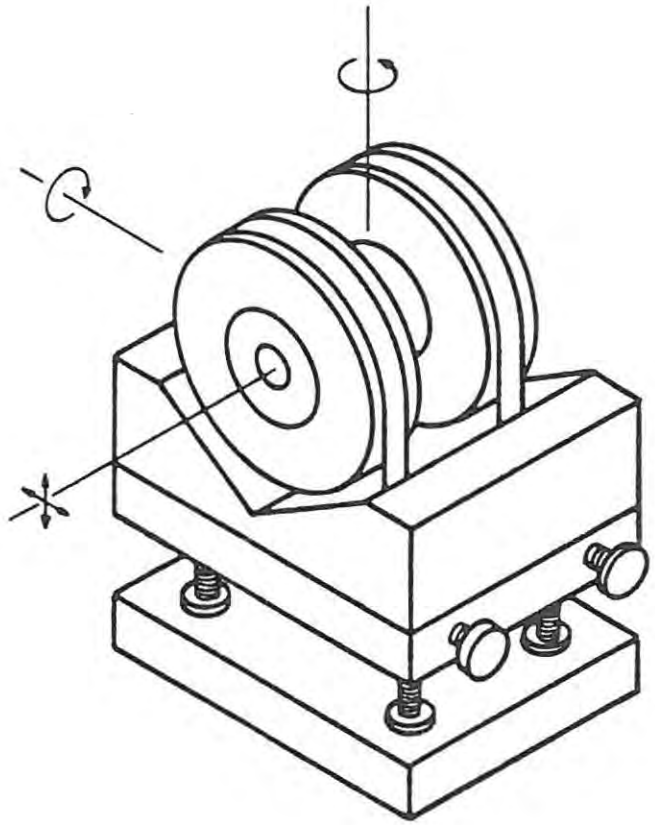

FIG. 4.7 ISOMETRIC VIEW OF THE POCKELS CELL IN ITS MOUNT. MOVEMENTS PROVIDED BY THE MOUNT ARE SHOWN.

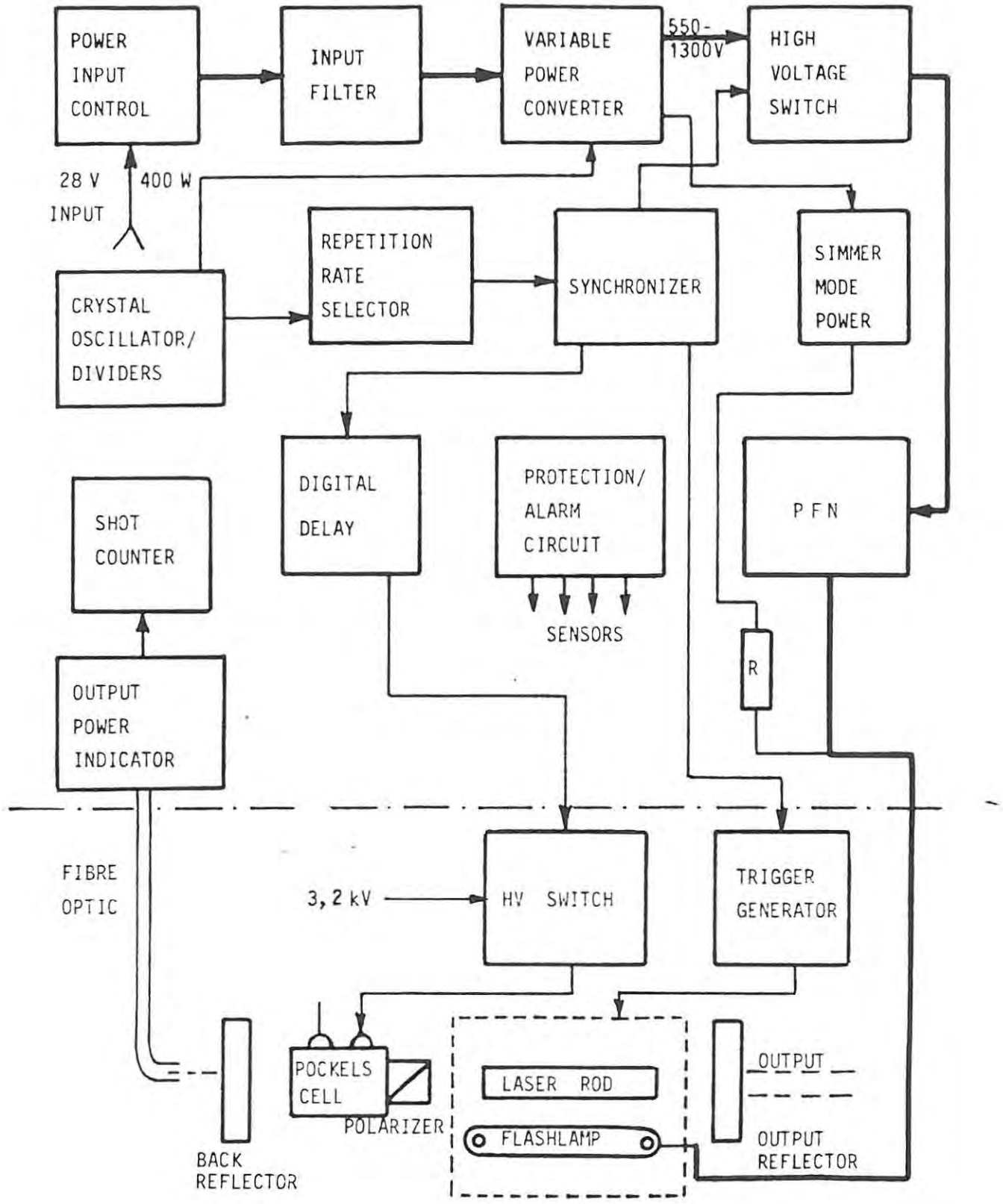

FIG. 4.8 BLOCK DIAGRAM OF THE HIGH REPETITION RATE ELECTRONIC CONTROL CIRCUIT

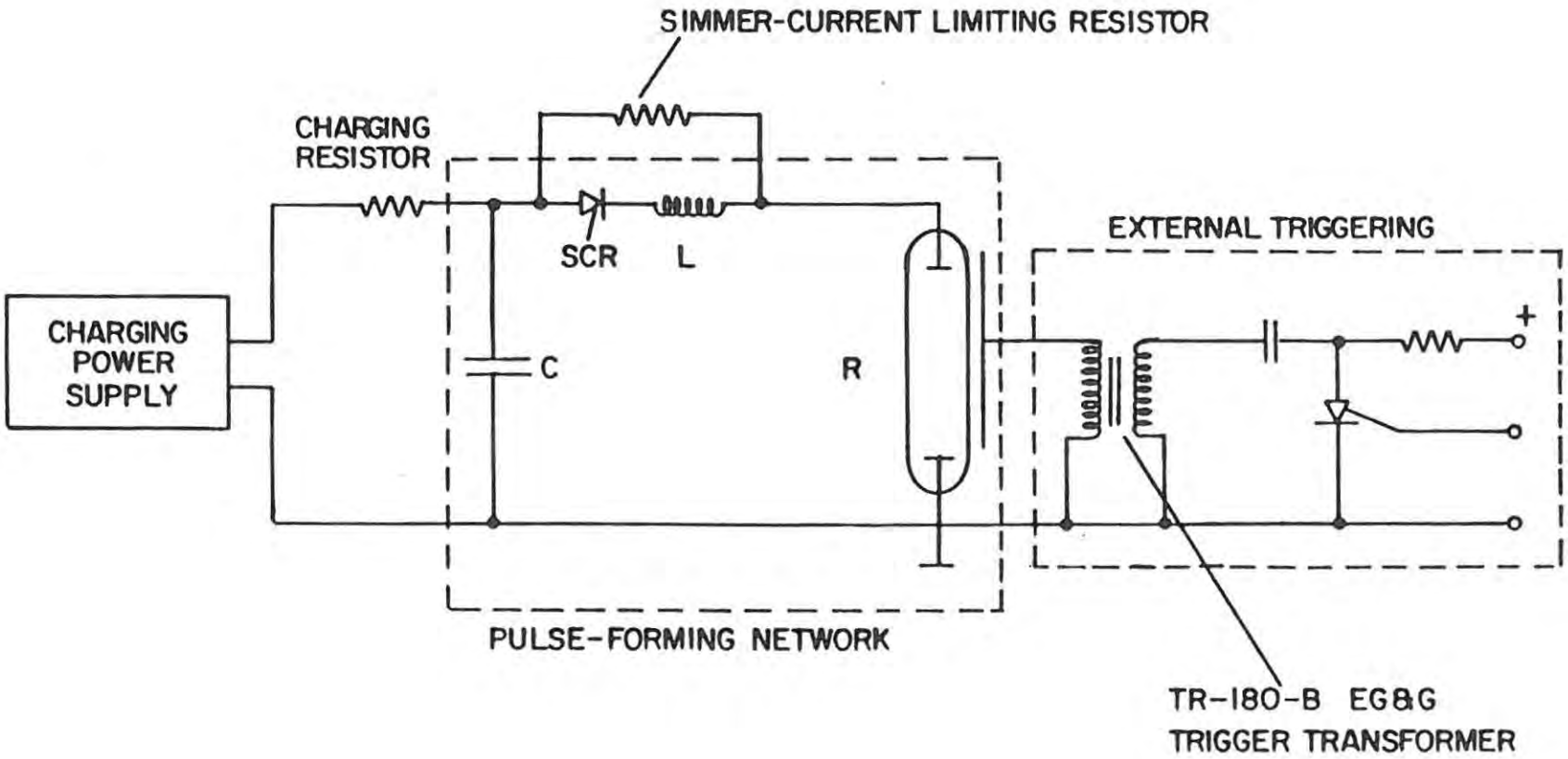

FIG. 4.9 DIAGRAM OF THE ELECTRONIC EXCITATION CIRCUIT OF THE LASER SHOWING SIMMER-MODE OPERATION

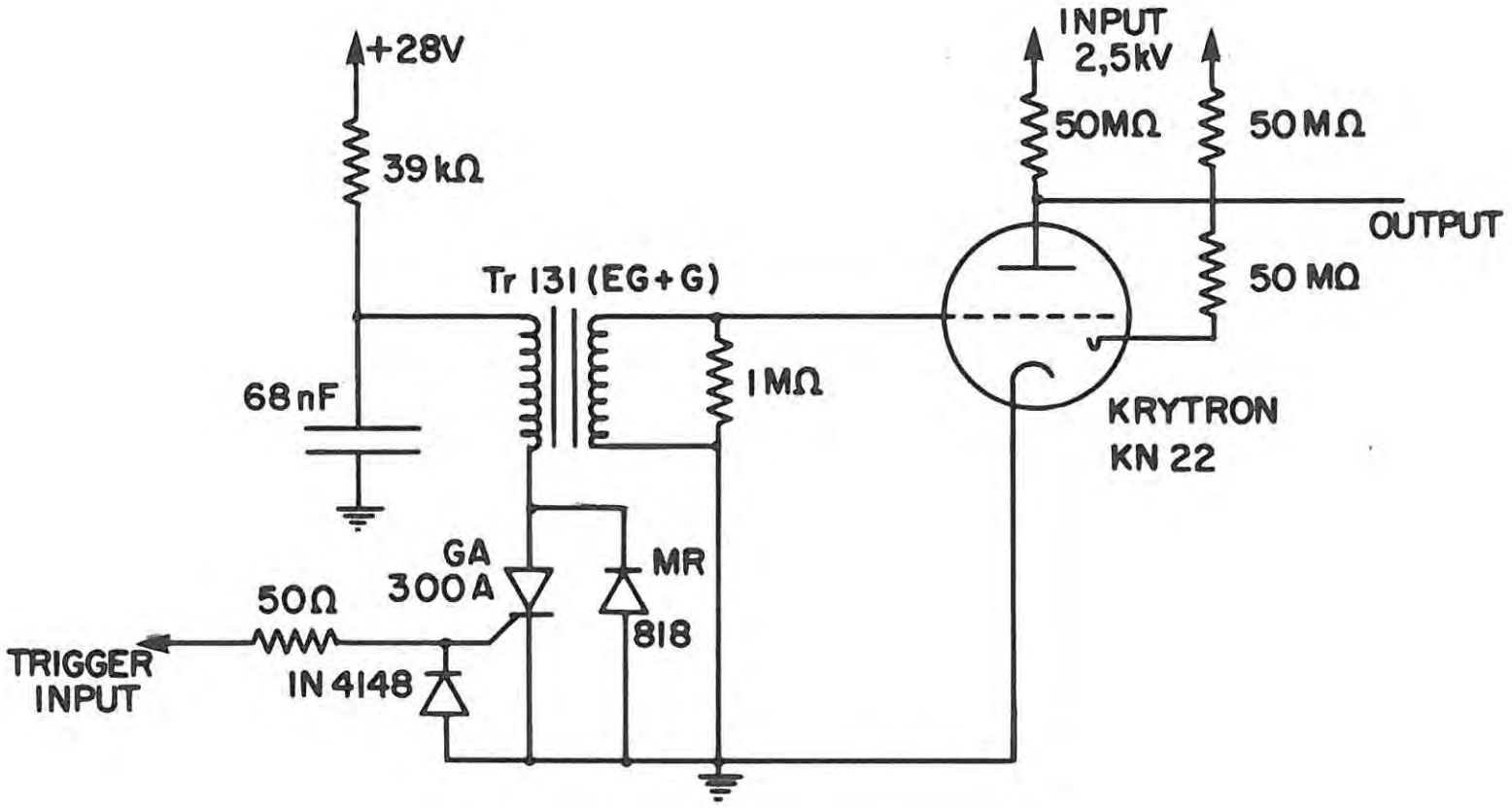

FIG. 4.10 POCKELS CELL SWITCHING CIRCUIT

Repetition rates of 1,25; 2,5; 5; 10 and 20 pulses per second were selectable by means of DIP switches. Q-switch delay times, i.e. the time between the start of the flashlamp pulse and the switching of the Pockels cell, could similarly be varied between 1 and 255 μs in 1 μs steps. A typical flashlamp current pulse is shown in Fig. 4.11.

4.4 MEASURING EQUIPMENT

4.4.1 OPTICAL DETECTORS

In order to measure laser parameters such as energy, pulse width and beam profile, different optical detectors were needed. For energy measurements a pyroelectric detector was used, and for pulse width measurements use was made of a silicon PIN photodiode. The beam profile measurements required the use of a silicon linear photodiode array.

4.4.1.1 PYROELECTRIC ENERGY HEAD

Pyroelectric detectors are thermal detectors whose output is proportional to the rate of change of its temperature. The pyroelectric effect is a change in the spontaneous polarization of a pyroelectric crystal when the temperature is changed. A voltage pulse is generated which is proportional to the energy of the incident laser pulse.

The detector we used was a Gen-Tec model ED-200 fast response joulemeter and the output voltage was measured with an oscilloscope. The manufacturers specified a flat response from the visible to 30 μm wavelength. When measuring high power laser pulses a negative lens was inserted in front of the detector in order to slightly expand the beam, so reducing energy density and damage possibilities on the detector. The detector had a diameter of 23 mm and a damage threshold of 0,5 J/cm^2 for Q-switched laser pulses.

4.4.1.2 SILICON PIN PHOTODIODE

Laser pulse widths were measured with an HP 5082-4207 PIN photodiode and a storage oscilloscope. A PIN photodiode is essentially an ordinary photodiode (p-n junction) with an intrinsic semiconductor sand-

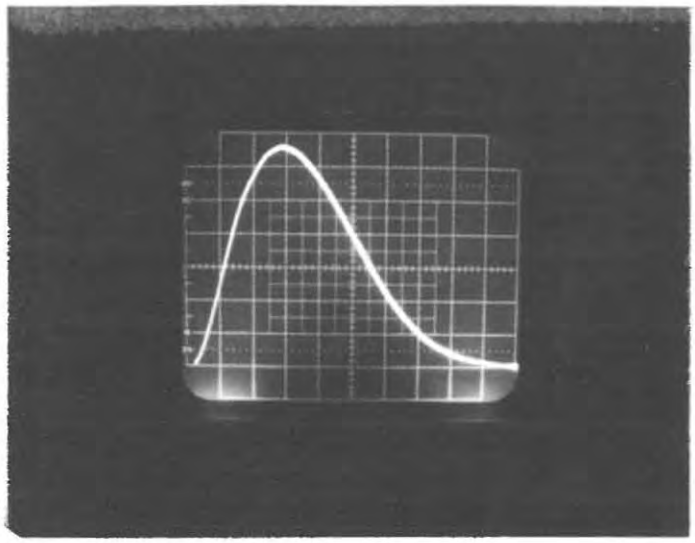

FIG. 4.11 A TYPICAL FLASHLAMP CURRENT PULSE
VERT. SCALE 80 A/div.
HORIZ. SCALE 20 μs/div.

wiched between the p-n regions, hence the name PIN. An intrinsic semiconductor is one doped to give equal numbers of holes and electrons, or undoped so that p=n. The PIN photodiode is operated reverse biased with the circuit shown in Fig. 4.12. In order to prevent saturation of the photodiode from the laser light, attenuation was provided by means of ground glass plates (scatter plates). The photodiode and scatter plates were mounted inside a closed box with a small opening, covered by a scatter plate, for the laser beam.

4.4.1.3 SILICON LINEAR PHOTODIODE ARRAY

The beam profiles of the laser were measured with a Reticon RL-64P solid state line scanner. It consisted of a row of 64 silicon photodiodes spaced on 50 μm centres each having a 41 μm x 50 μm aperture and covered with a quartz lid. Once again the processing electronics was designed by W van den Berg (1982). This enabled one to continuously observe the 64 elements on an oscilloscope. The beam profile was measured simply by placing the array in the beam after sufficient attenuation to prevent damage. In cases where the beam was larger than the array, photographs of the array output at three sections of the beam were obtained and joined together for the full profile (see section 5.3.3 and Figs. 5.7, 5.9, 5.10).

4.4.2 VOLTAGE AND CURRENT MEASUREMENTS

Static voltages like the flashlamp capacitor voltage were measured with a Fluke digital multimeter model 8022A together with a high voltage probe, Fluke 80K-40. For transient high voltages such as the voltage across the flashlamp during triggering, and Pockels cell voltages, a high voltage probe, Tektronix P6015(350 MHz), together with a storage oscilloscope, were used. Measurement of the flashlamp current pulses was done with a Rogowski coil, model 1025 from Pearson Electronics Inc. USA, and oscilloscope. The sensitivity was 40A/volt with 100 ns risetime.

4.4.3 OSCILLOSCOPE

All measurements were done with one fast, storage oscilloscope. This was a Tektronix 7633 (100 MHz) mainframe with a model 7A26 plug-in vertical amplifier and a model 7B80 plug-in timebase. The oscilloscope

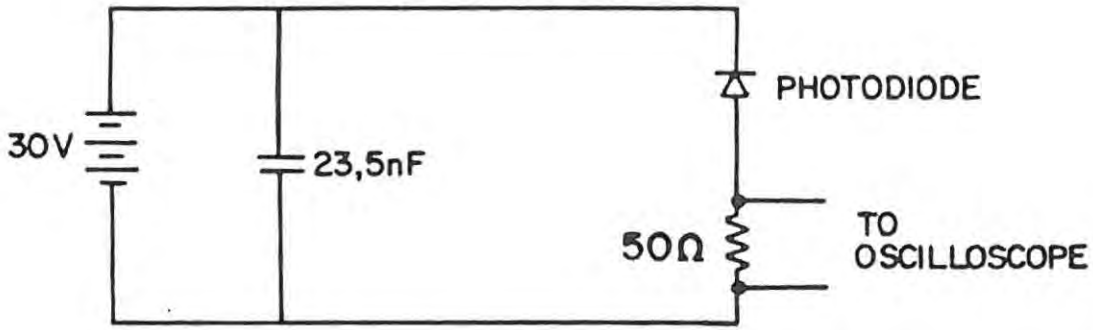

FIG. 4.12 CIRCUIT DIAGRAM OF PIN PHOTODIODE

was placed inside a Faraday cage to shield against electromagnetic interference. An isolation transformer was used in the power line of the oscilloscope to prevent voltage spikes on the line to the oscilloscope.

4.5 OPTICAL ALIGNMENT OF THE LASER

4.5.1 ALIGNMENT OF LASER ROD AND MIRRORS

The optical alignment of a laser employing an unstable resonator is a more complicated procedure than for a stable resonator. The small size of the output coupler mirror complicates matters even further. The usual techniques of using a He-Ne laser and aligning components by means of reflections back to the He-Ne laser failed to yield successful results. The fact that the output coupler consisted of two components (see Section 4.2.5) resulted in a large number of back reflected He-Ne spots and hence complete chaos for accurate alignment.

The alignment of unstable resonators has been the subject of a number of publications (Krupke & Sooy (1969), Koval'chuk & Sventsitskaya (1973), Hanlon & Aiken (1974), Chao & Schnurr (1984)). None of these papers provided exactly a technique which could be used by us, but a technique based on the ideas of Hanlon & Aiken (1974) was developed specifically for our purposes. The alignment procedure used a pellicle beamsplitter and a Davidson model D-275 alignment telescope together with a Schott (KL1500) fibre optic light source. A He-Ne laser was used for alignment of the back reflector mirror. The optical configuration for the alignment of the resonator is shown in Fig. 4.13 and is described below. It should be noted that the alignment was done before the insertion of the Pockels cell since it would have complicated matters as will be seen later.

The procedure was as follows:

(1) the telescope was aligned with respect to the laser rod via the beamsplitter so that its eyepiece cross hairs were centred on the laser rod and back reflections from the rod face were also centred.

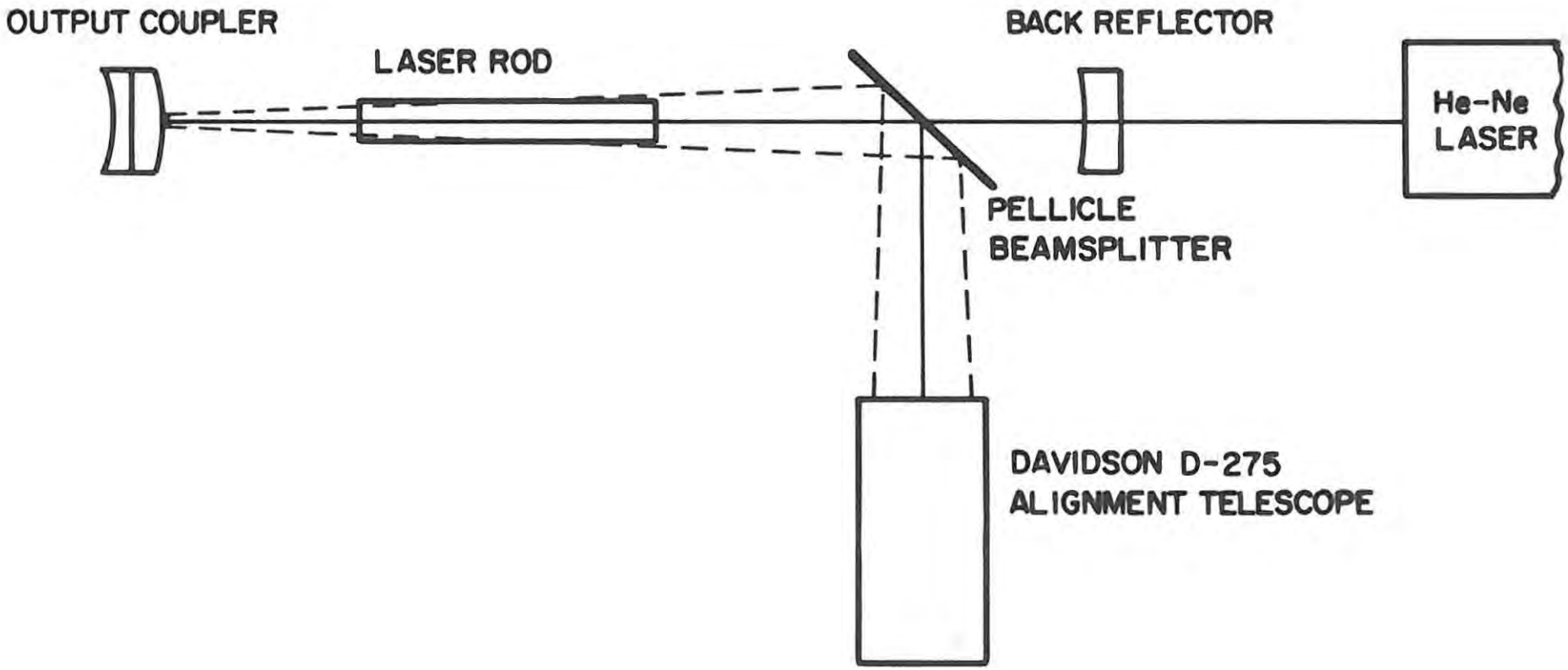

FIG. 4.13 DIAGRAM SHOWING THE METHOD OF ALIGNMENT OF THE LASER

(2) the He-Ne laser was aligned so that reflections from the laser rod surface were reflected by the beamsplitter into the telescope and onto the cross hairs. The use of a pellicle beamsplitter was essential so that the He-Ne laser beam was not displaced through the beamsplitter.

(3) next, the laser head was removed entirely from the U-channel after banking blocks had been positioned to mark its original position. The need for this was that the 6 mm laser rod aperture did not allow enough light from the telescope to the output coupler mirror and back again, hence the omission of the Pockels cell too.

(4) the output coupler mirror was then centred on to the telescope cross hairs by horizontal and vertical translations.

(5) the reflection from the output coupler was aligned by tilting of its mount. Due to the very weak reflection from the mirror, steps (4) and (5) were done in small alternate steps to accurately align and centre the mirror.

(6) the laser head was then replaced and its alignment confirmed.

(7) the beamsplitter was removed and the back reflector aligned with the He-Ne laser in the usual way.

This method of alignment was successful even on the first attempt. The laser could then be optimized by the adjustment of each mirror and observation of the burn mark of the beam on exposed polaroid film, as well as measurements of the laser output energy.

4.5.2 ALIGNMENT OF THE POCKELS CELL

A precision alignment technique for the Pockels cell is described by McCarthy (1973). This technique involves placing polarizers on either side of the Pockels cell with their axes crossed. In our case the integrally mounted polarizer of the Pockels cell was used as the one

polarizer. The He-Ne alignment laser was thus extinguished by this combination.

Insertion of a ground glass diffuser between the incoming polarizer and the Pockels cell results in a Maltese-cross pattern when observed on a screen. The Maltese-cross is produced by the different velocities of light transmitted along the oridinary and extraordinary axes of the birefringent crystal in the Pockels cell. This results in phase interference at the output end of the crystal and produces a cross surrounded by concentric rings of light and dark areas. By noting the relative positions of the cross and He-Ne laser beam, the cross can be superimposed over the laser beam by the tilt and translation facilities provided on the Pockels cell mount. Accurate optimization was done by observing the output energy and beam burn mark with the laser in operation.

CHAPTER 5

RESULTS AND DISCUSSION

5.1 INTRODUCTION

This chapter describes the experimental evaluation of the laser and will point out the differences between lasers using unstable resonators and other more conventional (stable) resonators. The experimental evolution of the laser from a single-shot, non-Q-switched device to a Q-switched, repetitively pulsed device is described.

5.2 SINGLE-SHOT, LONG-PULSE MODE OPERATION

In order to verify that it was possible to use an unstable resonator configuration at all, a single-shot, non-Q-switched laser was first built according to the design of Section 3.4.1. A list of the resonator and laser parameters is given here:

laser rod:	6,35 mm x 80 mm
pump reflector:	diffuse reflector
back reflector:	1 m radius of curvature (concave)
output coupler:	0,3 m radius of curvature (convex); 1,8 mm reflecting spot
output coupler to laser rod distance:	80 mm

With these components lasing was readily observed.

An efficiency curve between 10 and 20 J input energy for this single-shot device is shown in Fig. 5.1. It can be deduced that the lasing threshold is somewhat higher than that for a stable resonator system (typically 4J). This is understandable due to the much higher losses of unstable resonators over stable types.

As described in Section 2.3.1 the output of a non-Q-switched solid state laser is a train of pulses or relaxation oscillations extending

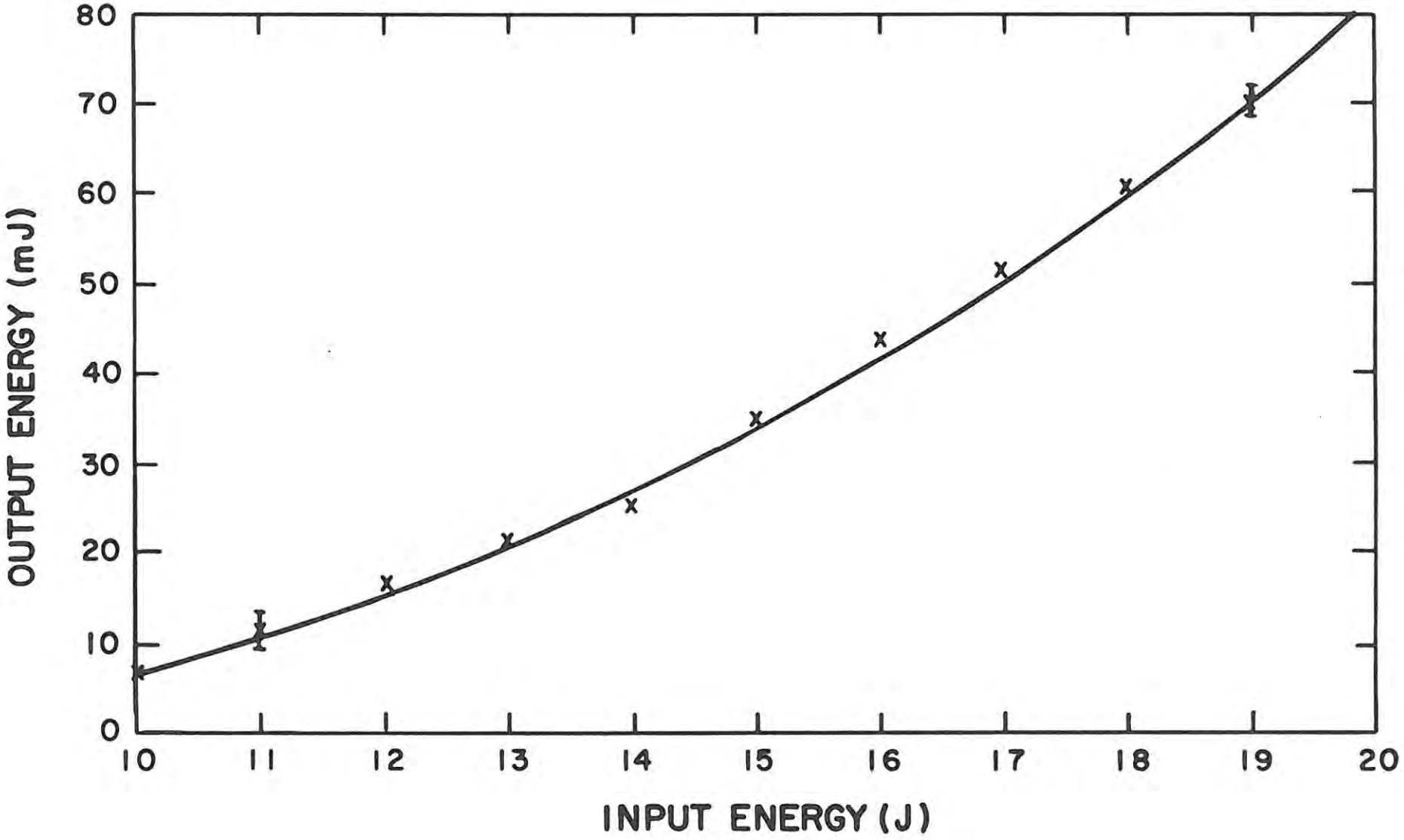

FIG. 5.1 SLOPE EFFICIENCY CURVE OF THE LASER (LONG-PULSE MODE)

over a number of microseconds. Such an output was observed and is shown in Fig. 5.2.

5.3 REPETITIVELY PULSED, Q-SWITCHED OPERATION

The pump cavity used in the repetitively pulsed experiments is also of the diffuse reflector type but was not the same cavity as used in 5.1 since the single-shot laser head has no facilities for the cooling of the laser rod and flashlamp.

5.3.1 OPTIMIZATION OF Q-SWITCH TIME DELAY

In Section 2.3.2 it was explained that the Q of the laser cavity is kept low until the population inversion is much larger than that required for the threshold of normal lasing, at which time the Q is made high.

The exact time at which the cavity Q is switched (relative to the flashlamp pulse) from a low to a high value is important for the extraction of the maximum amount of energy from the laser rod. If the Q is switched at a time before the inversion is a maximum, then lasing starts with a lower than maximum inversion resulting in a low output. Switching the Q at a time after the maximum inversion has been reached results in the population of the upper laser level decreasing by spontaneous emission and non-radiative processes. Robertson & Preussler (1982) have shown that as the switching time is increased, the peak power decreases while the laser pulse width increases. The speed (or risetime) of the switching voltage is also important. Effective Q-switched output requires risetimes of less than 100 ns. For risetimes greater than this value the laser pulse width increases and peak power decreases. For risetimes greater than 800 ns double pulsing of the laser output is observed.

Timing of the switching voltage must be optimized experimentally for each laser design since pumping, pump geometry and feedback determine the time of peak inversion. Even ageing of the flashlamp can cause peak inversion times to vary. As explained in Section 4.3 DIP switches

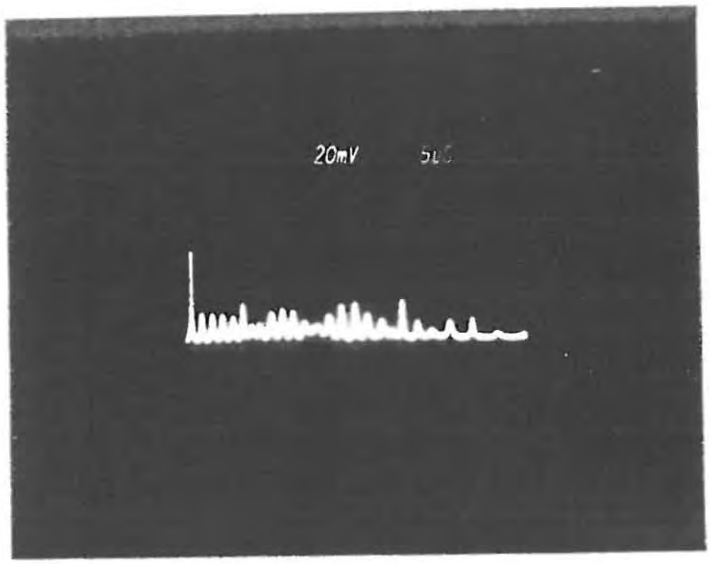

FIG. 5.2 RELAXATION OSCILLATIONS FROM THE NON-Q-SWITCHED LASER

enable one to adjust the Q-switching time relative to the start of the flashlamp pulse. Figure 5.3 shows the laser output energy as a function of the switching time or Pockels cell delay time. These measurements were done at an input energy of 25 J. Based on these results the Pockels cell delay time was set at 128 μs and remained at this setting throughout the experimental investigations which followed.

5.3.2 SLOPE EFFICIENCY OF THE LASER

The efficiency of the laser was measured for a range of input energies from 16 J to 36 J and is shown in Fig. 5.4. It can be seen that the threshold for lasing in this case is much higher than in the long-pulse mode case in Fig. 5.1. The reason for this is not clear at all since the insertion loss of the Pockels cell would be too low to account for this. A possible explanation is that the unstable resonator is a high loss system and would therefore be sensitive to, for example, a different pump cavity or laser rod. The reason for the slight curvature of the graph is not known, but a similar curvature is observed by Byer & Herbst (1978) for which no explanation is given. Other efficiency curves in the literature yield straight line graphs. Figure 5.5 gives a graphical comparison of Nd:YAG unstable resonator lasers already published.

5.3.3 DETERMINATION OF THE LASER BEAM PROFILES AND PARAMETERS

As mentioned in Chapter 1, one of the major advantages of unstable resonators is the superior beam quality which they provide. In particular they discriminate against higher order transverse modes and consequently provide low divergence beams. The necessity for measuring near- and far-field beam profiles is that despite the near-field "hole" in the profile, in the far-field the profile is "filled in" to yield a Gaussian shaped beam which has useful applications in, for example, the field of non-linear optics for stimulated Raman scattering and harmonic generation.

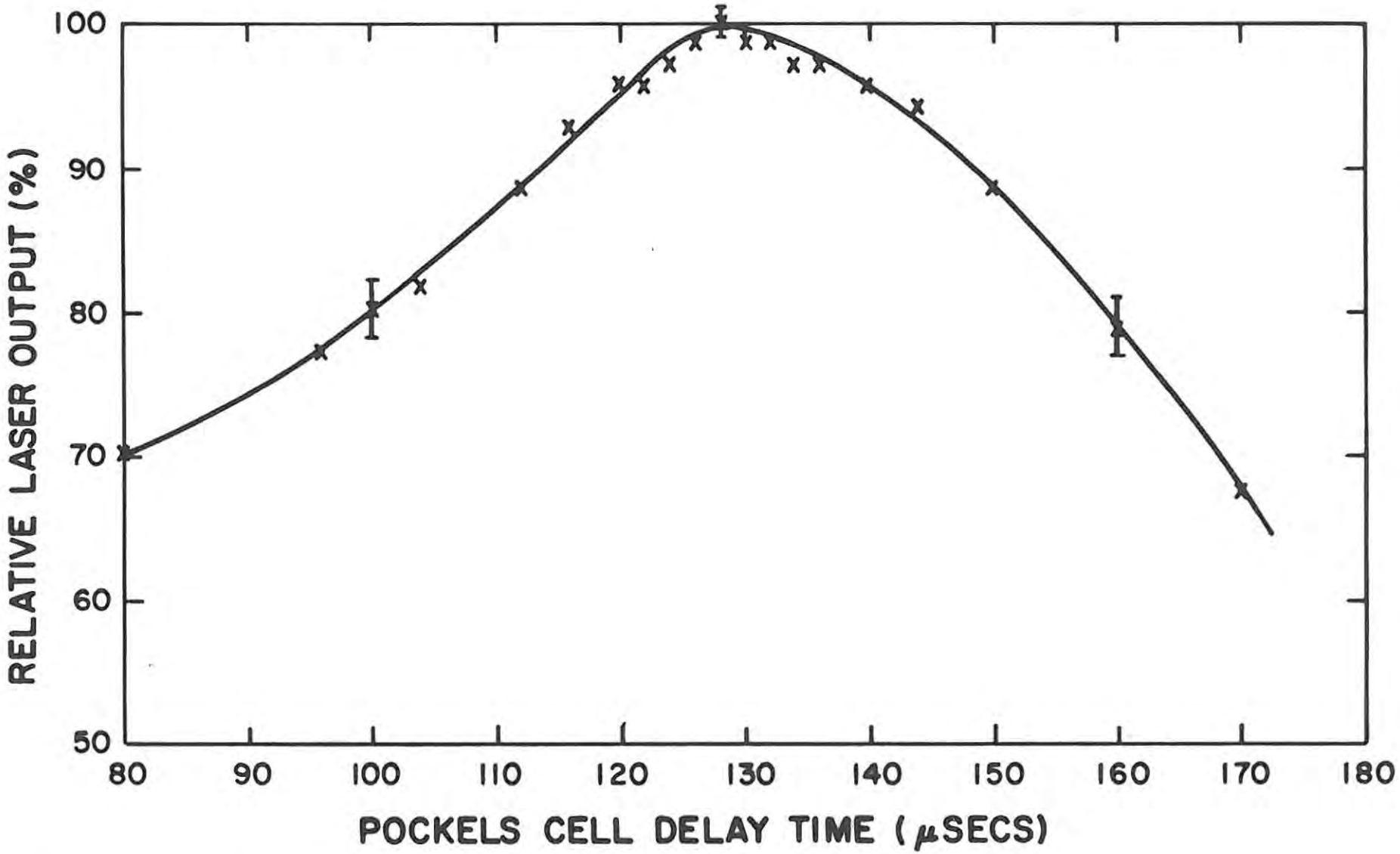

FIG. 5.3 LASER OUTPUT AS A FUNCTION OF POCKELS CELL DELAY TIME

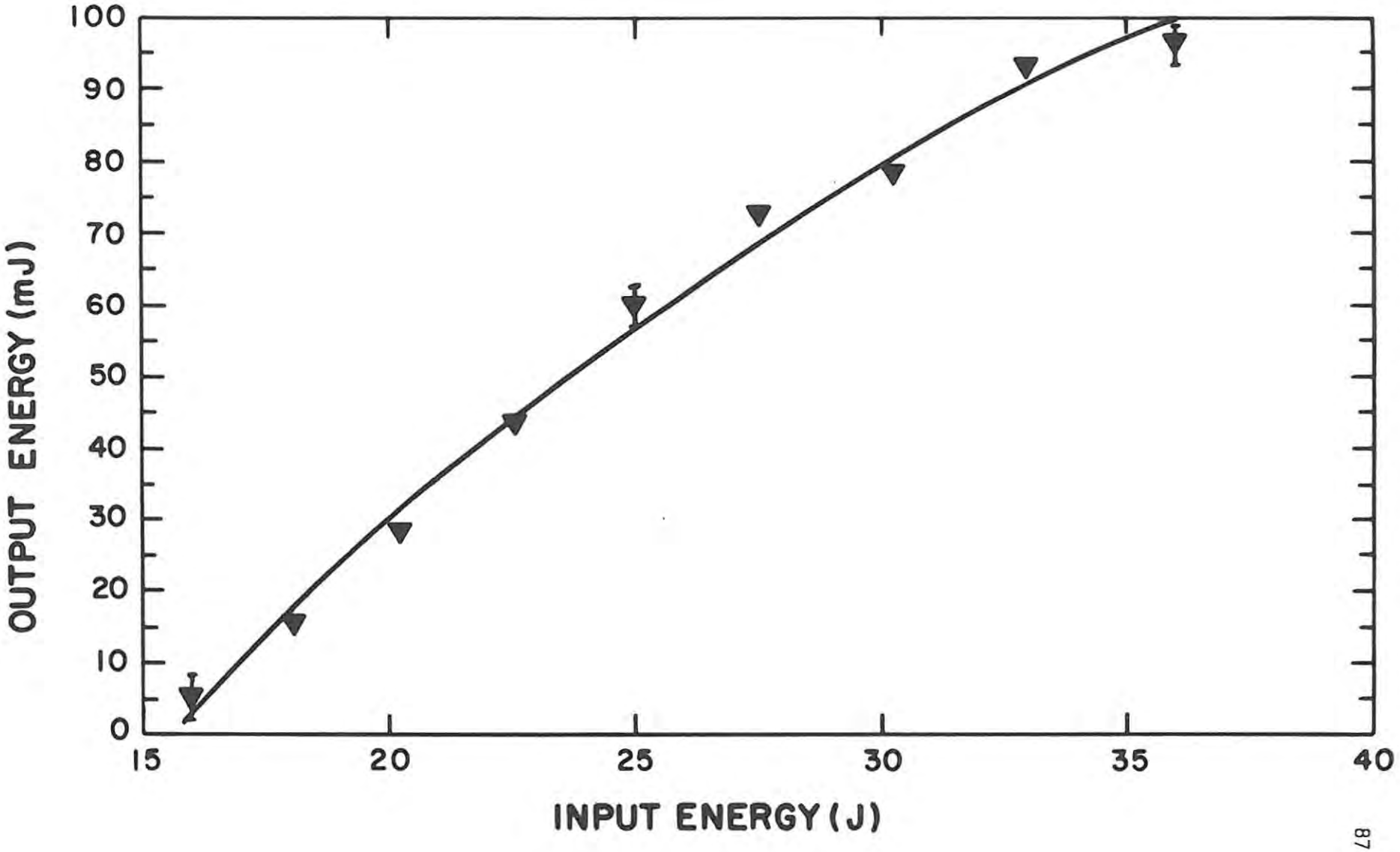

87

FIG. 5.4 SLOPE EFFICIENCY OF THE Q-SWITCHED LASER

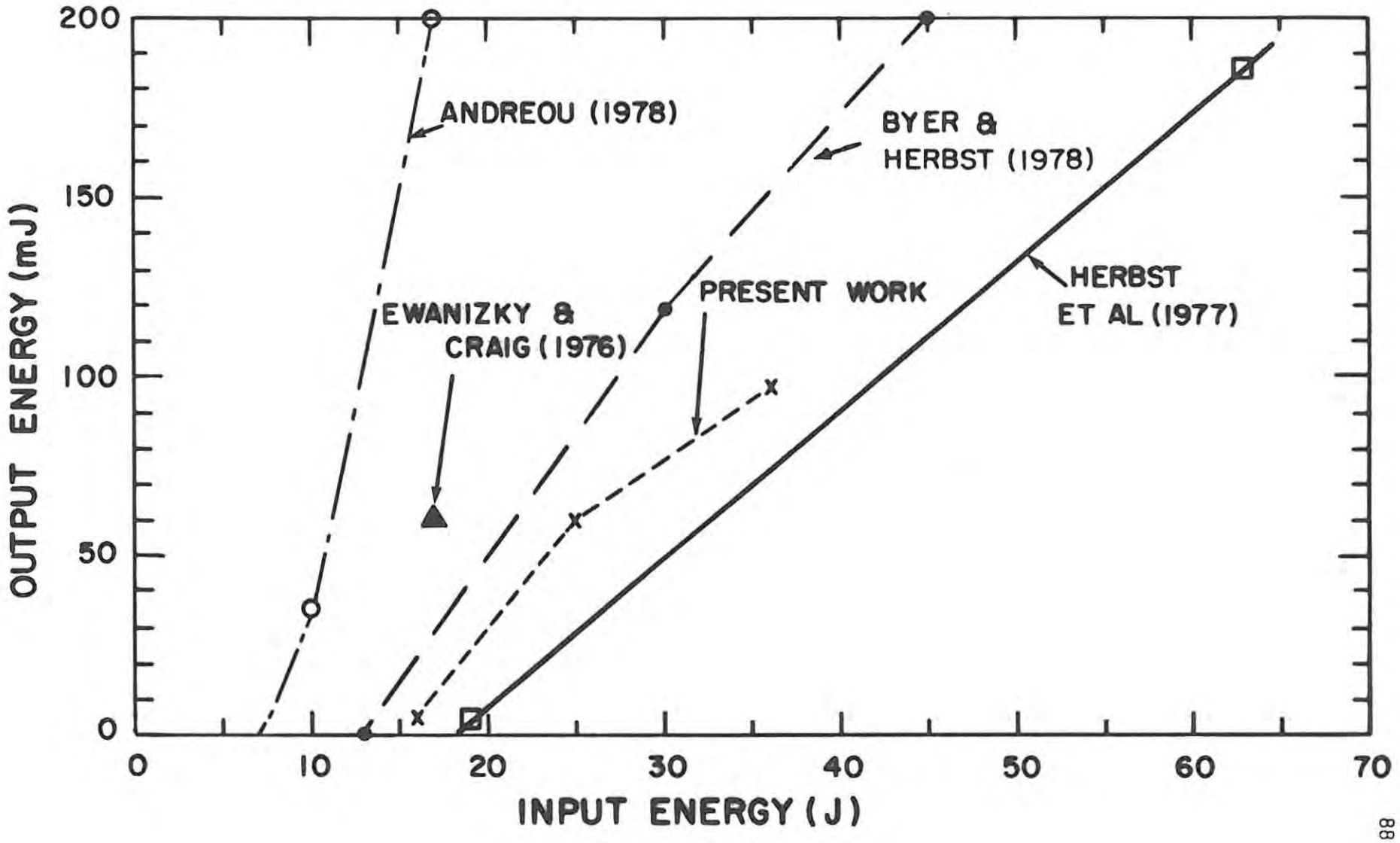

FIG. 5.5 COMPARITIVE CURVE OF EXISTING UNSTABLE RESONATOR Nd:YAG LASERS

5.3.3.1 MEASUREMENT OF THE INTERNAL LASER INTENSITY PROFILE

In stable resonator lasers the measurement of the internal intensity profile is achieved simply by observing the intensity profile of the outcoming beam close to the output mirror, since the output coupler is semi-transparent. The lowest order mode has a Gaussian intensity variation across the beam. In unstable resonators, however, the output is diffracted around the output coupler and transforms rapidly with distance so a more exact picture can only be obtained by observing the internal profile directly. Only one paper was found in the literature (Freiberg et al (1972)) which experimentally observed the internal beam profile and this was that of a CO_2 laser. Most papers dealing with unstable resonator lasers simply assume that the internal profile is uniform in intensity as predicted by the simple geometrical approximation (see Section 3.3).

Figure 5.6 shows the experimental setup which was used to determine the internal beam profile. A wedged plate (wedge angle ≈ 44 minutes, thickness ≈ 2,5 mm) was inserted in the resonator as close as possible to the output coupler and at a small angle so that the reflected beam passed unobstructed out of the resonator. One side of the plate was AR coated for 1 µm to reduce reflections while the other side was uncoated. Plane parallel plates and plates with very small wedges (≈ 3 min) were not suitable since they resulted in interference fringes being observed even if one surface was AR coated. The photodiode array (Section 4.4.1.3) was used to observe the vertical cross section of the reflection of the internal beam.

It should be noted that the insertion of a wedged plate into the resonator causes such optical axis deviations that realignment and recentring of the output coupler is necessary. After alignment of the output coupler the output energy of the laser was reduced by approximately 15 %.

The results of these investigations are shown in Fig. 5.7. An oscilloscope trace of a vertical section through the beam is shown together with a photographic recording of the beam made with a polaroid camera

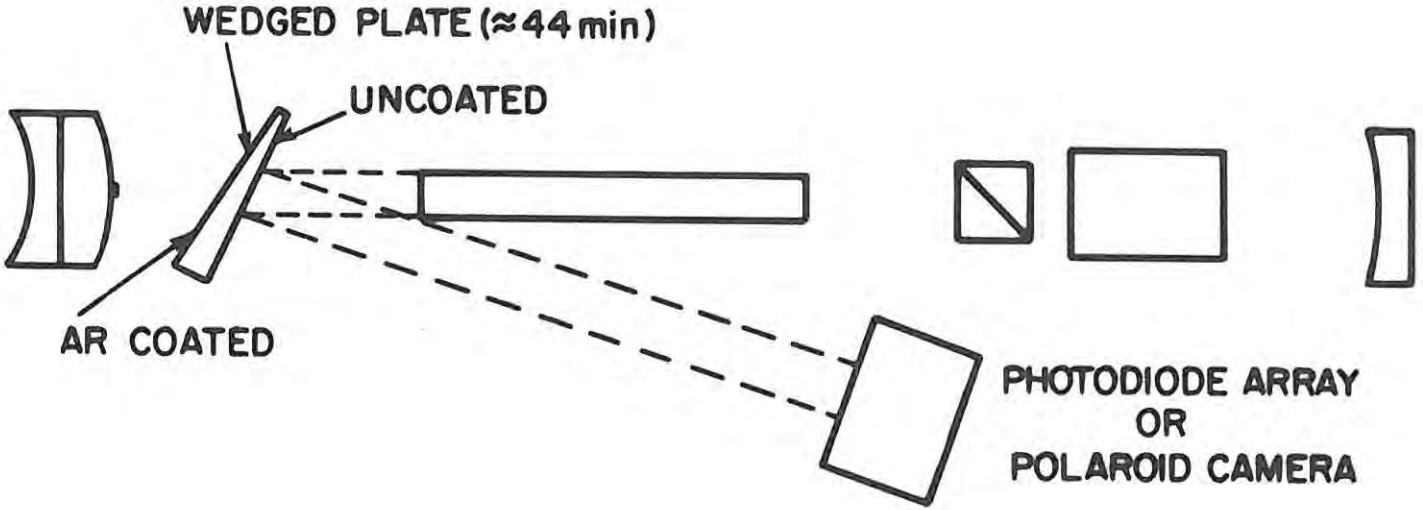

FIG. 5.6 DIAGRAM ILLUSTRATING THE METHOD OF MEASURING THE INTERNAL INTENSITY PROFILE OF THE LASER

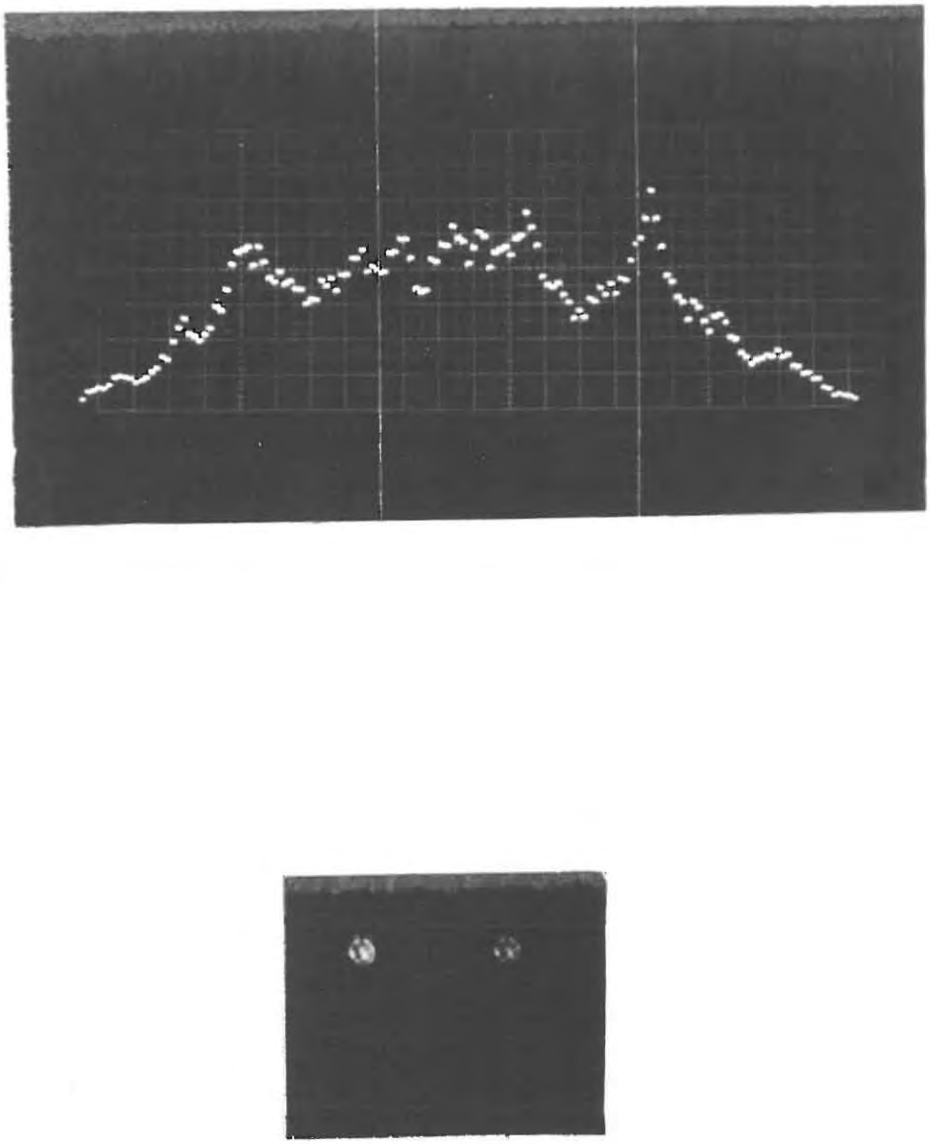

FIG. 5.7 OSCILLOSCOPE TRACE OF PHOTODIODE ARRAY SCAN OF THE INTERNAL LASER INTENSITY PROFILE TOGETHER WITH A PHOTOGRAPHIC RECORDING

back. Evident from the figure is the distinct ring shaped structure of the beam. According to the theoretical computer analysis of transverse mode structure (Section 3.3 and Siegman & Arrathoon (1967)) this concentric ring type structure is expected. The ring structure is explainable in terms of the Fresnel diffraction of light from the edge of the output coupler and the Nd:YAG rod (Byer & Herbst (1978)). It is important to note that the intensity is not radially uniform over the laser rod as assumed by the simpler unstable resonator analyses.

5.3.3.2 NEAR-FIELD BEAM PROFILE

Measurement of the near-field profile of the beam was achieved with the arrangement as shown in Fig. 5.8. Strong attenuation was achieved by reflecting the outcoming laser beam from two polished glass surfaces with ground backs. Further attenuation was achieved with neutral density filters and an RG 830 filter was used to discriminate against the flashlamp radiation. The photodiode array was mounted on an X-Y translation stage and was placed at approximately 35 cm from the output coupler. The results of this experiment can be seen in Fig. 5.9 together with burn marks in the near-field. The conditions under which the experiment was carried out were at 1,25 Hz and 25 J input energy. For comparison the experiment was repeated at a repetition rate of 10 Hz and the results are shown in Fig. 5.10. The resonator length was adjusted to compensate for thermal lensing. The burn marks in the figures clearly show the Poisson (or Arago) spot in the middle surrounded by some diffraction rings. The Poisson spot develops in the centre of the beam in the geometrical shadow of the mirror and its existence is explainable in terms of the Fresnel diffraction of light about a circular obstacle (Klein (1970)).

5.3.3.3 FAR-FIELD BEAM PROFILE AND BEAM DIVERGENCE

(i) Theoretical far-field diffraction pattern

Spherical wave analyses of unstable resonators predict the lowest order internal transverse mode as having a uniform intensity. Computer simulations (see Section 3.3) and our experimental investigations show a pronounced departure from the uniform intensity distribution. Nevertheless, one still finds in the published literature (Hanna & Laycock (1979), Ewanizky & Craig (1976)) that comparisons are made between the

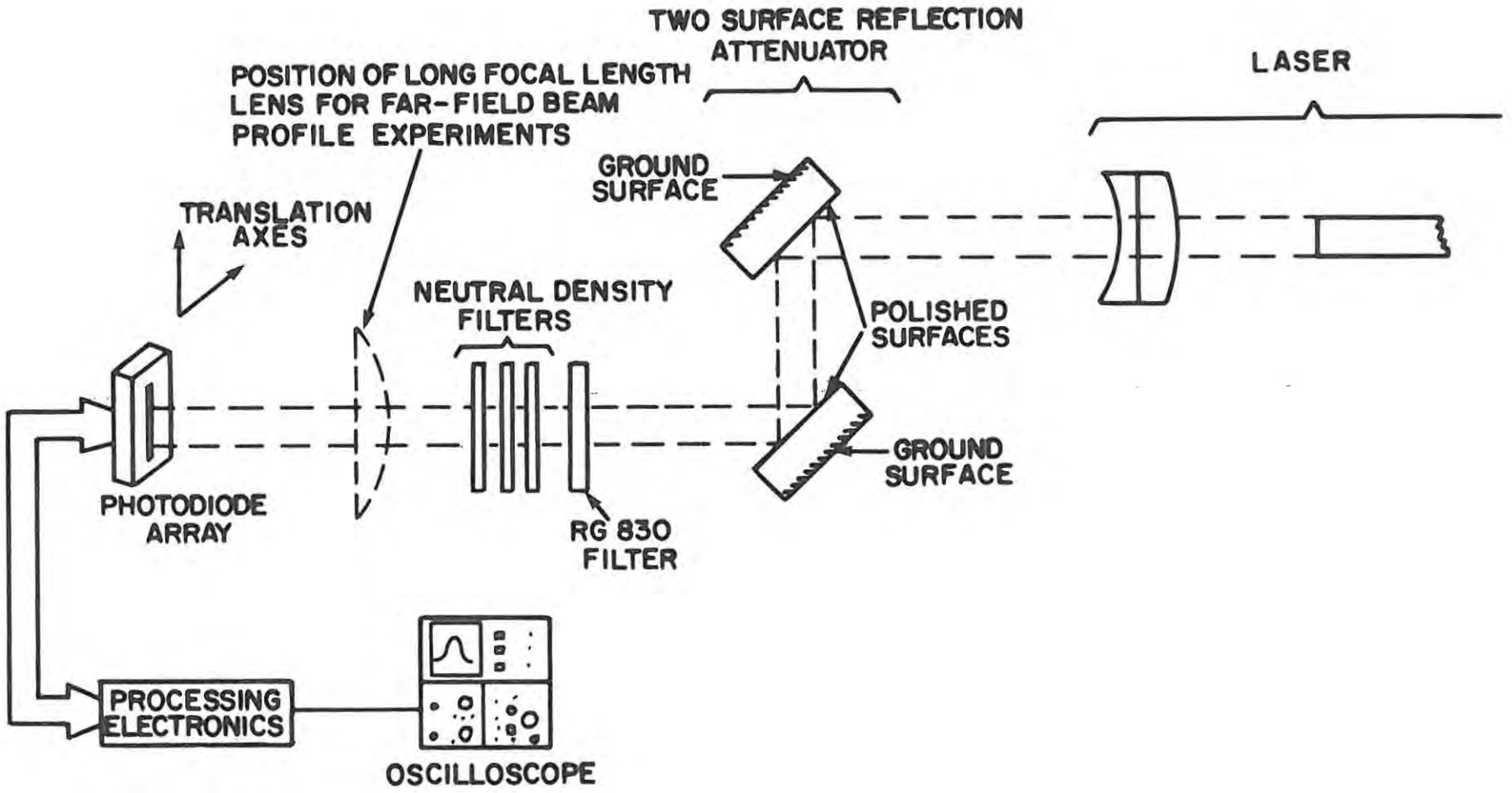

FIG. 5.8 DIAGRAM SHOWING THE METHOD OF MEASURING NEAR- AND FAR-FIELD INTENSITY PROFILES OF THE LASER

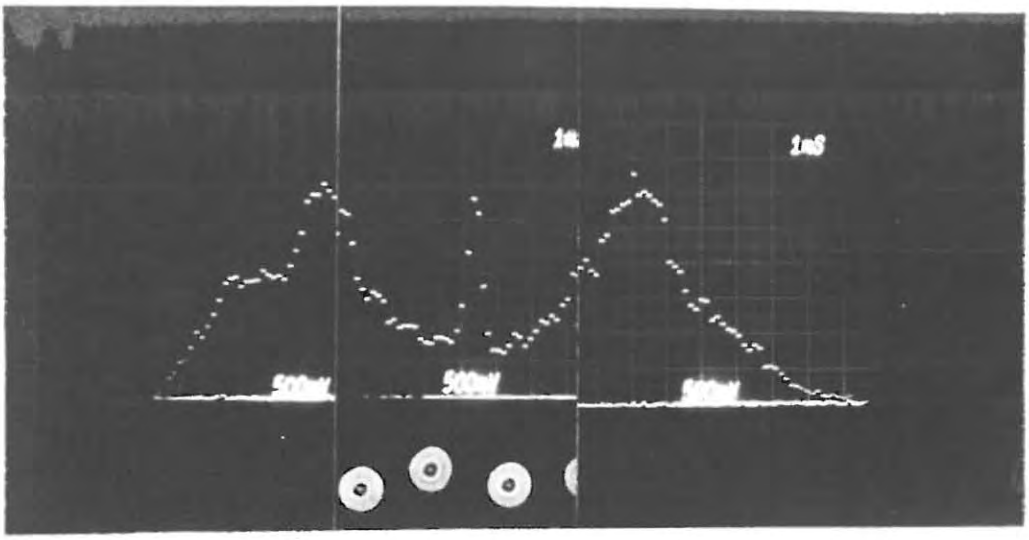

FIG. 5.9 NEAR-FIELD PROFILE OF LASER BEAM AT 1,25 Hz; 25 J

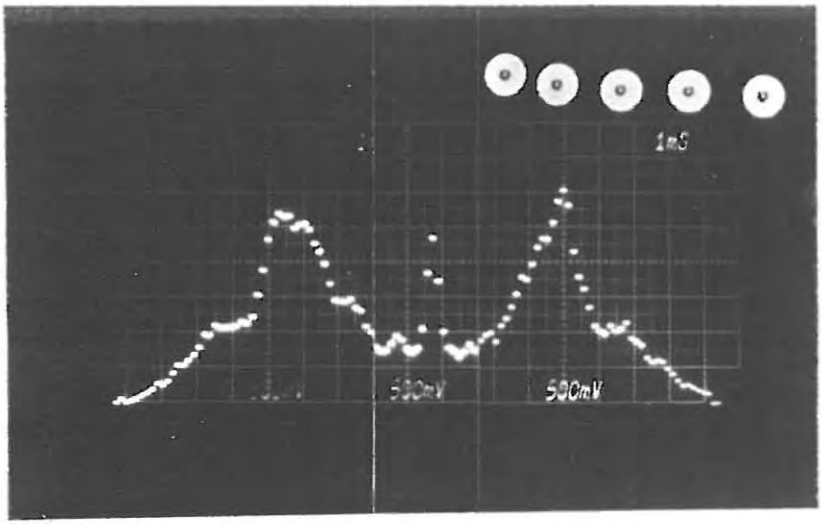

FIG. 5.10 NEAR-FIELD PROFILE OF LASER BEAM AT 10 Hz; 25 J

diffraction pattern of a uniformly illuminated annulus and the far-field diffraction pattern of a solid-state unstable resonator. The most likely explanation for this is the difficulty or perhaps the impossibility of being able to describe the internal mode profile in a mathematically simple or rigorous way. The correspondence between the experiment and the simple theoretical model is, nevertheless, usually remarkably good. We will also compare the experimental results to the simple model of uniform illumination.

The illumination of an annular aperture bounded by two concentric circles of radii a and εa, where $o<\varepsilon<1$, by a uniform plane wave results in a Fraunhofer pattern with an intensity distribution given by (Born & Wolf (1980))

$$I = \frac{1}{(1-\varepsilon^2)^2}\left[\left(\frac{2\ J_1(kas)}{kas}\right) - \varepsilon^2\left(\frac{2\ J_1(\varepsilon kas)}{\varepsilon kas}\right)\right]^2 \ I_o$$

where I_o is the intensity in the centre of the pattern

$J_1(x)$ is the first order Bessel function

$k = \frac{2\pi}{\lambda}$ is the wave number

$s = \sin\theta$ is the sine of the angle at any point in the pattern measured relative to the central direction

The zeros of intensity are given by the roots of the equation

$$J_1(kas) - \varepsilon J_1(k\varepsilon as) = 0 \quad (s \neq 0)$$

In our experimental arrangement we have $a = \frac{1}{2}$ (6,35) mm (due to rod) and $\varepsilon a = \frac{1}{2}$ (1,8) mm (due to output coupler) so $\varepsilon = 0{,}28$. Born & Wolf (1980) state that for the unobstructed aperture ($\varepsilon = 0$) the first zero occurs at

$$s = \frac{0{,}61\ \lambda}{a}$$

while for $\varepsilon = \frac{1}{2}$, $\quad s = \frac{0{,}50\ \lambda}{a}$

Using tables of Bessel functions we can show that for $\varepsilon = 0,28$

$$s = \frac{0,56\ \lambda}{a}$$

and since $s = \sin\theta \approx \theta$ for θ small in radians we get

$$\theta = \frac{0,56\ \lambda}{a}$$

Substituting for λ and a we get that the angle to the first minimum is 0,187 mrad.

(ii) Measurement of far-field beam parameters

In many laser applications the quality of the beam in the far-field is an extremely important factor. For applications where the beam is transmitted over long distances, for example, a low beam divergence is desirable. The far-field beam profile and the beam divergence of the laser were measured by observations in the focal plane of a long focal length lens.

If the focal length of the focussing lens is f and the full-angle beam divergence of the incoming laser beam is θ, then the size of the focussed spot in the focal plane of the lens is given approximately by

$$D = f\theta$$

The derivation of this formula is given in Appendix II.

So by measuring the size of the focussed spot and knowing the focal length of the lens one can determine the beam divergence of the laser. The longer the focal length of the lens, the better is the accuracy of the measurement.

The far-field beam profile and the beam divergence were measured with the photodiode array in the focal plane of a long focal length lens. The focussing lens was positioned just after the attenuator and filters as shown in Fig. 5.8. The results of the experiment are shown in Fig. 5.11 for two different focal length lenses used, a 2 m lens and a 6,417 m lens, both plano-convex. The shorter lens was used to show the

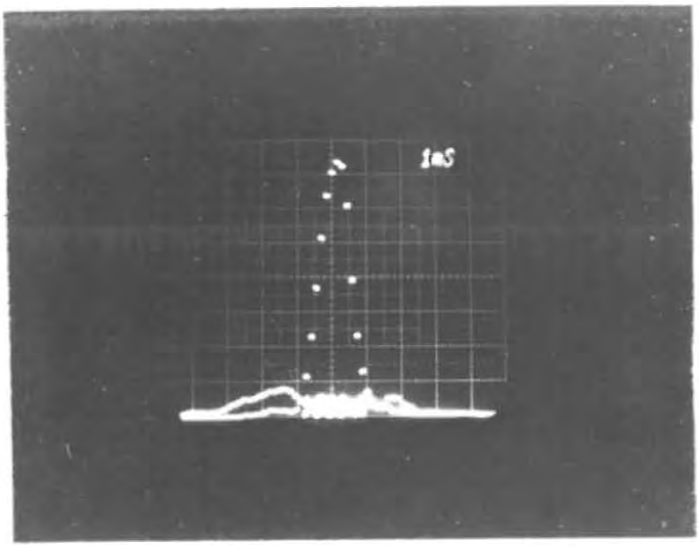

(a)

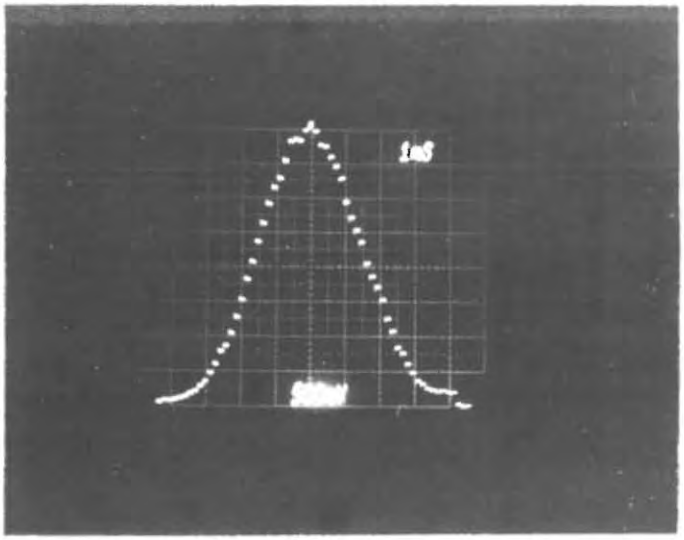

(b)

FIG. 5.11 FAR-FIELD PROFILES OF LASER BEAM

(a) 2 m FOCUSSING LENS

(b) 6,417 m FOCUSSING LENS

complete beam profile since with the longer lens the spot size is larger than the array size so that the side lobes are not seen. It can be seen that the side lobes of the far-field profile are very small and thus contain very little energy. A similar result was published by Byer & Herbst (1978). From the long focal length picture we can measure the beam divergence and the angle subtended by the first minimum. The beam divergence is measured at the $(1/e^2)$ points of the intensity and it can be seen to be represented by approximately 38 diodes. This corresponds to a beam size of 1,9 mm and a full-angle beam divergence of 0,296 mrad. This value of divergence is smaller than those quoted in the literature, for example,

Herbst et al (1977)	0,5 mrad (half-angle)
Andreou (1978)	0,25 mrad (not stated but appears half-angle)
Hanna & Laycock (1979)	0,25 mrad (half-angle)
Ewanizky & Craig (1976)	2 mrad (full-angle)

The angle subtended by the first minimum corresponds approximately to 28 diodes or 0,22 mrad. This is slightly larger than the value of 0,19 mrad calculated according to the diffraction of a uniformly illuminated annulus. As we have seen, the internal intensity profile of the laser is far from being uniformly illuminated and this is likely to cause a departure from the theoretical value. Slightly greater values for experimental cases compared to theoretical predictions have also been published in the literature (Ewanizky & Craig (1976) and Freiberg et al (1972)).

5.3.4 SENSITIVITY OF MIRRORS TO MISALIGNMENT

In this section a simple geometrical model for the sensitivity of an unstable resonator to mirror misalignment will be given. Included is the effect of mirror misalignment on beam steering angle of the output beam. The experimentally observed misalignment effects are given and compared to the simple model.

5.3.4.1 SIMPLE GEOMETRICAL MODEL FOR MIRROR MISALIGNMENT SENSITIVITY

A view commonly held in this field is that unstable resonators, and particularly the positive branch type, suffer from the disadvantage of sensitivity to mirror misalignment. "Small" tilts tend to steer the output beam while "large" tilts cause the output beam to deteriorate and may prevent lasing action completely.

In contrast to stable resonators, in an unstable resonator there is only one stationary light ray that does not walk out of the resonator. This ray is the optical axis and determines the direction of propagation of the output beam.

The treatment of misalignment sensitivity of the unstable resonator is based on the geometry shown in Fig. 5.12 and has been treated previously by Krupke & Sooy (1969) who investigated an unstable resonator CO_2 laser system. The laser rod is excluded from the treatment as it will be seen that lasing ceases due to the optical axis missing the output coupler completely before the axis misses the laser rod.

(i) Back reflector

Tilting the back reflector, M_2, by α with respect to its aligned condition moves the optical axis (ray through both centres of curvature) from its aligned position qc_1 to oc_1 (Fig. 5.12(a)). The direction of propagation of the output beam is then tilted by an angle ϕ (beam steering angle). The optical axis moves vertical distances h_1 and h_2 at M_1 and M_2, respectively. By geometrical considerations and assuming small angles it can be seen that:

$$\phi = \frac{\alpha R_2}{R_1 + R_2 - L}$$

$$h_1 = \phi \left| R_1 \right|$$

$$h_2 = \phi (L - R_1)$$

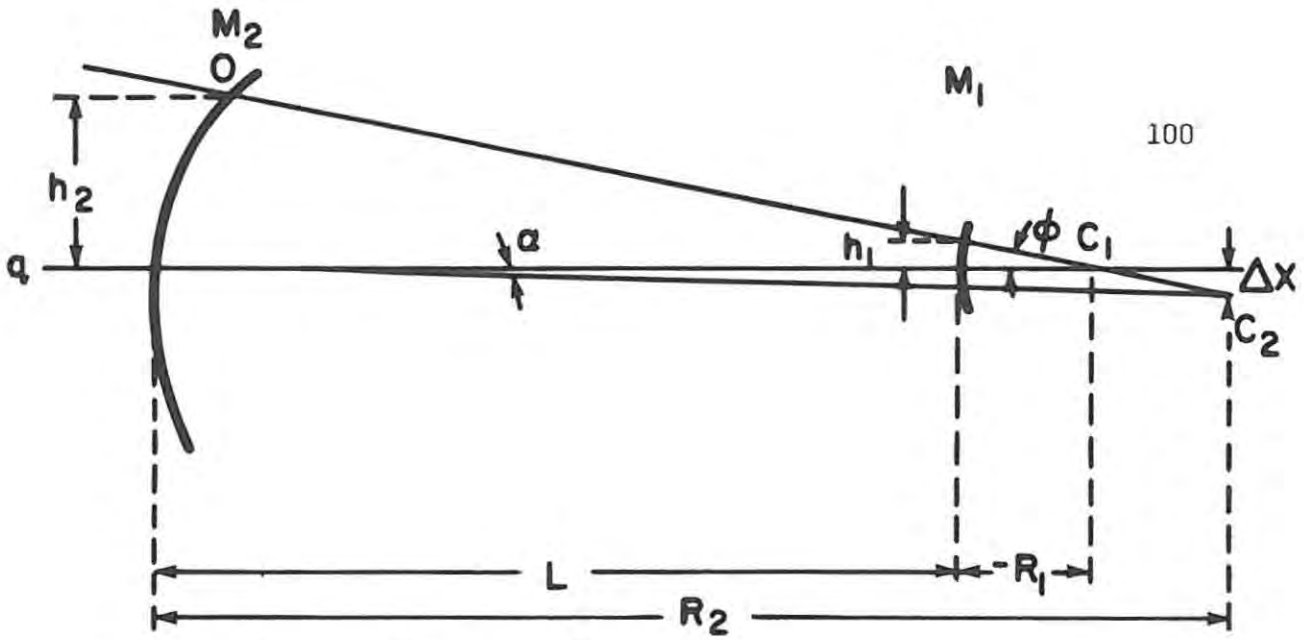

$$\phi = \frac{h_1}{|R_1|} = \frac{h_2}{L-R_1} = \frac{\Delta X}{R_2-(L-R_1)}$$

$$\alpha = \frac{\Delta X}{R_2} \text{ or } \Delta X = \alpha R_2 \text{ substituting gives}$$

$$\phi = \frac{\alpha R_2}{R_1+R_2-L} \text{ (Note that } R_1 \text{ is a negative distance)}$$

(a)

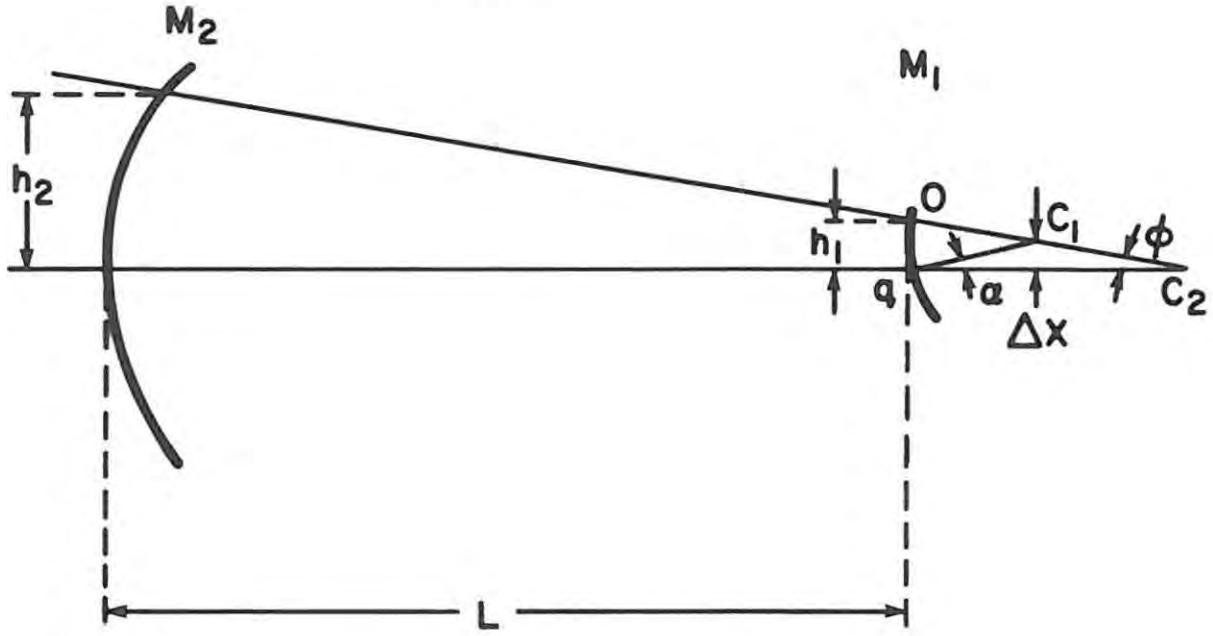

(b)

FIG. 5.12 GEOMETRICAL REPRESENTATION OF MIRROR MISALIGNMENT
(a) BACK REFLECTOR
(b) OUTPUT COUPLER

where R_1 and R_2 are the mirror radii and a convex mirror is defined to have a negative radius (see Section 3.2). Using equation (3.6) and (3.7)

$$R_1 = -\frac{2L}{M-1} \tag{3.6}$$

$$R_2 = \frac{2ML}{M-1} \tag{3.7}$$

we can obtain the above equations in terms of magnification and resonator length

$$\phi = \frac{2\,\alpha\,M}{M-1}$$

$$h_1 = \frac{4L\,\alpha\,M}{(M-1)^2}$$

$$h_2 = \frac{2L\,\alpha\,M(M+1)}{(M-1)^2}$$

We can make an order of magnitude calculation to find the maximum values of beam steering angle and tilt angle. The resonator length is approximately 400 mm. Lasing ceases when the optical axis misses the output coupler, i.e. when $h_1 > 0{,}9$ mm. Using $M = 3{,}56$ we get from the above equations

$$\alpha_{max} = 1{,}04 \text{ mrad} = 3{,}56 \text{ min}$$
$$\phi_{max} = 2{,}88 \text{ mrad} = 9{,}9 \text{ min and } \phi = 2{,}78\,\alpha$$

i.e. lasing should cease when the mirror is tilted by 3,56 min from its aligned condition. A graph of ϕ versus α is given in Fig. 5.16 and 5.17. A simple calculation shows that the optical axis would always pass through the laser rod and on these grounds it was omitted from the model.

(ii) Output coupler

Figure 5.12(b) shows the geometry for a tilt of the output coupler by an angle α. The symbols have the same meaning as for the previous case. By similar arguments it can be found that:

$$\phi = \frac{-\alpha R_1}{R_1 + R_2 - L}$$

$$h_1 = (R_2 - L)\phi$$

$$h_2 = R_2\phi$$

and on substituting for R_1 and R_2 we get

$$\phi = \frac{2\alpha}{M - 1}$$

$$h_1 = \frac{2L\,\alpha(M + 1)}{(M - 1)^2}$$

$$h_2 = \frac{4L\,\alpha\,M}{(M - 1)^2}$$

An order of magnitude calculation as done previously shows that

α_{max} = 1,62 mrad = 5,56 min

ϕ_{max} = 1,27 mrad = 4,35 min and ϕ = 0,78 α

A graph of ϕ versus α is given in Fig. 5.18.

5.3.4.2 EXPERIMENTAL RESULTS

(i) Misalignment effects on laser energy

The tilt of the 100 % mirror about vertical and horizontal axes and its effect on the energy of the laser are shown in Fig. 5.13. It can be seen that if we were to arbitrarily accept a 10 % drop in the output energy then a misalignment of the mirror of 0,5 mrad (from aligned position) could be tolerated. Lasing ceases when the mirror has been

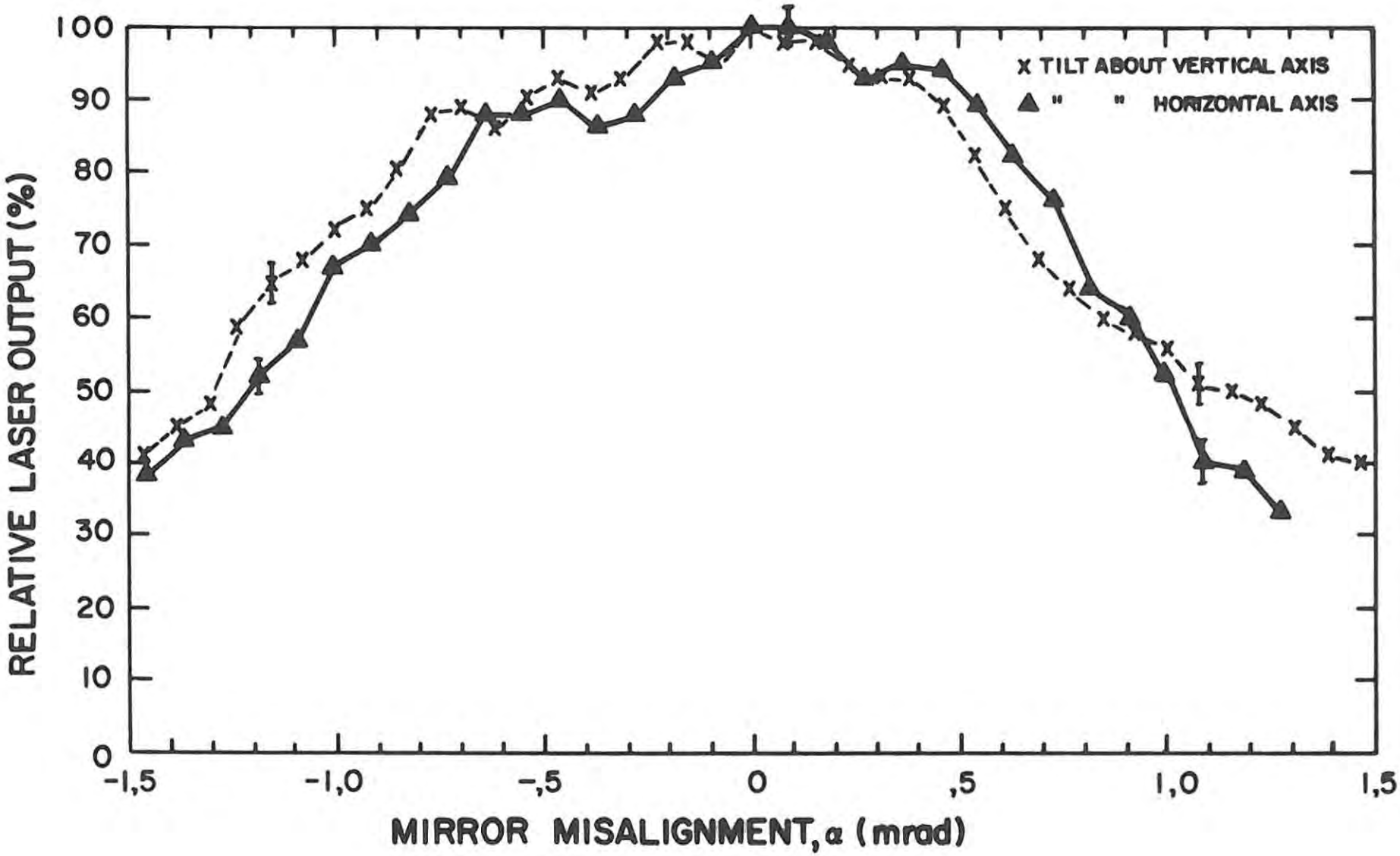

FIG. 5.13 LASER OUTPUT VERSUS MIRROR MISALIGNMENT (BACK REFLECTOR)

tilted approximately 2,3 mrad about a vertical axis and 2 mrad about a horizontal axis from its aligned condition. These figures are considerably larger than that predicted by the simple model (1,04 mrad).

Laser output energy as a function of output coupler tilt is shown in Fig. 5.14. A tolerance of 10 % energy drop would allow a mirror tilt of 0,7 mrad from the 100 % position. This is larger than the corresponding tilt of the back reflector showing that the back reflector is more sensitive to misalignment than the output coupler in agreement with theoretical predictions. For this reason the output coupler was mounted on a structure with a longer leverage. Lasing ceases when the mirror has been tilted by 4,4 mrad about a vertical axis and 3,5 mrad about a horizontal axis. Once again these values are considerably larger than that predicted by the simple model (1,62 mrad).

A very interesting fact arises when the misalignment sensitivity is compared to that of other resonators. According to the literature one of the main disadvantages of unstable resonators is their sensitivity to misalignment. Our results tend to contradict this statement. In Fig. 5.15 we show the alignment sensitivity of a stable cavity 30 cm long and with mirrors of 3 m radius of curvature (Roberton & Preussler (1982)), and our results from the sensitivity of the back reflector about a horizontal axis. Tilt about a horizontal axis was chosen for the comparison since from Fig. 5.13 and 5.14 it can be seen that its sensitivity is most marked.

Krupke & Sooy (1969) successfully used the theoretical model described above to account for misalignment sensitivity in a CO_2 unstable resonator. Even the predictions given by this model in our case, although not comparable to the experimental results, yield much larger misalignment angles than for the stable case.

(ii) Effects of mirror misalignment on far-field beam steering angle

The effect of mirror misalignment on the beam steering angle in the far-field was measured with the same configuration as shown in Fig. 5.8. The linear photodiode array was mounted on an X-Y translation

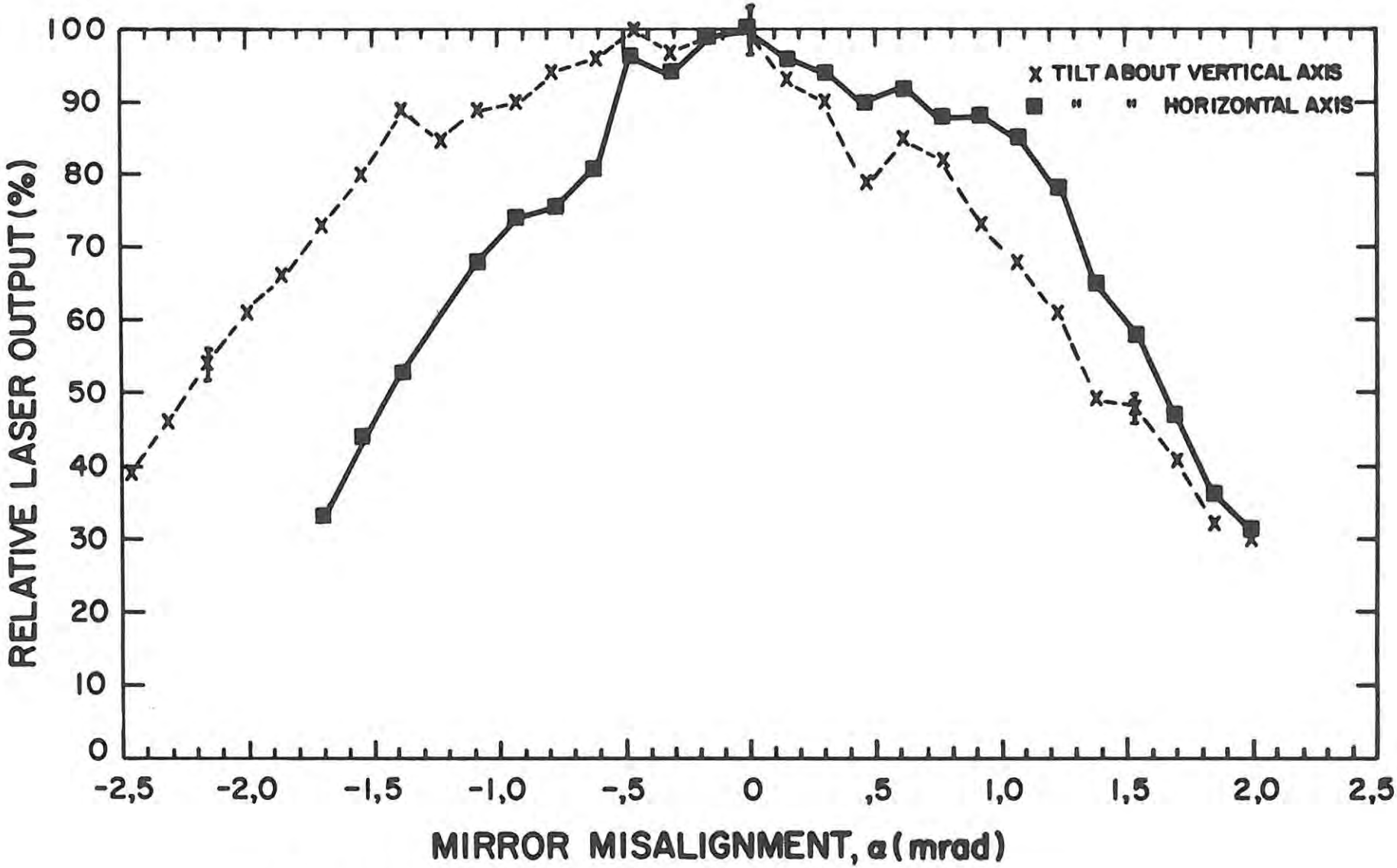

FIG. 5.14 LASER OUTPUT VERSUS MIRROR MISALIGNMENT (OUTPUT COUPLER)

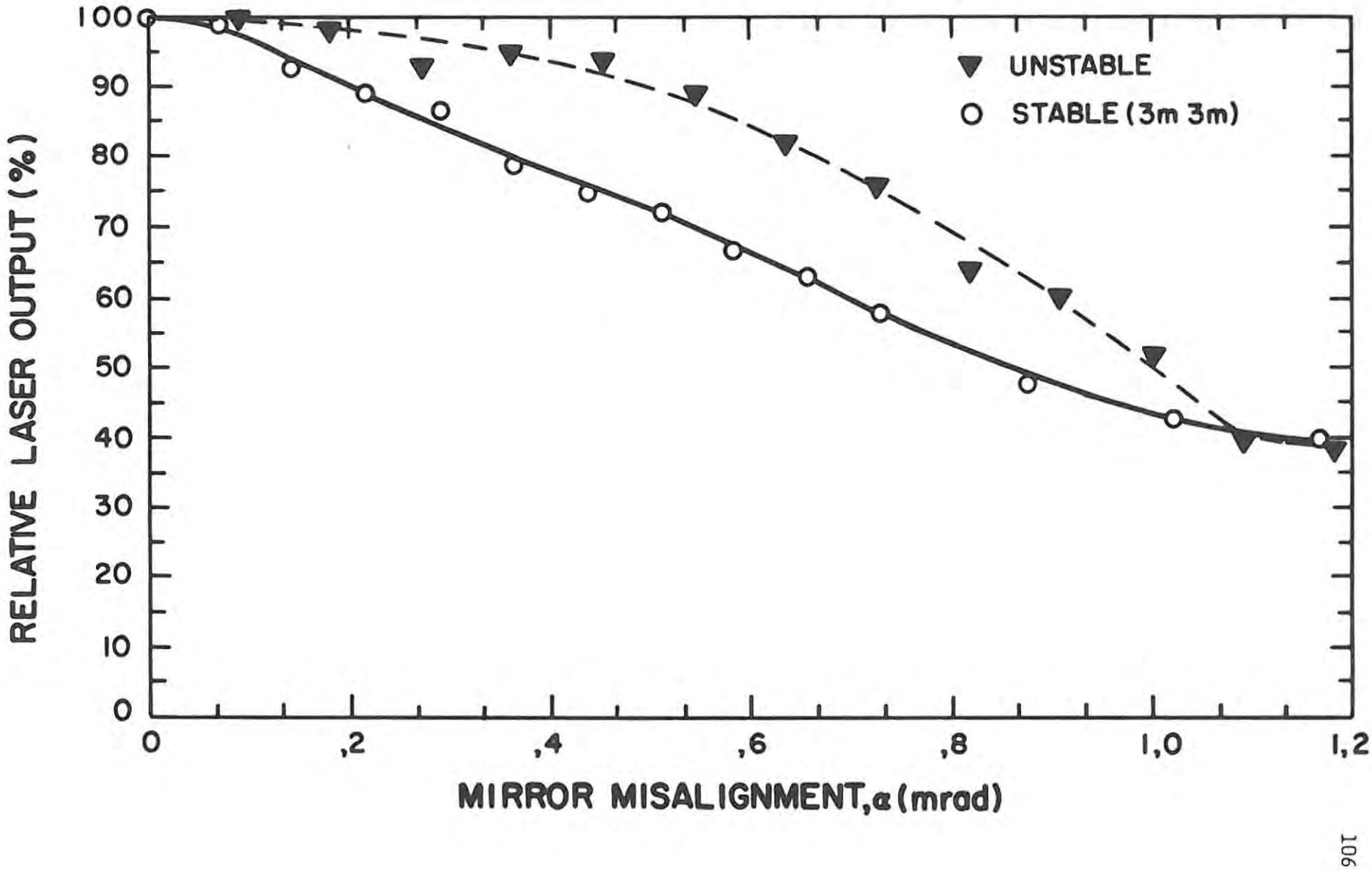

FIG. 5.15 COMPARISON OF MIRROR MISALIGNMENT SENSITIVITY FOR A STABLE RESONATOR WITH THAT OF THE PRESENT SYSTEM

stage to allow translation across the focussed beam. Beam steering was measured by tilting one of the laser mirrors and observing the amount by which the array had to be moved in order to centre the observed beam profile. The results are shown graphically in Figs. 5.16 to 5.18. Linear least square lines have been fitted to the experimental points. The correspondence between experimental and theoretical values is quite good. The experimental results were obtained at an input energy of 25 J and 1,25 Hz repetition rate.

5.3.5 EFFECT OF PULSE REPETITION RATE ON THE LASER PARAMETERS

As described in Section 3.4.2, the thermal lens effect is compensated for in the unstable resonator by moving the back reflector relative to the other components. Due to the fact that the focal length of the laser rod is inversely proportional to the pump power into the flashlamp (Section 2.4) it is clear that an increase in either the pulse repetition rate or input energy will result in a shorter focal length of the laser rod. In this investigation we consider the effect of a change of pulse repetition rate at a constant input energy of 25 J.

5.3.5.1 DETERMINATION OF THE BACK REFLECTOR TRANSLATION STAGE CHARACTERISTICS WITH TRANSLATION POSITION

The shift of the back reflector along the optical axis to compensate for the thermal lens effect should ideally be such that the mirror remains exactly aligned. This, however, is difficult to achieve and relies not only on accurate alignment of the translation stage but also on the straightness and flatness of travel of the stage. The translation characteristics, rise and fall and lateral shift with travel (defined in Fig. 5.19), were determined simply by glueing a flat mirror to the back reflector mount and observing the angular deviations, from a reference zero at one of the end positions, directly with the Davidson alignment telescope. The results of these experiments are shown in Fig. 5.20. A maximum rise and fall of just over 3 minutes (0,87 mrad) and a lateral shift of just over 0,5 minutes (0,15 mrad) was measured over the 50 mm range of travel.

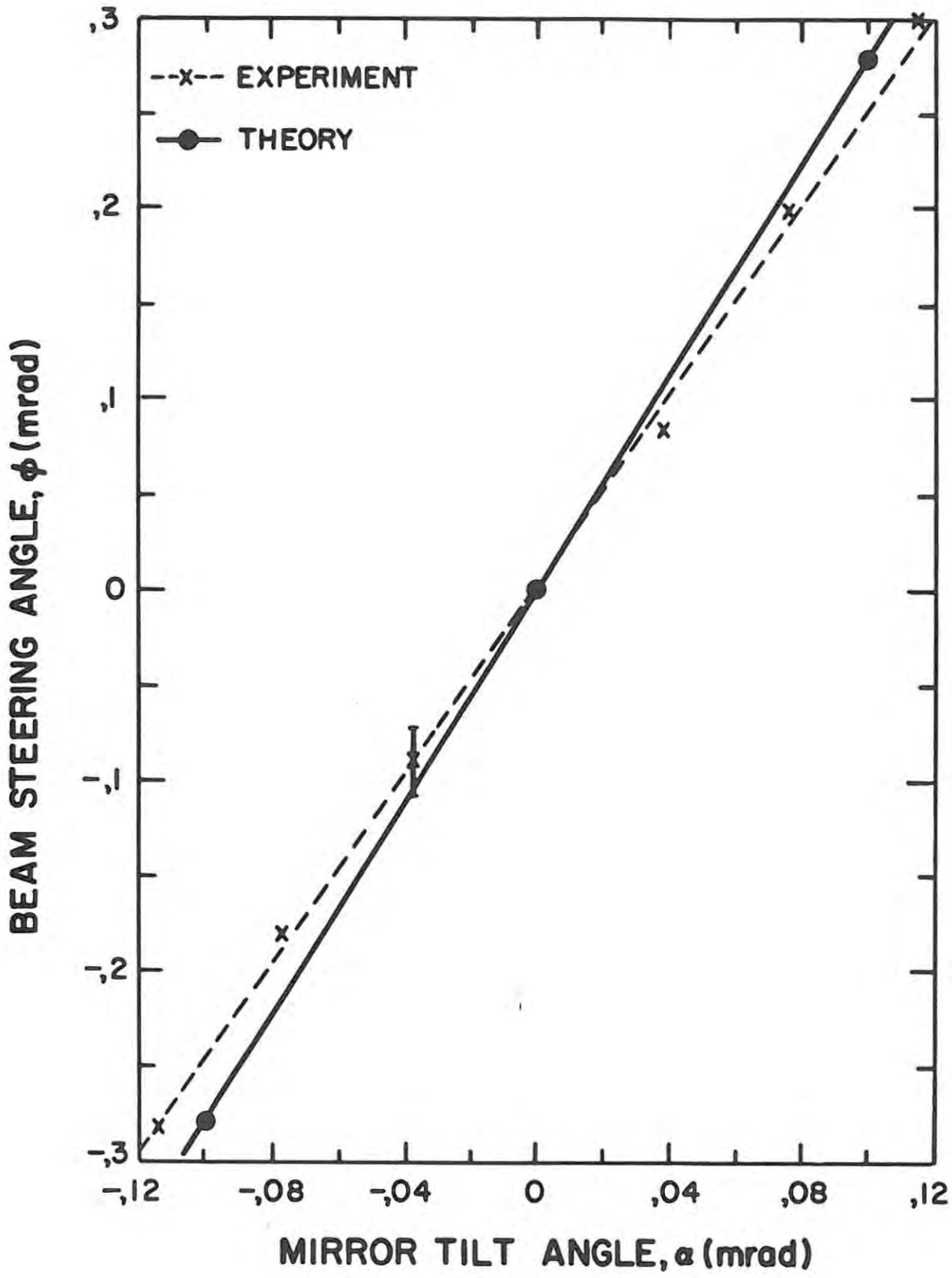

FIG. 5.16 BEAM STEERING ANGLE VERSUS TILT ANGLE OF BACK REFLECTOR ABOUT A VERTICAL AXIS.

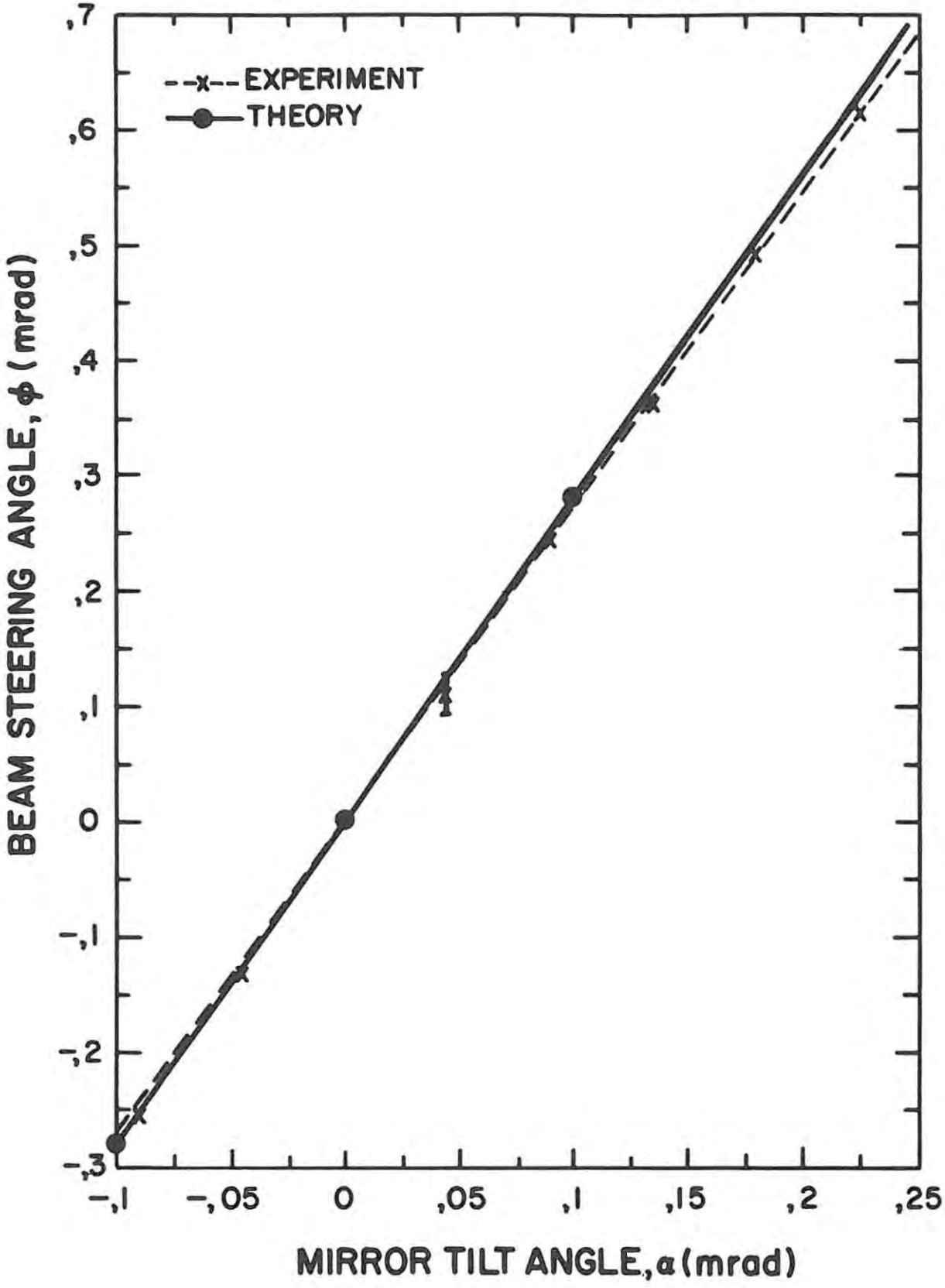

FIG. 5.17 BEAM STEERING ANGLE VERSUS TILT ANGLE OF BACK REFLECTOR ABOUT HORIZONTAL AXIS

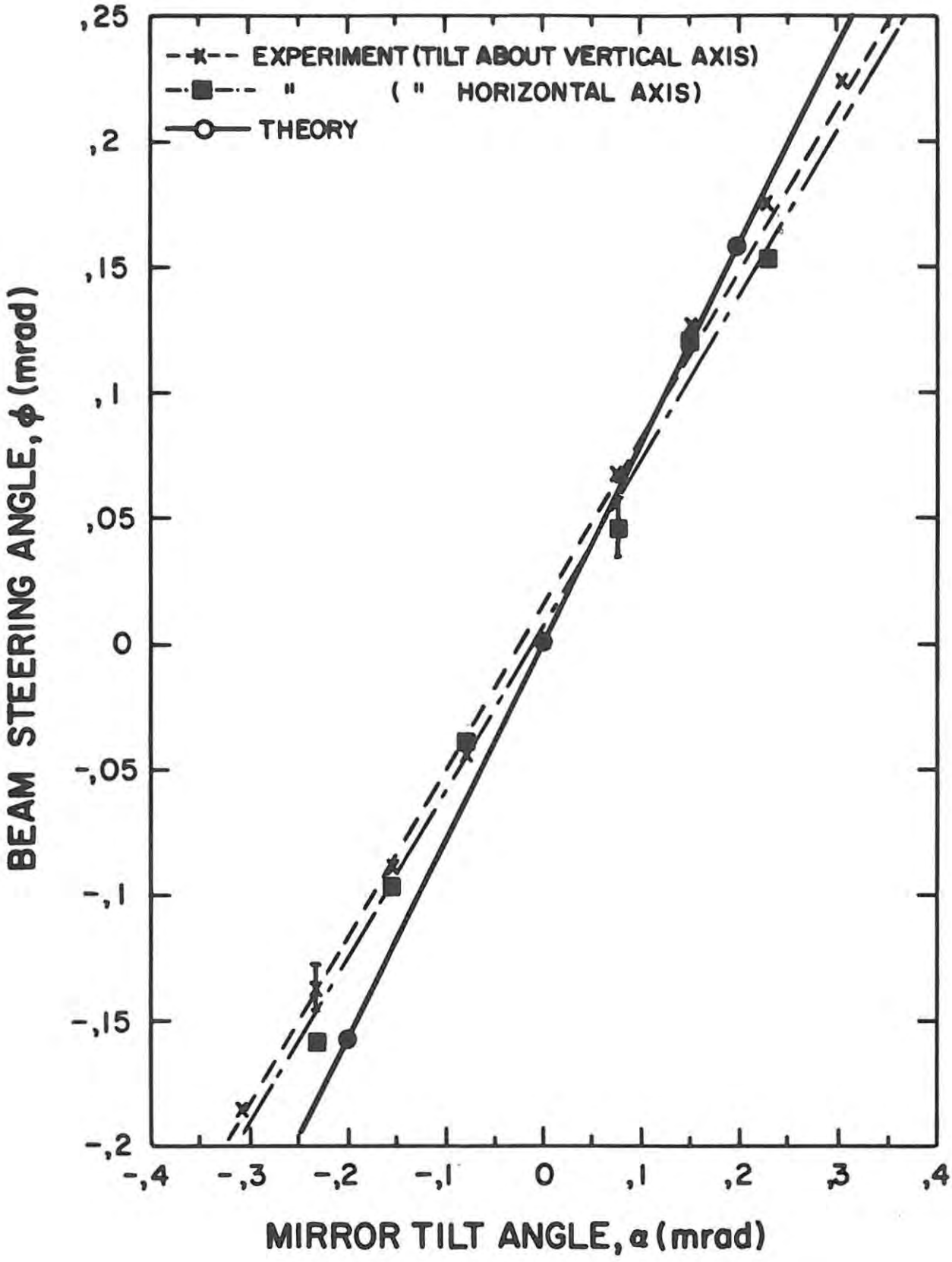

FIG. 5.18 BEAM STEERING ANGLE VERSUS TILT ANGLE OF OUTPUT COUPLER

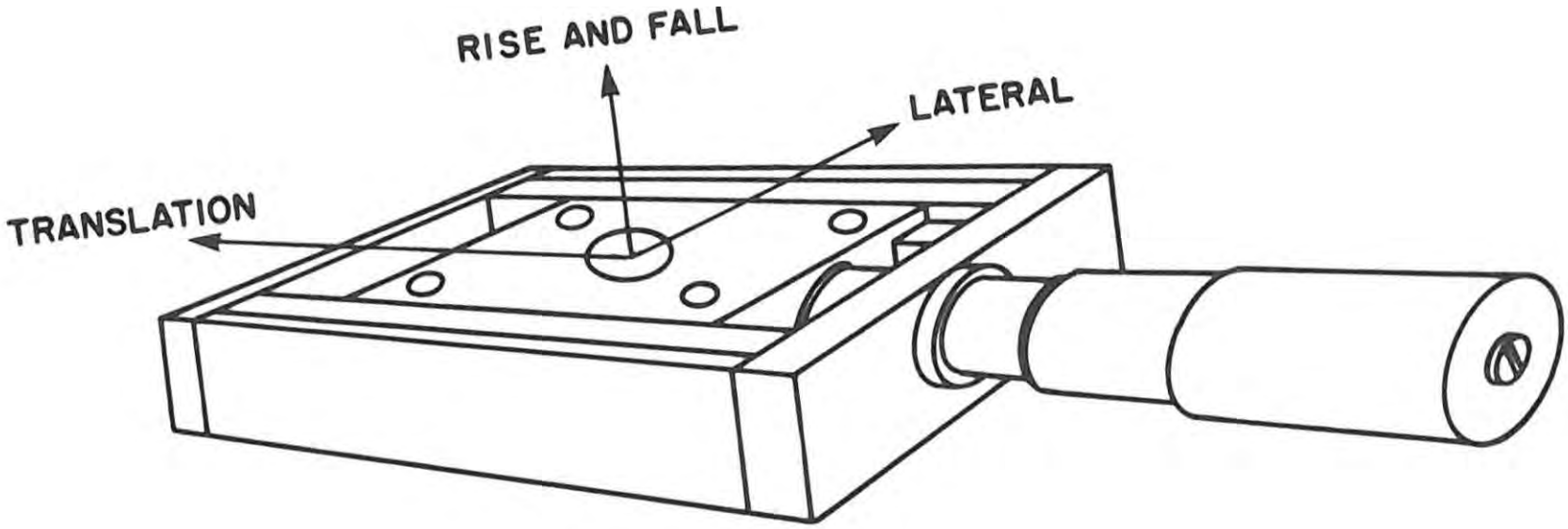

FIG. 5.19 DEFINITION OF TRANSLATION STAGE PARAMETERS

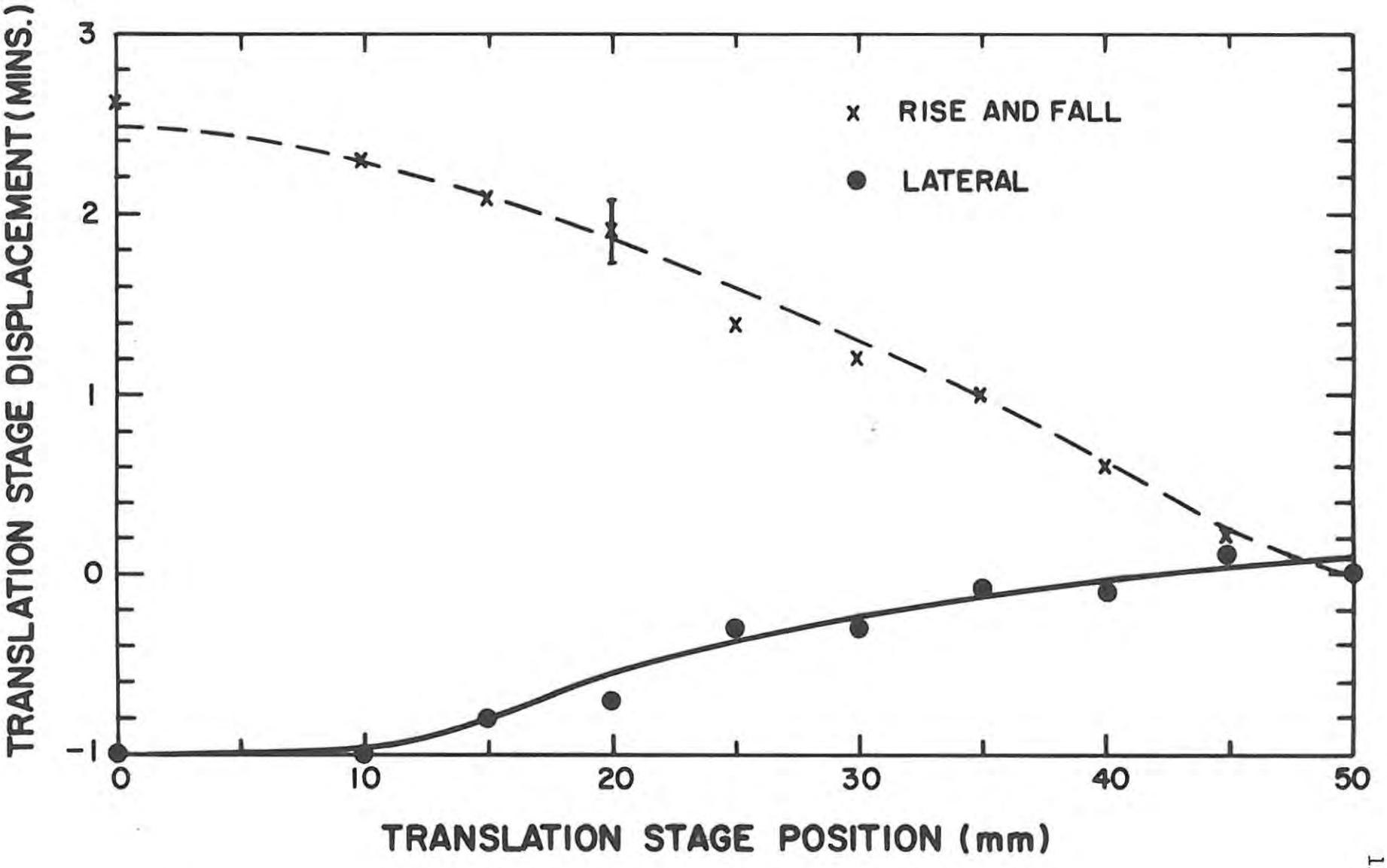

FIG. 5.20 TRANSLATION STAGE PARAMETERS AT VARIOUS POSITIONS DURING STAGE TRAVEL

While these figures indicate that we could still remain above the 90 % energy points, the beam burn mark showed a distinctly non-uniform annulus. From the energy point of view one could therefore use the laser at various repetition rates without reoptimization of the back reflector but not from a beam quality point of view.

5.3.5.2 OUTPUT POWER AND PULSE WIDTH

The effects of the translation stage misalignment characteristics on the peak output power of the laser and the laser pulse width were experimentally determined at the various repetition rates. These were measured with the silicon PIN photodiode (see Section 4.4.1.2) near the output coupler. The experiment was conducted in the following way. At 1,25 Hz the laser was optimized and the output power and pulse width measured. At 2,5; 5 and 10 Hz the back reflector was positioned for minimum beam divergence (Table 5-2) without reoptimizing the back mirror. This mirror position is given for each repetition rate on the right of the central column in Table 5-2. The peak power and pulse width were measured at these positions. The experiment was then repeated but this time the back mirror was reoptimized (as determined by the beam burn mark) at each of the translation stage positions corresponding to the minimum beam divergence. The results are tabulated in Table 5-1. (As the measurements yield relative values only, the results were left in the units in which they were observed, i.e. volts).

TABLE 5-1

Repetition rate (Hz)	Mirror position (mm)	Peak Power	
		mirror not optimized	Mirror optimized
1,25	35	1,64 V	1,64 V
2,5	32,5	1,64	1,64
5	22,5	1,1	1,64
10	17,5	1,24	1,64

The pulse width (FWHM) remained constant to within 2 ns at a value of 10 ns at 50 % power points. The peak power appears to vary considerably more than the output energy with translation stage position. The

burn mark showed clearly that the laser was not properly aligned. By reoptimizing the mirror alignment at each position of the translation stage we could get back to the same peak power. A typical laser pulse at 1,25 Hz is shown in Fig. 5.21. The pulse width shown is between 1,5 and 2 times shorter than that obtained with stable resonators built in this laboratory (≈ 20 ns) (Nortier (1981), Robertson & Preussler (1982)). We ascribe this to the fact that in the unstable resonator the inverted population is depleted faster due to the larger mode volume and higher power density in the resonator. Another reason is the higher threshold which causes lasing to start later and extinguish earlier.

5.3.5.3 FAR-FIELD BEAM DIVERGENCE

Measurement of the far-field beam divergence at various repetition rates was achieved with the same experimental arrangement as shown in Fig. 5.8. At each repetition rate the far-field pattern at the focal plane of the lens was observed and the $1/e^2$ width measured for various positions of the back reflector. The mirror was optimized at each position. These results are shown in Table 5-2. It can be seen that the movement of the back reflector by a considerable amount results in only a very small increase in beam divergence. It can be seen that without moving the back reflector, the thermal lensing effect of the laser rod results in a larger spot size in the focal plane and hence a larger beam divergence. Compensation of the thermal lens results in the same beam divergence at all repetition rates. Using equation (2.31), with P_{in} = 25 J x repetition rate, the focal length of the laser rod for each repetition rate can be calculated and plotted against back reflector position as shown in Fig. 5.22.

Clearly the position of the back reflector in Table 5-2 and Fig. 5.22 is not as clearly defined and critical as that computed in Section 3.4.2.2 and Fig. 3.14. This would then mean that the thermal lens in the laser rod is not as marked as we could expect and that possibly equation (2.31) does not accurately describe the induced thermal focal length. We have, however, shown the necessity to compensate for the resulting thermal lens.

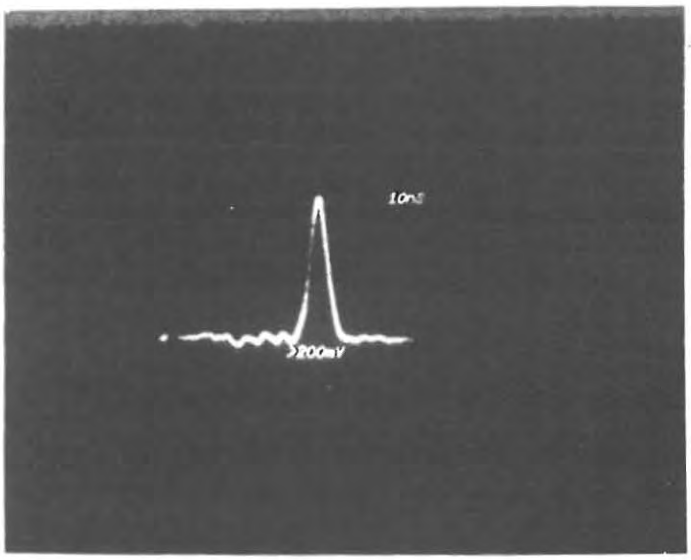

FIG. 5.21 A TYPICAL LASER PULSE

TABLE 5-2

Rep. rate (Hz)	Back reflector position (mm)		No. of diodes at $1/e^2$ points
1,25	50		42
	45		40
	40		38
	35	35	38
	30		39
	25		39
	20		44
2,5	50		43
	45		39
	40		37
	35	32,5	37
	30		37
	25		37
	20		40
	15		46
5	40		42
	35		38
	30		38
	25		37
	20	22,5	36
	15		41
	10		44
10	25		40
	20		37
	15	17,5	38
	10		39
	5		42
	0		45

† positions for minimum beam divergence

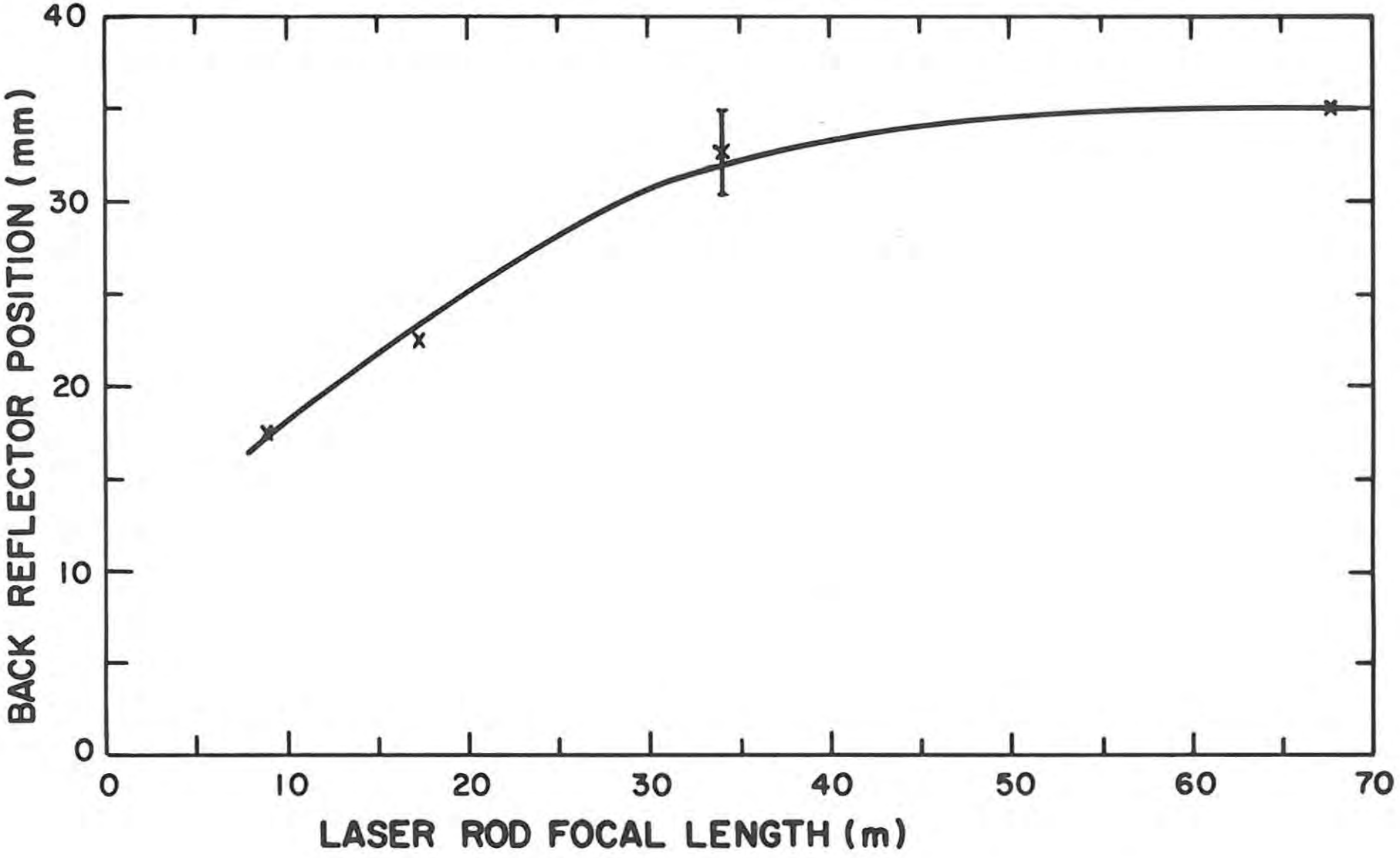

FIG. 5.22 POSITION OF BACK REFLECTOR WHICH GIVES MINIMUM BEAM DIVERGENCE AS A FUNCTION OF LASER ROD FOCAL LENGTH

CHAPTER 6

CONCLUSIONS

6.1 SUMMARY

A Q-switched Nd:YAG laser using a confocal positive-branch unstable resonator has been successfully designed and operated at repetition rates up to 10 Hz. The efficiency of the laser lies within the range of efficiencies reported in the literature. Due to the much shorter pulse lengths which were obtained, a somewhat higher peak output power could be achieved. Powers of the order of 5 MW were obtaind by Nortier (1981) and Robertson & Preussler (1982). Operating in the middle of the efficiency curve we could obtain powers of 6 MW (60 mJ, 10 ns). In terms of beam divergence and beam quality, the unstable resonator has proven its merits over stable resonators. A beam divergence of 0,3 mrad at all repetition rates was achieved compared to divergences greater than 1 mrad obtainable with stable resonators. A near-Gaussian far-field beam structure was also obtained.

In terms of sensitivity to mirror misalignment, we have shown, contrary to the theory and literature, that our specific laser is less sensitive to mirror misalignment than a comparable stable resonator laser.

At high repetition rates the induced thermal lens in the laser rod can be compensated for by a shift of the back mirror along the optical axis. Although theory and experiment show different amounts of shift with repetition rate, the expected tendency is observed. The misalignment effects introduced by the translation stage movement cause a reduction in output energy and power from the optimum and necessitate reoptimization of the back mirror for best output. While such a reoptimization could be tolerated in a laboratory type system, it would be undesirable for other applications.

6.2 SUGGESTIONS FOR FURTHER WORK

A number of aspects for the further improvement of the output characteristics of the unstable resonator need further investigation.

Firstly, the use of a close-coupled ellipse (Section 4.2.3) may improve the conversion of pumplight into laser light. Most unstable resonator lasers use this type of pumping geometry and this may improve the output and lower the threshold to some extent. The reason it was not done here was due to the unavailability of such a geometry at the time of the experiments.

Secondly, one could vary the size of the output coupler mirror. This would mean a change in the magnification, equivalent Fresnel number and resonator length. While it is suggested in the literature that one should operate at half-integer values of the equivalent Fresnel number, Hanna & Laycock (1979) have observed no significant change in output beam quality from half-integer to whole integer values. It may be possible that the choice of mirrors of different curvature, but consistent with the design equations, may result in a better (or worse) output since the difference between the design of Andreou (1978) and the present work is only in the radii of curvature and resonator length.

Another possibility for investigation would be the use of a negative-branch unstable resonator. Although, as we have stated previously, optical (or gas) breakdown problems could be encountered with the internal focal point, a very recent publication (Gobbi et al (1985)) describes a method of avoiding this problem. By making use of a field limiting aperture placed at the common focal plane of the mirrors, the hot spot inside the cavity can be removed. One of the most striking features of this resonator is the extremely regular and smooth behaviour of the intensity profile which in the results given is near-Gaussian shape in the near-field.

REFERENCES

Ananév Y.A., Vinokurov G.N., Koval'chuk L.V., Sventsitskaya N.A. and Sherstobitov V.E. (1970)
Telescopic-resonator laser
Sov. Phys.-JETP **31,** 3, p.420.

Ananév Y.A. and Sherstobitov V.E. (1971)
Influence of the edge effects on the properties of unstable resonators
Sov. J. Quant. Elect. **1,** p.263.

Andreou D. (1978)
Construction and performance of a 20-pps unstable Nd:YAG oscillator
Rev. Sci. Instrum. **49,** 5, p.586.

Ballhausen S.J.
Introduction to Ligand Field Theory
McGraw-Hill, Inc. New York

Born M. and Wolf E. (1980)
Principles of optics, 6th Edn.
Pergamon Press, New York.

Byer R.L. and Herbst R.L. (1978)
The unstable-resonator YAG
Laser Focus, July 1978, p.48.

Chao S.L. and Schnurr A.D. (1984)
Unstable resonator alignment using off-axis Gaussian beam propagation
Appl. Optics **23,** 13, p.2115.

Chen L.W. and Felson L.B. (1973)
Coupled-mode theory of unstable resonators
IEEE J Quant. Electr. **QE-9,** 11, p.1102.

Einstein A. (1917)
Zur quantentheorie der strahlung
Physik. Zeit. **18,** 6, p.121.

Ewanizky T.F. and Craig J.M. (1976)
A negative-branch unstable resonator Nd:YAG laser
Appl. Optics **15,** 6, p.1465.

Foster J.D. and Osterink L.M. (1970)
Thermal effects in a Nd:YAG laser
J. Appl. Phys. **11,** 9, p.3656.

Fox A.G. and Li T. (1961)
Resonant modes in a maser interferometer
Bell Syst. Tech. J. **40,** p.453.

Freiberg R.J., Chenausky P.P. and Buczek C.J. (1972)
An experimental study of unstable confocal resonators
IEEE J. Quant. Elect. **QE-8,** 12, p.882.

Geusic J.E., Marcos H.M. and Van Uitert L.G. (1964)
Laser oscillations in Nd-doped yttrium aluminium, yttrium gallium and gadolinium garnets
Appl. Phys. Lett. **4,** 10, p.182.

Gleason T.J. (1971)
Analysis of complex laser cavities
Report number HDL-TM-71-5, US Army Material Command, Harry Diamond Laboratories, Washington DC.

Gobbi P.G., Morosi S., Reali G.C. and Zarkasi A.S. (1985)
Novel unstable resonator configuration with a self-filtering aperture: experimental characterization of the Nd:YAG loaded cavity
Appl. Optics **24,** 1, p.26.

Hanlon J. and Aiken S. (1974)
Alignment technique for unstable resonators
Appl. Optics **13,** 11, p.2461.

Hanna D.C. and Laycock L.C. (1979)
An unstable resonator Nd:YAG laser
Opt. and Quant. Elect. **11**, 2, p.153.

Herbst R.L., Komine H. and Byer R.L. (1977)
A 200 mJ unstable resonator Nd:YAG oscillator
Optics Comm. **21**, 1, p.5.

Horwitz P. (1976)
Modes in misaligned unstable resonators
Appl. Optics **15**, 1, p.167.

Hotz R.F. (1973)
Thermal transient effects in repetitively pulsed flashlamp pumped YAG:Nd, Lu laser material
Appl. Optics **12**, 8, p.1834.

Kahn W.K. (1966)
Unstable optical resonators
Appl. Optics **5**, 3, p.407.

Klein M.V. (1970)
Optics.
John Wiley & Sons Inc., New York.

Koechner W. (1970)
Thermal lensing in a Nd:YAG laser rod
Appl. Optics **9**, 11, p.2548.

Koechner W. (1976)
Solid-state laser engineering.
Springer-Verlag, New York

Kogelnik H. and Li T. (1966)
Laser beams and resonators
Proc. IEEE **54**, 10, p.1312.

Koningstein J.A. and Geusic J.E. (1964)
Energy levels and crystal-field calculations of Neodymium in Yttrium Aluminium Garnet
Phys. Rev. **136,** 3A, p.A 711.

Koval'chuk L.V. and Sventsitskaya N.A. (1973)
Methods for alignment of lasers with unstable resonators
Sov. J. Quant. Elect. **2,** p.450.

Krupke W.F. and Sooy W.R. (1969)
Properties of an unstable confocal resonator CO_2 laser system
IEEE J. Quant. Electr. **QE-5,** 12, p.575.

Lengyel B.A. (1971)
Lasers. 2nd Ed.
Wiley-Interscience, New York

Maiman T.H. (1960)
Optical and microwave-optical experiments in ruby
Phys. Rev. Lett. **4,** 11, p.564.

McCarthy A.E. (1973)
Technique for precision alignment of a Pockels cell in a Q-switched laser cavity
Report SLA-73-0689, Sandia Labs., New Mexico.

Nortier F.M. (1981)
Investigation of a crossed Porro-prism resonator employed in a Q-switched Nd:YAG laser
M.Sc. Thesis, University of Natal.

Preussler D.R. (1980)
An experimental fast pulsing laser system with rotating prism Q-switch (FPLS-RP)
NPRL Internal report, March 1980.

Preussler D.R. and De Kock T.N. (1983)
Evaluation of a fast pulsing Nd:YAG laser system using a crossed Porro-prism resonator
NPRL Internal report, April 1983.

Rensch D.B. and Chester A.N. (1973)
Iterative diffraction calculations of transverse mode distributions in confocal unstable laser resonators
Appl. Optics **12**, 5, p.997.

Robertson S.H. and Preussler D.R. (1982)
An experimental fast pulsing Nd:YAG laser system with electro-optical Q-switch (conventional resonator)
NPRL Internal report, March 1982

Röss D. (1969)
Lasers, light amplifiers and oscillators
Academic Press, New York.

Siegman A.E. (1965)
Unstable optical resonators for laser applications
Proc. IEEE **53**, 3, p.277.

Siegman A.E. (1971)
Stabilizing output with unstable resonators
Laser Focus, May 1971, p.42.

Siegman A.E. (1971a)
An introduction to lasers and masers
McGraw-Hill, Inc., New York.

Siegman A.E. (1974)
Unstable optical resonators
Appl. Optics **13**, 2, p.353.

Siegman A.E. (1976)
A canonical formulation for analyzing multielement unstable resonators
IEEE J. Quant. Elect. **QE-12**, 1, p.35.

Siegman A.E. and Arrathoon R. (1967)
Modes in unstable optical resonators and lens waveguides
IEEE J. Quant. Electr. QE-3, 4, p.156.

Siegman A.E. and Miller H.Y. (1970)
Unstable optical resonator loss calculations using the Prony method
Appl. Optics 9, 12, p.2729.

Steele E.L. (1968)
Optical lasers in electronics
John Wiley & Sons Inc., New York.

Steier W.H. (1979)
Unstable resonators in Laser Handbook, Vol. 3 edited by M.L. Stitch
North Holland Publishing Company, Amsterdam.

Treacy E.B. (1969)
Diffractive coupling from a CO_2 laser
Appl. Optics 8, 6, p.1107.

Van den Berg W. (1982)
Development of a laser beam analyser
NPRL Internal report no. FIS 291, November 1982.

Wahlstrom E.E. (1960)
Optical Crystallography 3rd Edn.
John Wiley & Sons Inc., New York.

Weichel H. and Pedrotti L.S. (1976)
A summary of useful laser equations
EOSD, July 1976, p.22

Yariv A. (1975)
Quantum Electronics, 2nd Edn.
John Wiley & Sons Inc., New York.

APPENDIX I

HP-86 computer programme for calculating the total ray transfer matrix using the method of specifying the input ray height and angle at a reference plane (see Fig. 3.12).

```
10 OPTION BASE 1
20 DIM A1(2,2),A2(2,2),A3(2,2)
30 DIM A4(2,2),A5(2,2),X(2,2),Y(2,2),Z(2,2)
40 DISP "ENTER ROD LENGTH(MM)AND REFRACTIVE INDEX"
50 INPUT L,NO
60 DISP "ENTER INPUT RAY HEIGHT(MM) AND ANGLE"
70 INPUT R1,C1
80 DISP "ENTER ROD/P.C. SEPARATION(MM)"
90 INPUT D1
100 DISP "ENTER ROD FOCAL LENGTH(MM)"
110 INPUT F
120 DISP "ENTER P.C. 100% MIRROR SEPARATION"
130 INPUT DO
140 REM DEFINE LASER ROD MATRIX
150 A1(1,1)=1-L/(2*NO*F)
160 A1(1,2)=L/NO
170 A1(2,1)=-(1/F)
180 A1(2,2)=1-L/(2*NO*F)
190 REM DEFINE ROD/BACK MIRROR SEPARATION MATRIX
200 A2(1,1)=1
210 A2(1,2)=DO+D1+27.03
220 A2(2,1)=0
230 A2(2,2)=1
240 REM DEFINE BACK MIRROR MATRIX
250 A3(1,1)=1
260 A3(1,2)=0
270 A3(2,1)=-(2/1000)
280 A3(2,2)=1
290 FOR I=1 TO 2
300 FOR J=1 TO 2
310 Y(I,J)=A1(I,J)
320 NEXT J
330 NEXT I
340 REM MULTIPLY MATRICES
350 FOR I=1 TO 2
360 FOR J=1 TO 2
370 Z(I,J)=A2(I,1)*Y(I,J)+A2(I,2)*Y(2,J)
380 NEXT J
390 NEXT I
400 FOR I=1 TO 2
410 FOR J=1 TO 2
420 Y(I,J)=Z(I,J)
430 NEXT J
440 NEXT I
450 FOR I=1 TO 2
460 FOR J=1 TO 2
470 Z(I,J)=A3(I,1)*Y(1,J)+A3(I,2)*Y(2,J)
```

```
480 NEXT J
490 NEXT I
500 FOR I=1 TO 2
510 FOR J=1 TO 2
520 Y(I,J)=Z(I,J)
530 NEXT J
540 NEXT I
550 FOR I=1 TO 2
560 FOR J=1 TO 2
570 Z(I,J)=A2(I,1)*Y(1,J)+A2(I,2)*Y(2,J)
580 NEXT J
590 NEXT I
600 FOR I=1 TO 2
610 FOR J=1 TO 2
620 Y(I,J)=Z(I,J)
630 NEXT J
640 NEXT I
650 FOR I=1 TO 2
660 FOR J=1 TO 2
670 Z(I,J)=A1(I,1)*Y(1,J)+A1(I,2)*Y(2,J)
680 NEXT J
690 NEXT I
700 REM DEFINE COEFFICIENTS OF TOTAL MATRIX
710 A=Z(1,1)
720 B=Z(1,2)
730 C=Z(2,1)
740 D=Z(2,2)
750 REM CALCULATE OUTCOMING RAY HEIGHT AND ANGLE
760 R2=A*R1+B*C1
770 C2=C*R1+D*C1
780 DISP "COLLIMATION =";C2
790 DISP "FOCAL LENGTH OF ROD=";F
800 DISP "P.C./MIRROR SEPARATION=";DO
810 REM IS COLLIMATION CONDITION SATISFACTORY ?
820 DISP "SATISFIED?(Y/N)"
830 INPUT N$
840 IF N$="N" THEN 120 ELSE 850
850 DISP "DO YOU WANT TO USE ANOTHER FOCAL LENGTH FOR ROD(Y/N)?"
860 INPUT Y$
870 IF Y$="Y" THEN 100 ELSE 880
880 END
```

HP-86 computer programme for calculating the ray transfer matrix by the round-trip method.

```
10 OPTION BASE 1
20 DIM A1(2,2),A2(2,2),A3(2,2),A4(2,2),A5(2,2)
30 DIM X(2,2),Y(2,2),Z(2,2)
40 DISP "ENTER ROD LENGTH(MM) AND REFRACTIVE INDEX"
50 INPUT L,NO
60 DISP "ENTER O.C./ROD SEPARATION(MM) & ROD P.C. SEPARATION(MM)"
70 INPUT D2,D1
80 DISP "ENTER ROD FOCAL LENGTH(MM)"
90 INPUT F
100 DISP "ENTER P.C/MIRROR SEPARATION(MM)"
110 INPUT DO
120 REM DEFINE MATRIX OF DISTANCE BETWEEN O.C.AND LASER ROD
130 A1(1,1)=1
140 A1(1,2)=D2
150 A1(2,1)=0
160 A1(2,2)=1
170 REM DEFINE MATRIX OF LASER ROD
180 A2(1,1)=1-L/(2*NO*F)
190 A2(1,2)=L/NO
200 A2(2,1)=-(1/F)
210 A2(2,2)=1-L/(2*NO*F)
220 REM DEFINE MATRIX OF P.C. & DISTANCE TO BACK REFLECTOR(DO)
230 A3(1,1)=1
240 A3(1,2)=DO+D1+27.03
250 A3(2,1)=0
260 A3(2,2)=1
270 REM DEFINE MATRIX OF BACK MIRROR
280 A4(1,1)=1
290 A4(1,2)=0
300 A4(2,1)=-(2/1000)
310 A4(2,2)=1
320 REM DEFINE MATRIX OF OUTPUT COUPLER
330 A5(1,1)=1
340 A5(1,2)=0
350 A5(2,1)=2/300
360 A5(2,2)=1
370 REM MULTIPLY MATRICES TO GET TOTAL TRANSFER MATRIX
380 FOR I=1 TO 2
390 FOR J=1 TO 2
400 Y(I,J)=A5(I,J)
410 NEXT J
420 NEXT I
430 FOR I=1 TO 2
440 FOR J=1 TO 2
450 Z(I,J)=A1(I,1)*Y(1,J)+A1(I,2)*Y(2,J)
460 NEXT J
470 NEXT I
480 FOR I=1 TO 2
490 FOR J=1 TO 2
500 Y(I,J)=Z(I,J)
510 NEXT J
520 NEXT I
530 FOR I=1 TO 2
540 FOR J=1 TO 2
```

```
550 Z(I,J)=A2(I,1)*Y(1,J)+A2(I,2)*Y(2,J)
560 NEXT J
570 NEXT I
580 FOR I=1 TO 2
590 FOR J=1 TO 2
600 Y(I,J)=Z(I,J)
610 NEXT J
620 NEXT I
630 FOR I=1 TO 2
640 FOR J=1 TO 2
650 Z(I,J)=A3(I,1)*Y(1,J)+A3(I,2)*Y(2,J)
660 NEXT J
670 NEXT I
680 FOR I=1 TO 2
690 FOR J=1 TO 2
700 Y(I,J)=Z(I,J)
710 NEXT J
720 NEXT I
730 FOR I=1 TO 2
740 FOR J=1 TO 2
750 Z(I,J)=A4(I,1)*Y(1,J)+A4(I,2)*Y(2,J)
760 NEXT J
770 NEXT I
780 FOR I=1 TO 2
790 FOR J=1 TO 2
800 Y(I,J)=Z(I,J)
810 NEXT J
820 NEXT I
830 FOR I=1 TO 2
840 FOR J=1 TO 2
850 Z(I,J)=A3(I,1)*Y(1,J)+A3(I,2)*Y(2,J)
860 NEXT J
870 NEXT I
880 FOR I=1 TO 2
890 FOR J=1 TO 2
900 Y(I,J)=Z(I,J)
910 NEXT J
920 NEXT I
930 FOR I=1 TO 2
940 FOR J=1 TO 2
950 Z(I,J)=A2(I,1)*Y(1,J)+A2(I,2)*Y(2,J)
960 NEXT J
970 NEXT I
980 FOR I=1 TO 2
990 FOR J=1 TO 2
1000 Y(I,J)=Z(I,J)
1010 NEXT J
1020 NEXT I
1030 FOR I=1 TO 2
1040 FOR J=1 TO 2
1050 Z(I,J)=A1(I,1)*Y(1,J)+A1(I,2)*Y(2,J)
1060 NEXT J
1070 NEXT I
```

```
1080 REM DEFINE ELEMENTS OF TOTAL RAY TRANSFER MATRIX
1090 A=Z(1,1)
1100 B=Z(1,2)
1110 C=Z(2,1)
1120 D=Z(2,2)
1130 REM CALCULATE COLLIMATION CONDITION
1140 C1=A*D-1
1150 DISP "COLLIMATION =";C1
1160 REM CALCULATE RADIUS OF CURVATURE OF WAVE AT OUTPUT MIRROR
1170 R=(A-D+SQR ((A-D)^2+4*B*C))/(2*C)
1180 DISP "RADIUS OF CURVATURE(M)=";R/1000
1190 REM CALCULATE BEAM RADIUS AT OUTPUT MIRROR
1200 W=SQR (.86*.86*(A+B/R)^2/(A*D-B*C))
1210 DISP "BEAM RADIUS AT OUTPUT MIRROR(MM)=";W
1220 DISP "FOCAL LENGTH OF ROD(M)=";F/1000
1230 DISP "P.C/MIRROR SEPARATION(MM)=";DO
1240 DISP "SATISFIED?(Y/N)"
1250 INPUT N$
1260 IF N$="N" THEN 100 ELSE 1270
1270 DISP "DO YOU WANT TO USE ANOTHER FOCAL LENGTH FOR ROD(Y/N)?"
1280 INPUT Y$
1290 IF Y$="Y" THEN 80 ELSE 1300
1300 DISP "O.K. BYE"
1310 END
```

APPENDIX II

DERIVATION OF D = fθ

The derivation refers to Fig. A1.

It shows a Gaussian beam of waist diameter 2 W_{01} transformed into a Gaussian beam of waist diameter 2 W_{02} by a thin positive lens. The incoming beam waist is at a distance Z_1 from the lens and the focussed beam waist is at a distance Z_2 from the lens.

The position and size of the focussed beam waist are given by equations (A1) and (A2) below (Weichel & Pedrotti (1976)):

$$Z_2 = f + \frac{(Z_1 - f)f^2}{(Z_1 - f)^2 + \left(\frac{\pi W_{01}^2}{\lambda}\right)^2} \qquad (A1)$$

spot size of a focussed laser beam at Z_2

$$\frac{1}{W_{02}^2} = \frac{1}{W_{01}^2}\left(1 - \frac{Z_1}{f}\right)^2 + \frac{1}{f^2}\left(\frac{\pi W_{01}}{\lambda}\right)^2 \qquad (A2)$$

Equation (A3), from the same reference, gives the spot size at a distance Z from the beam waist W_{02}

$$W^2(Z) = W_{02}^2\left[1 + \left(\frac{\lambda Z}{\pi W_{02}^2}\right)^2\right] \qquad (A3)$$

So, to get the spot size at the focal plane of the lens we must propagate the beam, from the beam waist W_{02}, a distance $(Z_2 - f)$ in equation (A3) and we get

$$W^2 \text{ (at focal plane)} = W_{02}^2\left[1 + \left(\frac{\lambda(Z_2 - f)}{\pi W_{02}^2}\right)^2\right] \qquad (A4)$$

Inserting equations (A1) and (A2) in (A4) it can be shown by elementary algebraic manipulation that

$$W^2 \text{ (at focal plane)} = f^2\left(\frac{\lambda}{\pi W_{01}}\right)^2$$

or $$W \text{ (at focal plane)} = f \frac{\lambda}{\pi W_{01}}$$

and since $\theta = \frac{\lambda}{\pi W_{01}}$ is, by definition, the far-field half-angle beam divergence

$$W \text{ (focal plane)} = f \theta$$

or $$D = 2W = f \theta_{full}$$

This result shows that at the focal plane of the lens the spot size remains the same whether or not the lens is in the near-or far-field.

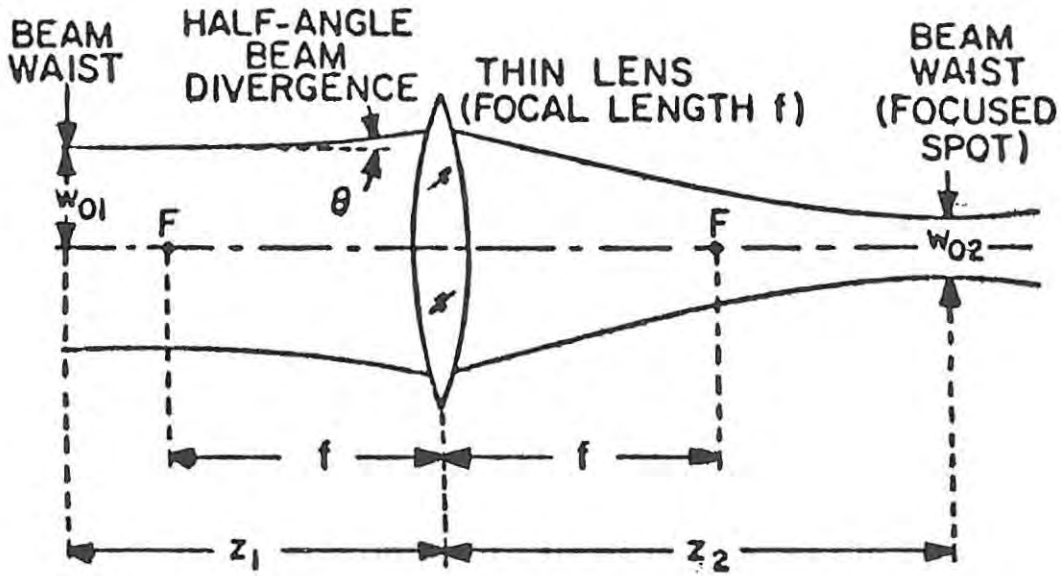

FIG. A1 GEOMETRY FOR THE DERIVATION OF D = fΘ